

Diss. ETH No. 13078

Groundwater Dynamics, Paleoclimate and Noble Gases

A dissertation submitted to the
SWISS FEDERAL INSTITUTE OF TECHNOLOGY ZÜRICH
for the degree of
DOCTOR OF NATURAL SCIENCES

presented by
URS BEYERLE
Dipl. Natw. ETH
born May 25, 1969
citizen of Zürich

accepted on the recommendation of
Prof. Dr. Dieter M. Imboden, examiner
Prof. Dr. Christoph Schär, co-examiner

Zürich 1999

Contents

Abstract	v
Kurzfassung	vii
Notation	ix
1 Introduction	1
1.1 GROUNDWATER AS A FRESHWATER RESOURCE	1
1.2 OLD GROUNDWATER AS ARCHIVE OF PAST CLIMATE	3
1.3 WHY NOBLE GASES?	4
1.4 OUTLINE	5
2 Noble gases in groundwater	7
2.1 ATMOSPHERIC NOBLE GASES	8
2.2 EQUILIBRIUM CONCENTRATION IN WATER	10
2.2.1 Isotopic fractionation of noble gases	17
2.3 EXCESS AIR	19
2.4 NON-ATMOSPHERIC SOURCES	25
2.4.1 Difference in helium ratios	25
2.4.2 Tritium (^3H)	29
2.4.3 Non-atmospheric Ne, Ar, Kr and Xe	33
3 A mass spectrometric system for the analysis of noble gases and tritium from water samples	35
3.1 INTRODUCTION	36
3.2 EXPERIMENTAL SECTION	37
3.2.1 Sampling	37
3.2.2 Gas extraction	39
3.2.3 He and Ne measurement	42
3.2.4 Ar, Kr, Xe measurement	43
3.2.5 Tritium measurement	45
3.2.6 Calibration	46

3.3	RESULTS AND DISCUSSION	49
3.3.1	Standard water samples	49
3.3.2	Equilibrated samples	53
3.3.3	Isotopic fractionation during solution	56
4	Recharge conditions and groundwater age deduced from noble gas concentrations	59
4.1	INTERPRETATION OF ATMOSPHERIC NOBLE GAS CONCENTRATIONS	60
4.1.1	The principle of the noble gas thermometer	60
4.1.2	Impact of ground and air temperature on noble gas temperature	62
4.1.3	Calculation of noble gas temperature and excess air	65
4.1.4	Determination of the recharge altitude	72
4.2	GROUNDWATER DATING	76
4.2.1	$^3\text{H}/^3\text{He}$ -dating method	79
4.2.2	Accumulation of radiogenic noble gases	84
4.3	EFFECT OF BINARY MIXING AND DISPERSION	94
4.3.1	Mixing	95
4.3.2	Dispersion	98
5	Infiltration of river water to a shallow aquifer investigated with $^3\text{H}/^3\text{He}$, noble gases and CFCs	107
5.1	INTRODUCTION	108
5.2	STUDY AREA	110
5.3	METHODS	114
5.3.1	Sampling and analysis	114
5.3.2	Evaluation of noble gas recharge temperature and excess air	115
5.3.3	$^3\text{H}/^3\text{He}$ dating of groundwater	116
5.4	RESULTS AND DISCUSSION	118
5.4.1	$^3\text{H}/^3\text{He}$ groundwater ages	118
5.4.2.	Noble gas data from the Linsental aquifer	122
5.4.3.	CFCs excess caused by contamination	125
5.4.4.	Variation in the dissolved oxygen concentration	128
5.4.5.	Radiogenic ^4He accumulation in the Linsental aquifer	130
5.5.	SUMMARY AND CONCLUSIONS	132

6 Climate and groundwater recharge during the last glaciation in an ice-covered region	135
References	147
Appendix	161
A1 SOLUBILITY DATA OF NOBLE GASES	161
Dank	165
Curriculum vitae	167

When you can measure what you are talking about, and express it in numbers, you know something about it; when you cannot express it in numbers, your knowledge is of a meager and unsatisfactory kind.

William Thompson Kelvin

Seite Leer /
Blank leaf

Abstract

The concentrations of dissolved noble gases and tritium in groundwater can be employed to deduce the physical conditions prevailing during recharge and to determine water residence times. Here, a method of determining the concentrations of noble gases and tritium in groundwater samples is described, the theory of the use of noble gases and tritium as environmental tracers is discussed, and two relevant case studies are described.

The most important stable isotopes of helium (He), neon (Ne), argon (Ar), krypton (Kr) and xenon (Xe), and the hydrogen isotope tritium (^3H) were analyzed by mass spectrometry. The experimental setup employed enables noble gas concentrations and isotopic ratios in water samples to be measured with an overall long-term accuracy typically better than 1%. Tritium samples can be measured routinely with an accuracy of 2% to 3% and a detection limit of 0.1 TU; both parameters can be improved by an order of magnitude by using larger samples.

The evolution and the various origins of the noble gases present in groundwater are discussed. After groundwater infiltration, the concentration of noble gases in groundwater depends mainly on the atmospheric equilibrium concentration modified by an additional atmospheric component called 'excess air'. With increasing residence time, non-atmospheric noble gases, such as radiogenic ^3He , ^4He and ^{40}Ar , accumulate in the groundwater during flow. It is shown how the atmospheric and non-atmospheric noble gas components can be identified and separated out, and how their concentrations can be interpreted in terms of groundwater age and climatic conditions. A least squares method is presented that allows the concentrations of the various noble gas components and the corresponding recharge temperature to be calculated.

The methods described were applied, in conjunction with other hydrological methods, to two research projects being conducted in northern Switzerland.

(a) The riverbank infiltration of a young groundwater The groundwater in the shallow Linsental aquifer is recharged by infiltration from the river Töss. The noble gas temperatures in the boreholes close to the river vary seasonally. However, the average noble gas temperature of all samples lies close to the mean annual temperature of the

river. Groundwater residence times were determined by the $^3\text{H}/^3\text{He}$ dating method. The largest groundwater residence times of about 3 yr were found in the deeper part of the aquifer and remained almost constant between 1995 and 1997. In contrast, the age of the samples obtained near the river depends on the amount of recent infiltrated water and is small during times of active river discharge. Three parameters correlate strongly with the $^3\text{H}/^3\text{He}$ water age (1) CFCs (chlorofluorocarbons) excess, (2) radiogenic ^4He , and (3) oxygen consumption. These correlations can be interpreted either in terms of mixing or in terms of accumulation/consumption rates.

(b) Climate and groundwater recharge during the last glaciation in an ice-covered region The groundwater in the Glatt Valley is shown to have residence times of up to almost 30,000 yr. A multitracer study indicates that the atmosphere in central Europe cooled by at least 5°C during the last glacial period. The relationship between oxygen isotope ratios ($\delta^{18}\text{O}$) and recharge temperatures reconstructed for this period is similar to the present-day one if a shift in the $\delta^{18}\text{O}$ value of the oceans during the ice age is taken into account. This similarity suggests that the present-day $\delta^{18}\text{O}$ -temperature relationship can be used to reconstruct paleoclimate conditions in northern Switzerland. A gap in calculated groundwater age between about 17,000 and 25,000 yr BP indicates that during the last glacial maximum, local groundwater recharge was prevented by overlying glaciers.

Kurzfassung

Die Konzentrationen von gelösten Edelgasen und von Tritium im Grundwasser lassen auf jene physikalischen Bedingungen schliessen, die zur Zeit der Grundwasserneubildung herrschten und erlauben eine Abschätzung der Grundwasseraufenthaltszeit. In dieser Arbeit wird eine Methode für die Messung von Edelgas- und Tritiumkonzentrationen in Wasser beschrieben und die Theorie über die Anwendung von Edelgasen und Tritium als natürliche Tracer erläutert. Die beschriebenen Methoden werden auf zwei Fallstudien angewendet.

Die wichtigsten stabilen Isotope von Helium (He), Neon (Ne), Argon (Ar), Krypton (Kr) und Xenon (Xe) sowie das Wasserstoffisotop Tritium (^3H) wurden massenspektrometrisch analysiert. Die verwendete Messtechnik erlaubt die Bestimmung von Edelgaskonzentrationen und Isotopenverhältnissen mit einer Genauigkeit von mindestens 1%. Tritium wird routinemässig mit einer Nachweisgrenze von 0.1 TU und einer Genauigkeit von 2 bis 3% gemessen; beide Werte können durch Verwendung von grösseren Proben um eine Grössenordnung gesenkt werden.

Die Quellen von gelösten Edelgasen im Grundwasser und die zeitliche Entwicklung der Edelgaskonzentrationen wird diskutiert. Die Edelgaskonzentration im Grundwasser hängt nach der Grundwasserneubildung vor allem vom Lösungsgleichgewicht mit der Atmosphäre und einer zusätzlichen atmosphärischen Komponente, die als 'excess air' bezeichnet wird, ab. Mit zunehmender Aufenthaltszeit werden im Grundwasser nicht atmosphärische Edelgaskomponenten wie radiogenes ^3He , ^4He und ^{40}Ar akkumuliert. Es wird gezeigt, wie die atmosphärischen und nicht atmosphärischen Edelgaskomponenten identifiziert und voneinander separiert werden können, und wie die Konzentration dieser Komponenten im Hinblick auf das Grundwasseralter und die zur Zeit der Infiltration herrschenden klimatischen Bedingungen interpretiert werden können. Eine Optimierungsmethode, basierend auf der Methode der kleinsten Quadrate, erlaubt die Berechnung der verschiedenen Edelgaskomponenten und der Infiltrationstemperatur.

Die beschriebenen Methoden wurden in Verbindung mit anderen hydrologischen Verfahren in zwei Forschungsprojekten in der Nordschweiz angewendet.

(a) Flussinfiltration in ein junges Grundwasser Im Linsental wird das Grundwasser durch die Flusswasser-Infiltration aus der Töss gebildet. Die Edelgastemperaturen in den Bohrungen nahe der Töss schwanken saisonal, wobei die durchschnittliche Edelgastemperatur aller Proben mit der Jahresmitteltemperatur des Flusses übereinstimmt. Die Grundwasser Aufenthaltszeiten wurden mit der $^3\text{H}/^3\text{He}$ -Datierungsmethode bestimmt. Die grössten Aufenthaltszeiten von etwa 3 Jahren, welche zwischen 1995 und 1997 praktisch gleich blieben, finden sich im tieferen Bereich des Grundwassersystems. Im Gegensatz dazu ist das Alter der Proben aus dem Nahbereich des Flusses abhängig von der Menge frisch infiltrierten Wassers und jeweils klein bei hohem Flusswasserstand. Drei Parameter zeigen eine starke Korrelation mit dem $^3\text{H}/^3\text{He}$ -Wasseralter (1) Überschuss an FCKWs (Fluorchlorkohlenwasserstoffe), (2) radio-genes ^4He und (3) Sauerstoffzehrung. Diese Korrelationen werden alternativ entweder in bezug auf Mischung oder in bezug auf Akkumulation-/Zehrungsraten interpretiert.

(b) Klima und Grundwasserinfiltration während der letzten eiszeitlichen Vergletscherung. Das untersuchte Grundwassersystem im oberen Glattal zeigte Aufenthaltszeiten von bis zu 30'000 Jahren. Die beschriebene Studie beruht auf der Anwendung von verschiedensten hydrologischen Tracern und deutet auf eine atmosphärische Abkühlung in Zentraleuropa von mindestens 5°C während der letzten glazialen Periode hin. Die Beziehung zwischen den gemessenen stabilen Sauerstoffisotopenverhältnissen ($\delta^{18}\text{O}$) und den rekonstruierten Edelgastemperaturen über die betrachtete Periode ist vergleichbar mit der heutigen $\delta^{18}\text{O}$ -Temperatur Beziehung, falls die entsprechende Veränderung des ozeanischen $\delta^{18}\text{O}$ berücksichtigt wird. Diese Ähnlichkeit lässt darauf schliessen, dass die heutige $\delta^{18}\text{O}$ -Temperatur Beziehung für die Rekonstruktion des Paläoklimas in der Nordschweiz benutzt werden kann. Bei den berechneten Grundwasseralter wurden keine Werte zwischen 17'000 und 25'000 Jahren vor heute gefunden. Dies deutet darauf hin, dass die lokale Grundwasserneubildung während dem Maximum der letzten Eiszeit durch die darüberliegenden Gletscher verhindert wurde.

Notation

Subscripts

Symbol	Name	Unit
C_{air}	noble gas concentration in air	[ppm]
C_{crust}	noble gas component derived from the crust	[cm ³ STP/g]
C_{eq}	equilibrium concentration	[cm ³ STP/g]
C_{ex}	excess air component	[cm ³ STP/g]
C_{init}	initial noble gas concentration after groundwater infiltration	[cm ³ STP/g]
C_{mantle}	noble gas component derived from the mantle	[cm ³ STP/g]
C_{mod}	modeled noble gas concentration	[cm ³ STP/g]
C_{na}	non-atmospheric noble gas component	[cm ³ STP/g]
C_{terr}	terrigenic noble gas component	[cm ³ STP/g]
C_{tot}	total noble gas concentration in groundwater	[cm ³ STP/g]
C_{tri}	tritogenic component due to ³ H decay	[cm ³ STP/g]

Variables and constants

Symbol	Name	Unit/Value
α	isotopic fractionation factor for He	[-]
α_x	longitudinal dispersivity	[m]
$\exp(-\alpha)$	attenuation factor	[-]
β_i	Bunsen coefficient	[cm ³ STP/cm ³ _{water}]
δ^3He_{eq}	difference between ³ He/ ⁴ He ratios in solution and air	[%]
$\delta^{36}Ar_{eq}$	difference between ³⁶ Ar/ ⁴⁰ Ar ratios in solution and air	[%]
$\delta^{20}Ne_{eq}$	difference between ²⁰ Ne/ ²² Ne ratios in solution and air	[%]
ΔNe	excess air component expressed as relative Ne excess	[%]
θ	aquifer porosity	[cm ³ _{water} /cm ³ _{rock}]

Notation

θ'	volume ratio between pore and matrix	$[\text{cm}^3_{\text{water}}/\text{cm}^3_{\text{total}}]$
κ	permeability	$[\text{m}^2]$
κ_{20}	electrical conductivity of water at 20°C	$[\mu\text{S}/\text{cm}]$
λ	decay constant	$[\text{yr}^{-1}]$
Λ_i	transport efficiency of noble gas i from rock to water	$[-]$
ν_w	kinematic viscosity of water	$[\text{m}^2/\text{s}]$
σ	experimental 1 σ -error	$[\%], [\text{cm}^3\text{STP}/\text{g}]$
τ	residence time, groundwater age	$[\text{yr}]$
$\rho, \rho_{\text{water}}$	water density	$[\text{kg}/\text{L}], [\text{g}/\text{cm}^3]$
ρ_{rock}	rock density	$[\text{g}/\text{cm}^3_{\text{rock}}]$
χ^2	chi-square	$[-]$
Ω	attenuation number	$[-]$
A	volume of excess air	$[\text{cm}^3\text{STP}/\text{g}]$
A_i	accumulation rate of noble gas i in water	$[\text{cm}^3\text{STP}/(\text{g}_{\text{water}}\cdot\text{yr})]$
c_{NaCl}	NaCl molarity	$[\text{mol}/\text{L}]$
CA	volume of the slow calibration gas	$[\text{cm}^3\text{STP}]$
CS_i	signal of a slow calibration i	$[\text{A}], [\text{Hz}]$
D_{crust}	diffusion coefficient in the crust	$[\text{cm}^2/\text{s}]$
D_{eff}	diffusion coefficient in porous media	$[\text{cm}^2/\text{s}]$
D_i	diffusion coefficient of noble gas i in pure water	$[\text{cm}^2/\text{s}]$
D_x	dispersion coefficient in x-direction	$[\text{m}^2/\text{s}]$
d	thickness of the aquifer	$[\text{m}]$
dh/dx	hydraulic gradient	$[-]$
E_i	ratio between slow and fast calibration	$[-]$
e_s	saturation water vapor pressure	$[\text{atm}]$
F	flux of radiogenic noble gas	$[\text{cm}^3\text{STP}/(\text{cm}^2\cdot\text{yr})]$
FS_i	signal of a fast calibration before calibration i	$[\text{A}], [\text{Hz}]$
FS_j	signal of a fast calibration before sample j	$[\text{A}], [\text{Hz}]$
G	production rate per unit volume	$[\text{cm}^3\text{STP}/(\text{cm}^3\cdot\text{yr})]$
g	acceleration of gravity	$9.81 \text{ m}/\text{s}^2$
${}^3\text{H}$	tritium concentration	$[\text{TU}]$
${}^3\text{He}_{\text{tr}}$	tritogenic ${}^3\text{He}$ component	$[\text{cm}^3\text{STP}/\text{g}], [\text{TU}]$
H	recharge altitude	$[\text{m}]$
H_0	scale height	$[\text{m}]$
h	hydraulic head	$[\text{m}]$
K	hydraulic conductivity	$[\text{m}/\text{s}]$

Notation

K_i	Setchenow coefficient for salinity	[L/mol]
k	Henry coefficient	[atm]
M_{NaCl}	molar mass of NaCl	58.443 g/mol
M_w	molar mass of water	18.016 g/mol
NGT	noble gas temperature	[°C]
P	(atmospheric) pressure	[atm]
P_0	standard pressure	1 atm = 1013.25 mbar
P_S	atmospheric pressure at sea level	[atm]
p	probability of the model	[-]
Pe	Peclet number	[-]
P_i	production rate of noble gas i in rock	[cm ³ STP/(g _{rock} ·yr)]
Q	non-atmospheric production rate for noble gases	[cm ³ STP/(g·s)]
q	Darcy flux, Darcy velocity	[m/s]
r	correlation coefficient	[-]
R	re-equilibration parameter	[-]
R_{air}	³ He/ ⁴ He ratio in air	1.384·10 ⁻⁶
R_{eq}	³ He/ ⁴ He ratio in solution at equilibrium	[-]
R_{gas}	universal gas constant	82.058 cm ³ atm/(mol·K)
S	salinity	[%]
SA_j	noble gas volume in sample j	[cm ³ STP]
SS_j	signal of sample j	[A], [Hz]
STP	standard temperature and pressure condition	0°C, 1 atm
T	water temperature	[K], [°C]
T_0	standard temperature	0°C = 273.15 K
T_a	annual amplitude of soil temperature	[°C]
T_{air}	air temperature	[°C]
T_s	soil temperature	[°C]
$T_{1/2}$	half-life	[yr]
t	time	[yr]
t_0	time of infiltration	[yr]
Th	thorium concentration in rock	[μg/g]
U	uranium concentration in rock	[μg/g]
V_0	molar volume of an ideal gas	22414 cm ³ /mol
V_i	molar volume of noble gas i	[cm ³ /mol]
v_x	effective groundwater velocity	[m/s]
x	distance	[m]

Notation

x_0	distance from the recharge area	[m]
x_i	mole fraction of noble gas i in equilibrium	[-]
z	depth below surface	[m]
\bar{z}	penetration depth of seasonal temperature variation	[m]
z_i	volume fraction of noble gas i	[-]

Introduction

1.1 Groundwater as a freshwater resource

Groundwater constitutes by far the largest reservoir of liquid freshwater on Earth. Less than 2% of the total freshwater consists of surface water in lakes, rivers and man-made reservoirs (see Table 1.1), making groundwater the key global freshwater resource. Today, however, man is threatening the quality of groundwater and mismanaging its available quantity. Although groundwater is normally less polluted than surface water, it can be easily contaminated, for example by the infiltration of industrial waste products and by pesticides and herbicides from agriculture. Once groundwater is polluted, recovery is very slow due to its long residence time and slow renewal, and cleaning up contaminated aquifers is usually extremely difficult and expensive, or even unfeasible.

In regions where groundwater recharge rates are low and where groundwater is often the only available freshwater resource, groundwater is frequently over-utilized. Over-exploitation of groundwater often results in a significant lowering of the local water table, allowing the encroachment of saline water from the sea or from deeper aquifers. The scarcity of groundwater, and its pollution, will be even more critical in the near future because of steadily increasing demand for high-quality fresh water due to population growth and rising standards of living. Consequently, it is evident that the sustainable utilization of groundwater is a matter of the greatest urgency. Viewing groundwater as a water resource, sustainability means that pumping be limited to the rate of groundwater recharge and that water quality be preserved. To conform with these guidelines, detailed knowledge of groundwater systems and their dynamics is indispensable.

Table 1.1: Global water reservoirs (Mather, 1984).

Category	Storage (10^3 km^3)	% of total	% of liquid freshwater
Total global volume of water	1,384,000	100	
Oceans and salt water lakes	1,350,000	97.5	
Glaciers and ice caps	25,000	1.8	
Liquid fresh water (details see below)	9,000	0.65	100
Groundwater	8,800	0.64	98.3
Freshwater lakes	125	0.009	1.4
Soil moisture	22	0.001	0.25
Man-made reservoirs	2.5	-	0.03
Rivers	1.7	-	0.02

The methods employed here, all of which are based on environmental tracers, are useful for quantifying the natural flow dynamics of groundwater, i.e. flow velocities, flow directions, residence times and recharge rates. Knowledge of these parameters is usually scarce or vague, although these quantities yield valuable information for groundwater management and therefore help in assessing the consequences of anthropogenic intervention. If the methods presented here are combined, for example, with knowledge on the origin and behavior of groundwater contaminants, they can provide a quantitative framework for the assessment of all aspects of groundwater quality and quantity. Moreover, they enable the calibration and verification of groundwater models that are themselves effective tools in groundwater studies.

As an example, these new approaches of tracer-based groundwater management were applied to a young groundwater system in northern Switzerland which is used for the local water supply.

1.2 Old groundwater as archive of past climate

Studies on groundwater yield information not only on groundwater dynamics, but also on the environmental conditions under which the groundwater infiltrated. This makes the investigation of paleogroundwaters especially interesting, since these can be used as archives of past climate. Questions of interest include: What was the ambient temperature during the last glacial period as compared to the present conditions? What temperatures prevailed during the inter-glacial periods? And how abrupt were the climate changes?

Answering these questions help in understanding global climate dynamics and are of particular interest for assessing possible climate changes induced by anthropogenic activities such as the release of greenhouse gases. Furthermore, a more complete global set of paleoclimate records is fundamental for the calibration of global climate models employed to analyze the development of the climate in the future.

Since the basic work of Münnich and Vogel (1962) and Mazor (1972), stable isotope ratios and noble gas concentrations in groundwater have been used to estimate paleotemperatures during the last glacial period. In addition to paleotemperature reconstructions, the relationship between calculated recharge temperatures and stable isotope ratios in a paleogroundwater can help in the interpretation of stable isotope data from other continental climate archives (such as lake sediments, ice cores and speleotherms).

Up until now, paleogroundwater studies have been conducted primarily in permanently ice-free regions. In contrast, the paleogroundwater studied in this work has its recharge area in a region that was temporarily ice-covered during the last glaciation period. It was therefore uncertain whether the noble gas methods could be validly applied in such a region to reconstruct paleoclimate. Assuming this can be shown to be so, however, the reaction of the groundwater system to ice cover in the infiltration area can be additionally investigated.

1.3 Why noble gases?

This work focuses mainly on the interpretation of noble gas concentrations in groundwater with regard to groundwater dating and the reconstruction of recharge conditions. The use of noble gases as hydrological tracers has a number of advantages:

(i) Noble gases are not involved in any chemical or biological activity under natural conditions. Relatively simple and well-known physical processes, such as diffusion, partition between different phases, and radiogenic production, govern their behavior in nature. Hence, noble gases are ideal to study and trace these physical processes.

(ii) Noble gases enter groundwater from several sources: from the atmosphere by gas exchange during infiltration; from non-atmospheric sources such as aquifer rocks by the flushing of radiogenic products; from the water itself via the radioactive decay of tritium; and from the earth mantle or crust. These different sources can often be identified based on the elemental signatures of the noble gases. If the atmospheric and non-atmospheric components can be separated out, determination of the latter, which continuously accumulate during groundwater flow, can allow the residence time of the groundwater to be estimated.

(iii) The initial concentrations of atmospheric noble gases in groundwater are mainly controlled by the ambient temperature and the altitude (i.e., the atmospheric pressure) of the recharge area. Once groundwater has reached the saturated zone, no further addition of atmospheric gases is possible. With the exception of the processes prevailing during groundwater recharge, groundwater can be regarded as a closed system with respect to atmospheric gases. This allows the physical conditions in general, and the temperature in particular, at which the groundwater infiltrated to be calculated from the atmospheric noble gas concentrations.

1.4 Outline

This thesis is organized as follows. In **chapter 2** the different origins of the noble gases in groundwater is discussed. After groundwater infiltration, the concentration of noble gases in groundwater depends mainly on the atmospheric equilibrium concentration (section 2.2.) modified by an additional atmospheric component known as 'excess air' (section 2.3). The reasons for the presence of this excess air component in groundwater are not yet completely understood. However, the problem of the generation and composition of the excess air component is crucial to any interpretation of the results of the noble gas thermometer, and to all dating methods based on gaseous tracers. During groundwater flow, the noble gas concentrations which pertained during recharge can be changed by the addition of non-atmospheric noble gases (section 2.4).

Chapter 3 outlines the design and set-up of the mass spectrometric system used for the analysis of the noble gas isotopes and tritium in water samples. The performance and precision of a typical measurement is discussed. To verify the reliability of the noble gas measurements, samples equilibrated under controlled conditions at different temperatures are compared to solubility data. This chapter has been submitted as a paper to *Environmental Science & Technology* (Beyerle et al., 1999b).

In **chapter 4**, a short description is given of the most relevant applications that make use of stable noble gas isotopes and tritium in groundwater, and of their limitations. It is shown that the measurement of the five noble gases helium (He), neon (Ne), argon (Ar), krypton (Kr), and xenon (Xe) allows the temperature at which groundwater last equilibrated with the atmosphere to be reconstructed (section 4.1). In special cases it is also possible to identify some additional parameters which control the solubility of noble gases, such as for example the altitude of the recharge area. In section 4.2, the determination of groundwater residence times is discussed. In young groundwater (water age < 50 yr) tritium (^3H) in combination with its decay product helium-3 (^3He) allows water ages to be determined with a high degree of accuracy (section 4.2.1). In old groundwater, the accumulation of radiogenic noble gases (^4He , ^{40}Ar , and ^{21}Ne) offers the possibility to obtain estimates of groundwater residence times of up to millions of years (section 4.2.2). Knowing the age of groundwater is central to

groundwater management and provides the time scale essential for the use of groundwaters as paleoclimate archives. The last section discusses how the groundwater age and the calculated noble gas temperature are altered by dispersion and mixing (section 4.3).

The last two chapters concern case studies on two aquifers located in northern Switzerland. The first of these deals with a young alluvial groundwater system with a residence time of a few years, whereas the second focuses on a paleogroundwater system with a maximum groundwater age of almost 30,000 yr. At both sites, the noble gas methods were applied in combination with other hydrological methods.

Chapter 5 describes a project in which noble gases, tritium, and CFCs (chlorofluorocarbons) are used to study the infiltration of river water into a shallow aquifer used as a source of drinking water. This project was carried out as a part of a larger interdisciplinary research program directed at evaluating the possible impacts of a planned natural rehabilitation of a Swiss perialpine river, the Töss. This chapter has been published in the *Journal of Hydrology* (Beyerle et al., 1999a).

Chapter 6 concentrates on a paleogroundwater system that provides information about climatic and recharge conditions during the last glacial period in an ice-covered area. It is shown that groundwater recharge was prevented during the last glaciation maximum by overlying glaciers. This chapter has been published in *Science* (Beyerle et al., 1998b).

Noble gases in groundwater

The concentrations of noble gases in groundwater are a result of different physical processes. First, at recharge, water is in gas exchange with air during its infiltration and dissolves atmospheric noble gases. The initial concentrations are mainly determined by the thermodynamic equilibrium, but are normally elevated due to a ubiquitous excess of atmospheric gases called excess air. Later, the concentration of noble gases in groundwater can be altered by molecular diffusion, groundwater dispersion and accumulation of non-atmospheric noble gases from the aquifer rocks or deeper strata. This chapter focuses on gas exchange during infiltration and on non-atmospheric sources of noble gases in groundwater. By definition, the total concentration C_i^{tot} of noble gas i dissolved in groundwater can be described as

$$C_i^{tot} = C_i^{eq} + C_i^{ex} + C_i^{na} \quad [\text{cm}^3\text{STP/g}] \quad (2.1)$$

where C_i^{eq} is the equilibrium component (section 2.2), C_i^{ex} is the excess air component (section 2.3) and C_i^{na} represents any non-atmospheric noble gas component (section 2.4). The effect of dispersion within the aquifer and mixing of different groundwater components on the noble gas concentration will be discussed in section 4.3.

2.1 Atmospheric noble gases

The atmosphere is the major reservoir of terrestrial noble gases. There are documented reasons (Mamyrin, 1970; Ozima and Podosek, 1983; Oliver, 1984) to assume that air has an uniform composition that is generally constant over time (Table 2.1 and 2.2). The atmospheric production of noble gases with exception of some rare isotopes (e.g., ^3He , ^{37}Ar , ^{85}Kr) is not relevant compared to the total amount in air.

In contrast to Ne, Ar, Kr, and Xe the light noble gas isotopes ^3He and ^4He can relative easily escape from the terrestrial reservoir into space. On time scales less than millions of years the atmospheric concentration of helium represents an approximate balance between the continuous input from the interior of the earth (see section 2.4), and escape from the upper atmosphere into space. It has been firmly established that the atmospheric helium volume fraction below heights of 100 km is constant with a volumetric concentration of 5.24 ppm (Ozima and Podosek, 1983) and a constant $^3\text{He}/^4\text{He}$ ratio of $1.384 \cdot 10^{-6}$ (Clarke et al., 1976).

Compared to helium, neon has a higher concentration of 18.18 ppm in air, with the natural isotopic abundances being 90.5% for ^{20}Ne , 0.268% for ^{21}Ne and 9.23% for ^{22}Ne . The most abundant Ne isotope ^{20}Ne has for most practical purpose no significant radiogenic subsurface sources. Although ^{21}Ne and ^{22}Ne are produced in the crust, this source that is much smaller than for ^4He (Kennedy et al., 1990) is negligible compared to the large quantities found in the atmosphere.

The most frequent noble gas in the atmosphere is Ar (9340 ppm). The dominant isotopes are ^{40}Ar , ^{38}Ar , and ^{36}Ar . ^{40}Ar accounts for 99.6% of the total amount of Ar in air and is largely the result of the release of ^{40}Ar from the decay of ^{40}K in solid Earth. The atmospheric $^{40}\text{Ar}/^{36}\text{Ar}$ ratio of 296.0 ± 0.5 was originally determined by Nier (1950). However, the value 295.5 came into widespread use. Steiger and Jäger (1977) have recommended its adoption as a convention for geochronology. As listed in Table 2.1, the noble gases Kr and Xe have several dominant isotopes in air summing up to the total concentrations of 1.14 ppm for Kr and 0.087 ppm for Xe.

Noble Gases in Groundwater

Table 2.1: Concentrations and isotopic abundances of noble gases in dry air (Ozima and Podosek, 1983).

Noble gas	Volume fraction z_i	Isotope	Abundance (%)	Noble gas	Volume fraction z_i	Isotope	Abundance (%)
He	$(5.24 \pm 0.05) \cdot 10^{-6}$	^3He	0.001384 ⁽¹⁾	Xe	$(8.7 \pm 0.1) \cdot 10^{-8}$	^{124}Xe	0.0951
		^4He	~ 100			^{126}Xe	0.0887
Ne	$(1.818 \pm 0.004) \cdot 10^{-5}$	^{20}Ne	90.50	^{128}Xe		1.919	
		^{21}Ne	0.268	^{129}Xe		26.44	
		^{22}Ne	9.23	^{130}Xe		4.070	
Ar	$(9.34 \pm 0.01) \cdot 10^{-3}$	^{36}Ar	0.3371 ⁽²⁾	^{131}Xe		21.22	
		^{38}Ar	0.0632	^{132}Xe		26.89	
		^{40}Ar	99.60	^{134}Xe		10.43	
Kr	$(1.14 \pm 0.01) \cdot 10^{-6}$	^{78}Kr	0.347	^{136}Xe		8.857	
		^{80}Kr	2.257				
		^{82}Kr	11.52				
		^{83}Kr	11.48				
		^{84}Kr	57.00				
		^{86}Kr	17.40				

⁽¹⁾ The $^3\text{He}/^4\text{He}$ ratio of $1.384 \cdot 10^{-6}$ is taken from Clarke et al. (1976).

⁽²⁾ The $^{40}\text{Ar}/^{36}\text{Ar}$ ratio of 295.5 was recommended by Steiger and Jäger (1977) and is used as a convention for geochronology.

Table 2.2: Most frequently used atmospheric noble gas ratios calculated from Table 2.1.

Isotopes	Ratio	Ratio x_i/y_j	x_i				
			He	Ne	Ar	Kr	Xe
$^3\text{He}/^4\text{He}$	$1.384 \cdot 10^{-6}$	He	1	3.47	$1.78 \cdot 10^3$	0.218	0.0166
$^3\text{He}/^{20}\text{Ne}$	$4.408 \cdot 10^{-7}$	Ne	0.288	1	514	0.0627	$4.79 \cdot 10^{-3}$
$^4\text{He}/^{20}\text{Ne}$	0.3185	y_j Ar	$5.61 \cdot 10^{-4}$	$1.95 \cdot 10^{-3}$	1	$1.22 \cdot 10^{-4}$	$9.31 \cdot 10^{-6}$
$^{20}\text{Ne}/^{22}\text{Ne}$	9.80	Kr	4.60	15.9	$8.19 \cdot 10^3$	1	0.0763
$^{40}\text{Ar}/^{36}\text{Ar}$	295.5	Xe	60.2	209	$1.07 \cdot 10^5$	13.1	1

2.2 Equilibrium concentration in water

The most important source of noble gases in natural waters is the solution of atmospheric gases according to Henry's law:

$$p_i = k_i(T, S, \dots) \cdot x_i \quad [\text{atm}] \quad (2.2)$$

Thus, the equilibrium concentration of the dissolved gas i in the solution (here expressed as mole fraction x_i) is proportional to its partial pressure p_i in the gas phase. The proportionality is given by the Henry coefficient k_i which depends for noble gases to large extend mainly on temperature and salinity. In the literature, common expressions for the solubilities are

- (i) the Henry coefficient k (in atm), as in Equation (2.2);
- (ii) the mole fraction x (in moles of gas per moles of solution) in equilibrium with a gas phase at a specified partial pressure (normally 1 atm);
- (iii) the Bunsen coefficient β , (in $\text{cm}^3\text{STP}/\text{cm}^3_{\text{water}}$), which is defined as the volume of gas measured at STP (Standard Temperature: 0°C , and Pressure: 1 atm) absorbed per unit volume of solution, when the partial pressure of the gas is 1 atm;
- (iv) the atmospheric equilibrium concentration C_{eq} , (in $\text{cm}^3\text{STP}/\text{g}_{\text{water}}$), which is normally given as the gas volume (at STP) per unit weight of solution in equilibrium with moist air at a total atmospheric pressure of 1 atm.

Assuming an ideal gas, cm^3STP can be converted to moles or atoms according to

$$1 \text{ cm}^3\text{STP} = \frac{1}{V_0} \text{ mol} = 4.4615 \cdot 10^{-5} \text{ mol} = 2.6868 \cdot 10^{19} \text{ atoms} \quad (2.3)$$

The standard molar volume V_0 of an ideal gas is given in Equation (2.8).

Since measured noble gas concentrations in water are usually reported in $\text{cm}^3\text{STP}/\text{g}$, and because it is reasonable to assume that equilibration occurred with moist (water vapor saturated) air, the last form of gas solubilities is the most convenient for practice. Atmospheric equilibrium concentrations of this form have been reported for

He, Ne, Ar, and Kr by Weiss (1970b, 1971), and Weiss and Kyser (1978), both for fresh water and seawater. The corresponding values for He and Ne are commonly used in oceanographic (e.g., Jenkins, 1987; Schlosser et al., 1990), limnological (e.g., Torgersen et al., 1977; Aeschbach-Hertig et al., 1996) and hydrological (e.g., Solomon et al., 1992; Stute et al., 1997) applications of the $^3\text{H}/^3\text{He}$ dating method.

Benson and Krause (1976) gave Henry coefficients k_i for all noble gases in pure water. They claimed a very high precision of their values (better than $\pm 0.2\%$). Critical evaluations of the literature on noble gas solubilities were published as part of the IUPAC solubility data series by Clever (1979a, 1979b, 1980). These compilations used the results of the above mentioned studies and others to derive fit equations for the mole fraction solubilities in pure water. In Appendix A1 the coefficients and constants are listed that were used to calculate the different noble gas solubilities.

In addition to pressure and temperature, the equilibrium concentration depends on the salinity of the water. The Setchenow relation can describe the effect of salinity:

$$\ln\left(\frac{\beta_i(T,0)}{\beta_i(T,S)}\right) = K_i \text{ (L/mol)} \cdot c_{\text{NaCl}} \text{ (mol/L)} \quad [-] \quad (2.4)$$

where K_i is the Setchenow or salting coefficient of gas i and c_{NaCl} the NaCl molarity. Empirical salting coefficients for all noble gases in NaCl solutions were reported by Smith and Kennedy (1983) (see Appendix A1). These data can be combined with the fresh water solubilities of Benson and Krause (1976) and Clever (1979a, 1979b, 1980) to obtain complete sets of expressions for the noble gas solubilities.

In applied studies involving all five noble gases (e.g., Stute and Schlosser, 1993), the data of Weiss (1970b, 1971) for He, Ne, and Ar have usually been complemented by the solubilities of Kr and Xe as given by Clever (1979b) paired with the salt dependency of Smith and Kennedy (1983).

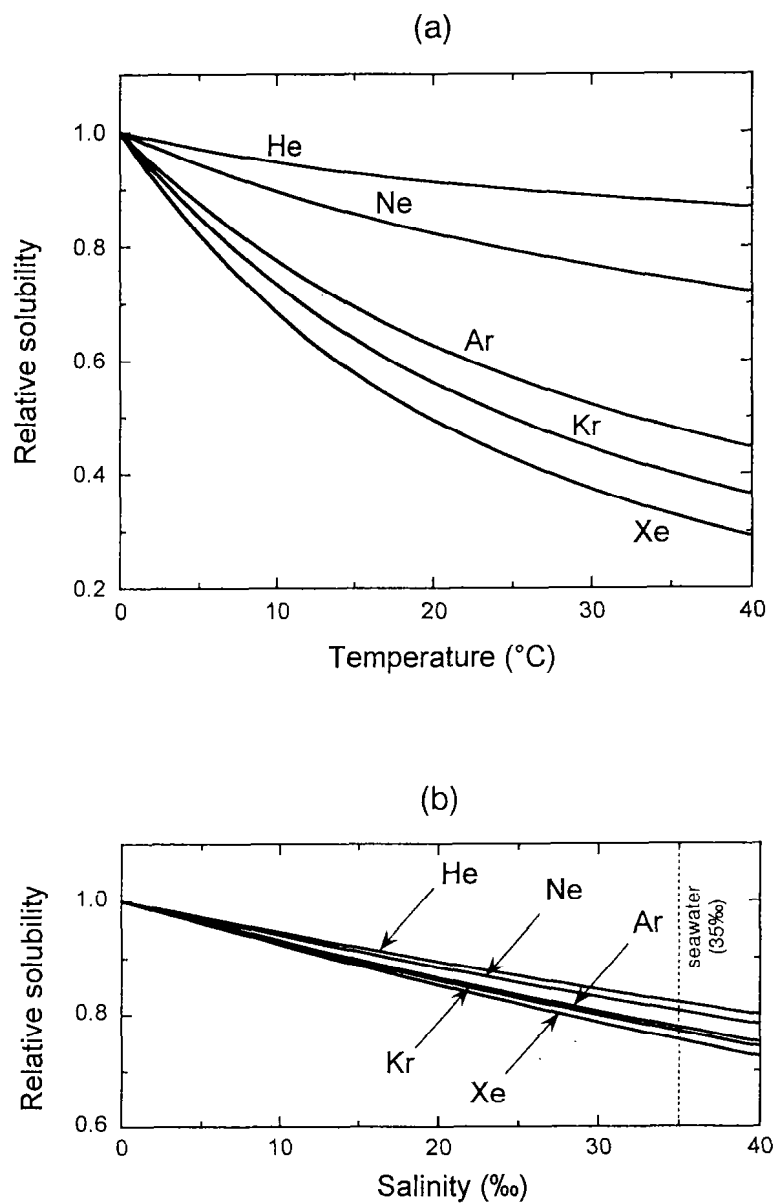


Figure 2.1: *Weiss solubilities* for noble gases (a) relative to water at 0°C as a function of temperature T (salinity $S = 0$), and (b) relative to pure water as a function of salinity S (temperature $T = 10^\circ\text{C}$). For the definition of the *Weiss solubilities* see text.

To compare noble gas solubilities three different sets of solubilities were calculated (Figure 2.1 and Figure 2.2):

- (i) the *Weiss solubilities*: combining the data of Weiss (1970b, 1971) and Weiss and Kyser (1978) for He, Ne, Ar, and Kr, with those of Clever (1979b) and Smith and Kennedy (1983) for Xe;
- (ii) the *Clever solubilities*: Clever (1979a, 1979b, 1980) with Smith and Kennedy (1983);
- (iii) the *Benson solubilities*: Benson and Krause (1976) with Smith and Kennedy (1983).

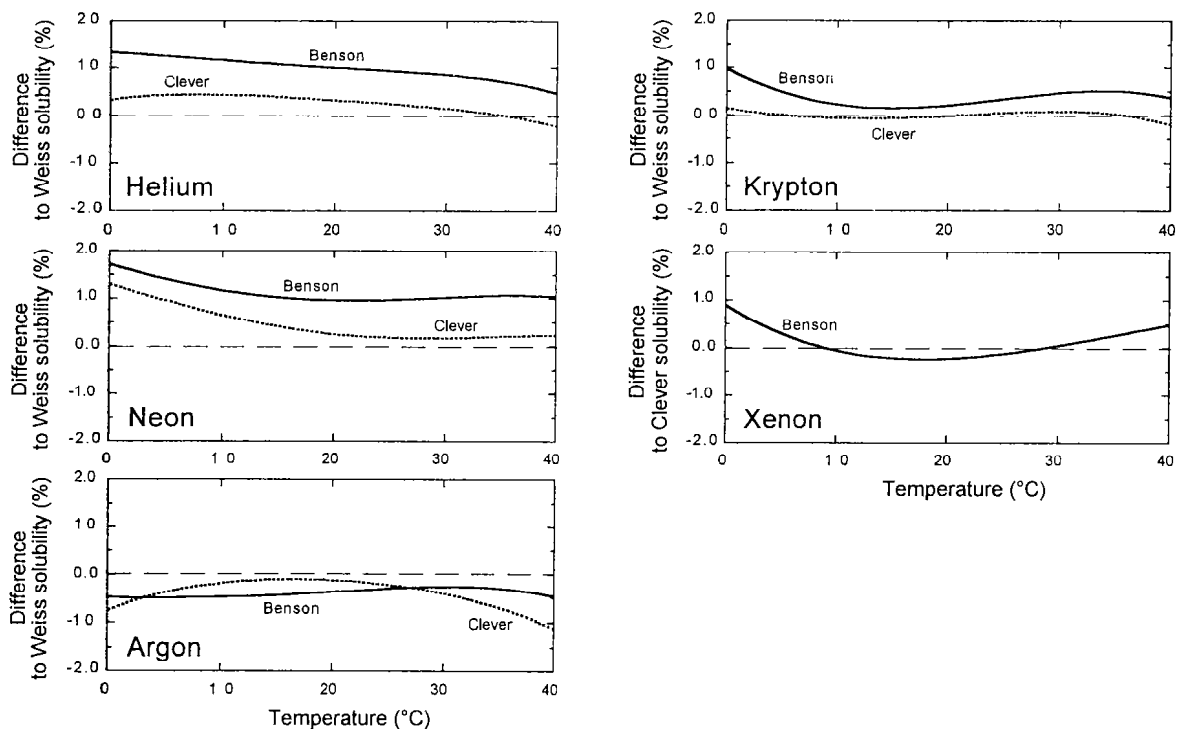


Figure 2.2: Differences in percent between noble gas solubility data in pure water ($S = 0$). The *Weiss solubilities* are compared with the *Clever solubilities* and *Benson solubilities*, respectively. For the definition of solubility sets see text. Between 0°C and 40°C the difference between the various solubilities hardly exceeds 1%.

For the guarantee of reproducibility, in the following the steps taken to calculate equilibrium concentrations $C_{eq}(T,S,P)$ from the literature data are discussed in some detail.

A first problem arises from the different parameterizations of salinity in the literature. Weiss (1970b, 1971) and Weiss and Kyser (1978) use seawater salinity S in g/kg (or ‰), whereas Smith and Kennedy (1983) use the molar concentration c_{NaCl} of pure NaCl solutions. The two parameters S and c_{NaCl} can be related by equating the mass of salt per unit volume:

$$c_{NaCl} = \frac{S \cdot \rho(T,S)}{M_{NaCl}} \quad [\text{mol/L}] \quad (2.5)$$

where M_{NaCl} is the molar mass of NaCl (58.443 g/mol) and $\rho(T,S)$ is the density of a sea-salt solution in kg/L (Equations (A.5) and (A.6) in Appendix A1; Gill, 1982). Justification for this simple approach is given by the results of Weiss and Price (1989), who showed that gas solubilities in Dead Sea water could be estimated from those in seawater with an error of less than 10% by assuming an equal salting-out effect by an equal mass of dissolved salt. In fresh waters, salinity may be estimated from κ_{20} , the electrical conductivity at 20°C, according to the methods outlined by Wüest et al. (1996). For small salinities any rough approximation of S is sufficient. Therefore the following relation established for CaHCO₃-dominated waters is commonly used:

$$S (\text{‰}) = 0.87 \cdot 10^{-3} \cdot \kappa_{20} (\mu\text{S/cm}) \quad (2.6)$$

In lakes κ_{20} rarely exceeds 500 $\mu\text{S/cm}$, thus S is below 0.5‰, and the influence of S on the solubilities is less than 0.5%. In chemically evolved groundwaters κ_{20} may be substantially higher, but relevant for the solution of noble gases is the salinity at the time of infiltration, which is usually close to zero.

For the conversion of units, the literature values for k_i in pure water are converted to Bunsen coefficients β_i by:

$$\beta_i(T,0) = \frac{\rho(T,0) \cdot V_i}{M_w} \cdot \frac{P_0}{k_i} \quad [\text{cm}^3 \text{STP/cm}^3_{\text{water}}] \quad (2.7)$$

where $\rho(T,0)$ is the density of pure water, M_w its molar mass (18.016 g/mol), P_0 is the reference pressure at which x_i is given (normally 1 atm), and V_i is the molar volume of

the gas i (in $\text{cm}^3\text{gas/mol}$). For an ideal gas the standard molar volume V_0 is given by the ideal gas law, according to

$$V_0 = \frac{R_{gas} \cdot T_0}{P_0} = 22414 \text{ cm}^3/\text{mol} \quad (2.8)$$

$$\text{with } R_{gas} = 82.058 \text{ cm}^3 \cdot \text{atm}/(\text{mol} \cdot \text{K})$$

$$T_0 = 273.15 \text{ K (0}^\circ\text{C)}$$

$$P_0 = 1 \text{ atm}$$

However, in this work real gas not ideal values of V_i are used (see Table A.5 in Appendix A1). The real volumes are calculated from the van der Waals equation of state with constants as given by Lide (1994). These real gas corrections are of minor importance in comparison to experimental uncertainties, even for Kr (0.3%) and Xe (0.6%).

In a next step, the salting coefficients K_i of Smith and Kennedy (1983) and Equation (2.4) are used to introduce the salt dependence:

$$\beta_i(T, S) = \beta_i(T, 0) \cdot e^{-K_i \cdot c_{NaCl}(S)} \quad [\text{cm}^3\text{STP}/\text{cm}^3_{\text{water}}] \quad (2.9)$$

At last, the Bunsen coefficient β_i of noble gas i can be converted to a moist air equilibrium concentration C_i^{eq} at a total atmospheric pressure P as follow:

$$C_i^{eq}(T, S, P) = \frac{\beta_i(T, S)}{\rho(T, S)} \frac{(P - e_s(T))}{P_0} z_i \quad [\text{cm}^3\text{STP}/\text{g}_{\text{water}}] \quad (2.10)$$

where z_i is the volume fraction of gas i in dry air (Table 2.1), P_0 is the reference pressure at which β is given (1 atm), and $e_s(T)$ is the saturation water vapor pressure as a function of T , e.g., Gill (1982):

$$e_s(T) = \frac{10^{\frac{a_1 + a_2 \cdot T}{1 + b \cdot T}}}{1013.25} \quad [\text{atm}] \quad (2.11)$$

$$\text{with } a_1 = 0.7859 ; \quad a_2 = 0.03477 ; \quad b = 0.00412$$

Equations (2.9) and (2.10) can be combined to give:

$$C_i^{eq}(T, S, P) = \frac{1}{k_i} \frac{\rho(T, 0)}{\rho(T, S)} \frac{V_i}{M_w} (P - e_s(T)) z_i \cdot e^{-K_i \cdot c_{NaCl}(S)} \quad [\text{cm}^3\text{STP/g}] \quad (2.12)$$

Equations (2.2) and (2.12) handle the conversion from Henry constants or mole fraction solubilities to atmospheric equilibrium concentrations. The solubilities of Weiss are already in this form, but there is a caveat. Because of the water vapor pressure, the moist air equilibrium concentrations are not simply proportional to P . The correct pressure dependence is:

$$C_i^{eq}(T, S, P) = C_i^{eq}(T, S, P_0) \frac{(P - e_s(T))}{(P_0 - e_s(T))} \quad [\text{cm}^3\text{STP/g}] \quad (2.13)$$

Sometimes in the literature it seems that the water vapor correction is forgotten.

The atmospheric pressure P in Equations (2.12) and (2.13) is related to the altitude H of the water surface. For groundwaters systems, H is reasonable approximated given by the altitude of the recharge area. The atmospheric pressure P can be calculated by a barometric altitude formula of the form:

$$P = P_S \cdot \exp\left(-\frac{H}{H_0}\right) \quad [\text{atm}] \quad (2.14)$$

where P_S is the pressure at sea level and H_0 is the typical scale height in meter for a given meteorological situation. This conversion is not unique, and should be adapted to local conditions, since H_0 is a function of temperature and humidity (e.g., Gill, 1982) and P_S can also deviate locally from global average. For instance, in northern Switzerland, the average atmospheric pressure reduced to sea level is 1.004 atm (Schüepp and Gisler, 1980). If no regional altitude-pressure function is known, the constant values $P_S = 1$ atm and $H_0 = 8300$ m were used in Equation (2.14). The pressure as function of the altitude of such a standard atmosphere is plotted in Figure 2.3. As approximation, an increase of 100 m in the altitude results in a 1.2% smaller equilibrium noble gas concentration.

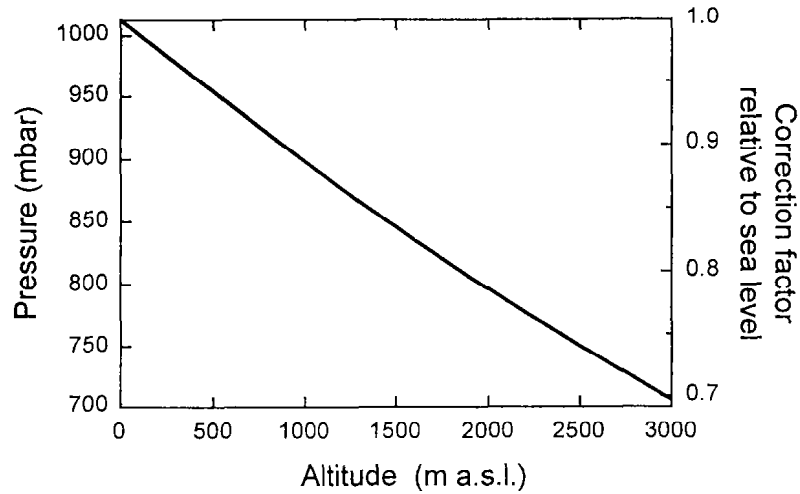


Figure 2.3: Atmospheric pressure variation as a function of altitude according to Equation (2.14) ($P_s = 1 \text{ atm} = 1013.25 \text{ mbar}$, $H_0 = 8300 \text{ m}$). Correction factors on the right axis serve to convert solubility values at sea level to values at given altitude (multiplying by the factor).

2.2.1 Isotopic fractionation of noble gases

The solubility of the chemically inert noble gases is mainly depending on the size of their electron shell and therefore light noble gases are less soluble than heavier noble gases (Figure 2.1). Similarly but to much lesser extend, fractionation should also influence the solubility of different isotopes of a noble gas. Besides the helium isotopes ^3He and ^4He , hardly any information is available for noble gas isotope fractionation in equilibrated water.

The isotopic fractionation factor for He, α is defined as (Benson and Krause, 1980a):

$$\alpha \equiv \frac{(^3\text{He}/^4\text{He})_{eq}}{(^3\text{He}/^4\text{He})_{air}} = \frac{R_{eq}}{R_{air}} \quad [-] \quad (2.15)$$

The difference between the $^3\text{He}/^4\text{He}$ ratios in solution and air at equilibrium can directly be expressed in terms of α :

$$\delta^3\text{He}_{eq} (\%) = \frac{R_{eq} - R_{air}}{R_{air}} \cdot 100 = \left(\frac{R_{eq}}{R_{air}} - 1 \right) \cdot 100 = (\alpha - 1) \cdot 100 \quad [\%] \quad (2.16)$$

Isotopic fractionation of He were determined by Weiss (1970a), Benson and Krause (1980a), Top et al. (1987), and Butzin (1994). In this work the most precise measurements of Benson and Krause (1980a), which were later confirmed by Top et al. (1987) and Butzin (1994), are used. The $\delta^3\text{He}_{eq}$ and the corresponding R_{eq} are plotted in Figure 2.4 and show an almost linear increase between 0 and 40°C. As measured by Benson and Krause (1980a), the effect of the salinity to the isotopic fraction is very small.

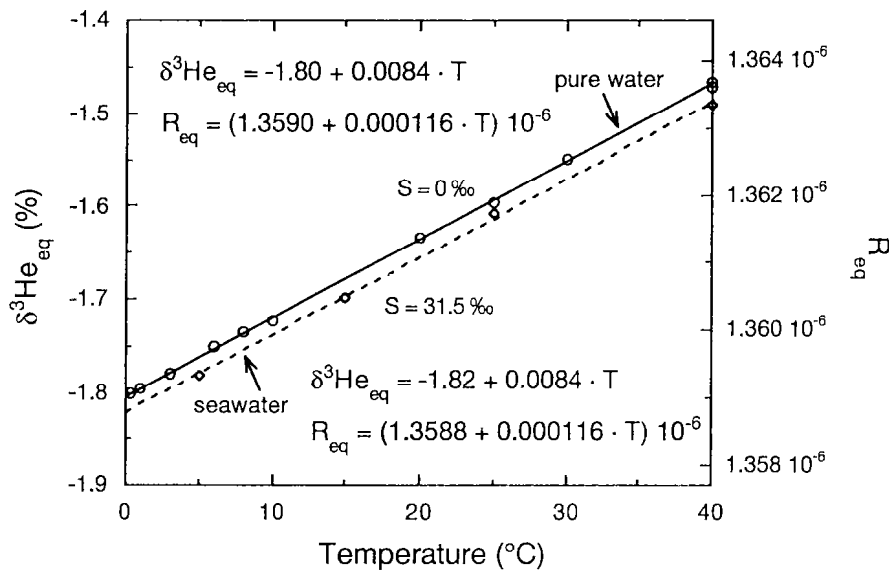


Figure 2.4: Isotopic fraction of He in pure water and seawater. R_{eq} is the ratio between ^3He and ^4He isotopes in solution ($R_{air} = 1.384 \cdot 10^{-6}$) and $\delta^3\text{He}_{eq}$ is the difference between R_{eq} and R_{air} relative to R_{air} . The equations are the result of linear fits between 0 and 40°C to the data of Benson and Krause (1980a).

Aside from the helium isotopes hardly any information is available for noble gas isotope fractionation in equilibrium. Aeschbach-Hertig (1994) estimated on the basis of 240 lake samples that the fractionation between ^{20}Ne and ^{22}Ne ($\delta^{20}\text{Ne}_{eq}$) in equilibrium with the atmosphere is about -1‰. This value is in the same range as the fractionation of oxygen molecules ($^{32}\text{O}_2/^{34}\text{O}_2$) of about -0.8‰ (Benson and Krause, 1980b). As the relative mass difference for ^{36}Ar and ^{40}Ar is as large as for ^{20}Ne and ^{22}Ne , a similar large fractionation can also be expected for Ar. Estimations of the Ne and Ar fractionation factors are given in chapter 3.3.3.

2.3 Excess air

In addition to the equilibrium concentrations $C_{eq}(T,S,P)$, an excess of atmospheric noble gases is commonly present in groundwaters (Heaton and Vogel, 1981). The elemental composition of the excess air component is usually assumed to be atmospheric. It can be described by the volume A of dry air injected per g of water (in $\text{cm}^3\text{STP/g}$):

$$C_i^{ex} = A \cdot z_i \quad [\text{cm}^3\text{STP/g}] \quad (2.17)$$

where z_i is the volume fraction of the noble gas i in dry air (Table 2.1). The excess air is best detectable with Ne, which is the less soluble noble gas of purely atmospheric origin. Therefore the excess air component is often expressed as a relative Ne excess ΔNe , i.e. the percentage of the Ne excess relative to the Ne equilibrium concentration:

$$\Delta Ne(\%) = \frac{Ne_{ex}}{Ne_{eq}} \cdot 100 \quad [\%] \quad (2.18)$$

As approximation, 1% ΔNe corresponds to $A = 10^{-4} \text{ cm}^3\text{STP/g}$. In the ocean, small air excess equivalents of a few percent ΔNe are very common and are attributed to injection of air bubbles by breaking waves (e.g., Craig and Weiss, 1971; Bieri, 1971). In groundwater, an even larger excess air component is present being attributed to complete dissolution of air trapped in the pore space (e.g., Andrews, 1992). Air bubbles with diameters smaller than about $1\mu\text{m}$ tend to collapse under their high surface tension (Osenbrück, 1991) and will inject all their gases in water phase. Gas excesses produced by complete air solution have the same elemental ratios as unfractionated atmospheric air.

In some groundwaters, the assumption of a purely atmospheric composition of the excess air cannot satisfactorily explain the observed noble gas abundances. A possible explanation could be incomplete dissolution of trapped air. Normally the ambient pressure is assumed to be equal with the atmospheric pressure. But, due to fluctuation of the groundwater table, the gas phase in lower part of the unsaturated zone comes under increasing pressure and air bubbles that do not dissolve completely will discharge their gas into water according to Henry's law. As the concentration at equilibrium is proportional to the pressure, a higher pressure increases all noble gas

concentration by the same relative amount. However, assuming incomplete dissolution of air bubbles under an increased hydrostatic pressure would make it difficult to directly relate the prevailing pressure to the altitude of the recharge area as in Equation (2.14).

As alternative to pressure fluctuation, a model of partial loss of the initial excess air by diffusive re-equilibration across the water table has been proposed to explain deviation from complete air dissolution (Stute et al., 1995b). Note that this degassing happens shortly after infiltration, close to the water table. Re-equilibration during recharge should not be confused with possible degassing during sampling (Stute, 1989). The process of partial re-equilibration leads to a systematic elemental fractionation of the excess component relative to atmospheric air in which the heavier noble gases are overabundant over the light ones. To characterize the degree of re-equilibration that occurred a new parameter is introduced. Stute et al. (1995b) expressed this parameter as the remaining fraction of the initial Ne excess:

$$\frac{C_i^{ex}}{C_i^{ex}(0)} = \left(\frac{C_{Ne}^{ex}}{C_{Ne}^{ex}(0)} \right)^{D_i/D_{Ne}} \quad [-] \quad (2.19)$$

where C_i^{ex} is the remaining excess of gas i after partial re-equilibration, $C_i^{ex}(0)$ the initial excess, and D_i the molecular diffusion coefficient, which governs the degassing process. The degassing term can be rewritten in such a way that directly refers to the underlying physical degassing process, by defining the re-equilibration parameter $R = -\ln(C_{Ne}^{ex}/C_{Ne}^{ex}(0))$:

$$C_i^{ex} = C_i^{ex}(0) \cdot e^{-R \frac{D_i}{D_{Ne}}} \quad [\text{cm}^3\text{STP/g}] \quad (2.20)$$

Values for D_i are published by Jähne et al. (1987) except for Ar. In Table 2.3 D_{Ar} was interpolated from the diffusion coefficients of the other noble gases assuming that D is indirect proportional to the square root of the atomic mass.

Table 2.3: Molecular diffusion coefficients of noble gases in water at different temperatures (Jähne et al., 1987; Stute, 1989). The diffusion coefficient for ^3He can be approximated by $D(^3\text{He}) \approx \sqrt{4/3} \cdot D(^4\text{He}) = 1.155 \cdot D(^4\text{He})$.

T (°C)	He	Ne	Ar	Kr	Xe
($10^{-5} \text{ cm}^2/\text{s}$)					
5	5.10	2.61	1.63	1.02	0.774
10	5.74	2.94	1.87	1.20	0.929
15	6.30	3.28	2.13	1.41	1.12
25	7.22	4.16	2.69	1.84	1.47
35	8.48	4.82	3.29	2.40	1.94

In Figure 2.5 the basic concepts of the formation of excess air are shown. It is reasonable to assume that during infiltration water has enough time to equilibrate with air until it reaches the saturated zone. Therefore with regard to the equilibrium concentration any kinetic fractionation of the noble gases can be excluded.

Usually it is supposed that during recharge water traps small air bubbles and that these bubbles are dissolved completely. This process elevates the noble gas concentrations compared to the equilibrium concentrations. Note that light noble gases react more sensitively to any kind of air injection because they are less soluble in water than heavy noble gases.

If the groundwater is already isolated from the atmosphere at the time when air bubbles collapse completely (i.e. no further gas exchange is possible), the excess air component remains undisturbed (case 1 in Figure 2.5: unfractionated excess air). However, in case the groundwater is still in gas exchange with the atmosphere or with soil air the supersaturated water starts to degas (case 2 in Figure 2.5: fractionated excess air). It is normally assumed that degassing happens after the dissolution of air bubbles (i.e., bubbles collapse much faster than excess air is affected by degassing).

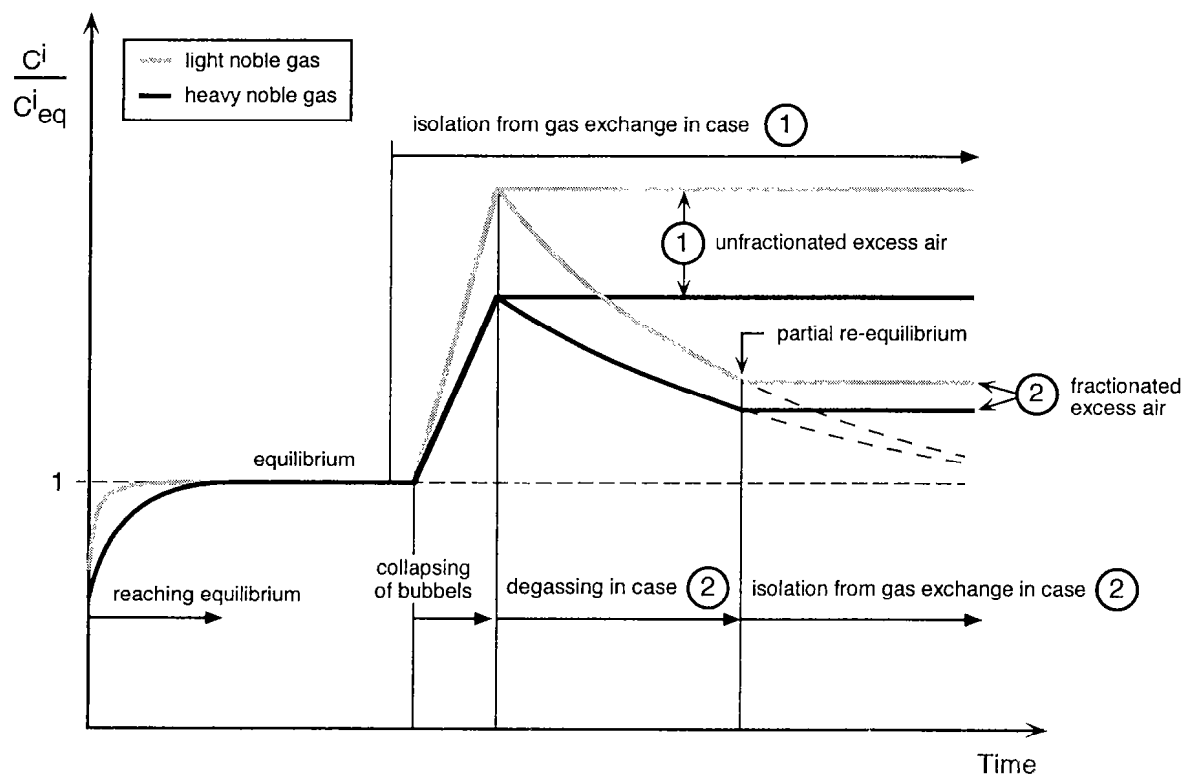


Figure 2.5: Formation of unfractionated and fractionated excess air plotted for light and heavy noble gas species. Case 1: The isolation from gas exchange happens before the complete dissolution of air bubbles. The result is an unfractionated excess air component. Case 2: The isolation from gas exchange happens after the complete dissolution of air bubbles. In the mean time the supersaturated water starts to degas. The result is a fractionated excess air component. Further explanation see text.

According to the Equations (2.19) and (2.20) degassing can be described as a re-equilibration process. If the groundwater is separated from gas exchange during re-equilibration, the equilibrium concentration is not completely reached and the excess air component remains fractionated (case 2 in Figure 2.5). However, it is also possible to postulate other degassing scenarios; as for example, supersaturated water degasses into a closed volume of soil air (e.g., into 'big bubbles') or the dynamic of the degassing process is governed by the square root of the molecular diffusion constant. In fact, a comprehensive description of the processes generating fractionated excess air is still lacking.

In any case, degassing affects preferentially the light noble gases. Therefore in fractionated excess air heavy noble gases are normally enriched relative to light noble gases, i.e. $(C^l / C^h)_{frac.} < (C^l / C^h)_{unfrac.} = (C^l / C^h)_{air}$ where the noble gas l is lighter than the noble gas h .

In Figure 2.6 the excess air component (ΔNe) found in a young groundwater system is plotted versus the groundwater age. The groundwater in the alluvial Linsental aquifer in northern Switzerland is predominately formed by river infiltration and has a maximum age of about 3 years (see chapter 5). Compared to the river samples being in saturation, all measured groundwater samples contain excess air with a maximum value of 30% ΔNe . Only in three out of 60 samples the composition of excess air is different from unfractionated atmospheric air. In these cases the assumption of a partial re-equilibration after excess air formation can explain the measured noble gas concentrations. However, the calculated initial ΔNe (i.e. excess air before degassing) would be in the order of 100%. Since this initial excess air component is much higher than any measured ΔNe in the Linsental aquifer, these calculations question about the physical realism of the re-equilibration process. It is certainly one of the major challenges of the noble gas method to verify the re-equilibration process, or to find alternative models to describe the observation of fractionated excess air.

All other measured samples support the idea that excess air is formed by the complete dissolution of air during recharge. In the Linsental aquifer ΔNe hardly correlates with the groundwater residence time (Figure 2.6). This finding leads one to suppose that the formation of excess air happens during or immediately after groundwater infiltration. In addition, the ΔNe seems to converge with increasing age to an average value. Presumably the mean value of 15% excess air is characteristic for this aquifer, but can vary due to different infiltration conditions.

A recent study by Wilson and McNeill (1997) try to prove that in some young groundwaters the amount of excess air is controlled by the lithology of the investigated aquifer. However, additional field and laboratory data is necessary to decide which processes influence air entrapment in groundwater (e.g., precipitation, water table fluctuation, pore size, grain size distribution, or even biological activities).

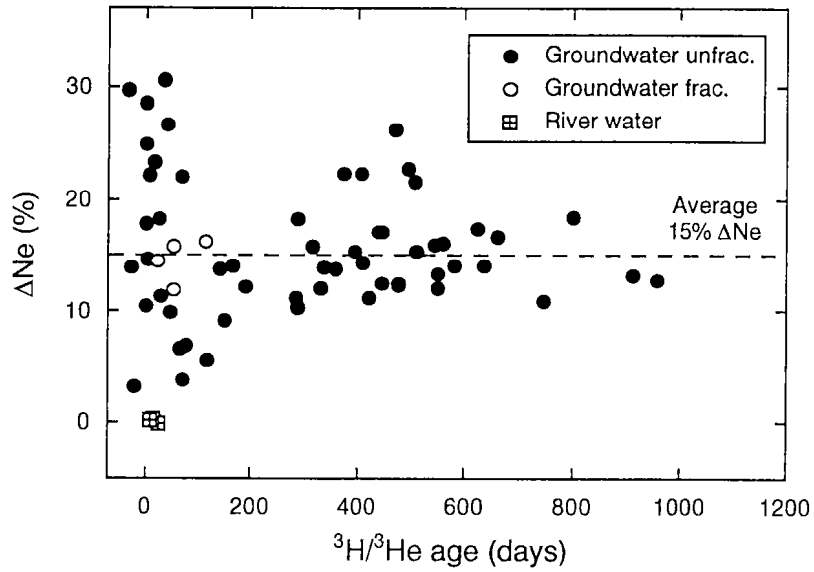


Figure 2.6: Excess air versus $^3H/^3He$ water age in the Linsental aquifer. With increasing water age the ΔNe converges to a mean value of about 15%. Note that no general correlation is found between excess air and the season of sampling and between excess air and the sampling depth below water table.

2.4 Non-atmospheric sources

In addition to noble gases derived from the atmosphere, some noble gas isotopes dissolved in groundwater originate from other sources. The most prominent noble gas isotopes that can lead to non-atmospheric excesses in groundwater are ^3He , ^4He , ^{40}Ar , and ^{21}Ne . In general, accumulation of non-atmospheric noble gas in groundwater can be used to derive residence times (section 4.2). Two major formation processes of noble gas isotopes can be distinguished: First, noble gas isotopes are directly produced by decay of radioactive isotopes in the groundwater or the surrounding rocks (e.g., ^3He , ^4He , ^{40}Ar , and several isotopes of Kr and Xe). Second, noble gas isotopes are produced indirectly by the interaction of α -particles with neighboring elements in the crystal lattice of rock forming minerals (e.g., ^{21}Ne , ^{22}Ne). In the following the sources of non-atmospheric noble gases in groundwater are discussed in some detail.

2.4.1 Difference in helium ratios

On Earth the He isotope ratio varies by many orders of magnitude, depending on the different origin of terrestrial helium. Three distinct sources can be distinguished (Table 2.4). Incorporation and mixing of He from these primary sources results in geosphere components (rocks, minerals and natural gases and waters), with characteristic $^3\text{He}/^4\text{He}$ ratios (Table 2.5).

Table 2.4: Major sources for He isotopes (Mamyrin and Tolstikhin, 1984).

Source	Production mechanism	$^3\text{He}/^4\text{He}$ ratio
Primordial He	nuclear fusion	$3 \cdot 10^{-4}$
Radiogenic He	radioactive decay	$2 \cdot 10^{-8}$
Spallogenic He	cosmic-ray bombardment	$2 \cdot 10^{-1}$

Table 2.5: Typical $^3\text{He}/^4\text{He}$ ratios in natural systems.

Geosphere component	$^3\text{He}/^4\text{He}$ ratio	Genetic source
Mantle	10^{-5}	mainly primordial
Active tectonic areas	$10^{-5} - 10^{-7}$	radiogenic and primordial
Crust	$10^{-7} - 10^{-8}$	mainly radiogenic
Rocks enriched in U, Th	$> 10^{-10}$	high radiogenic input
Atmosphere	$1.384 \cdot 10^{-6}$ ⁽¹⁾	all sources

⁽¹⁾ Clarke et al. (1976)

Terrestrial ^4He are mainly produced during α -decay of U- and Th-series nuclides. The main nuclear reaction producing ^4He in the subsurface are:



Based on the α -decay processes for U and Th, Kugler and Clarke (1972) suggested by interpreting ^3He as uncompleted α -particle that the resulting $^3\text{He}/^4\text{He}$ ratio should be in the order of $8 \cdot 10^{-12}$. This direct α decay related $^3\text{He}/^4\text{He}$ ratio is much less than the observed ratio in rocks and waters, suggesting other sources of ^3He . In groundwater system, ^3He is produced: (i) by the α induced reaction on Lithium (i.e., $^6\text{Li} (n, \alpha) ^3\text{H}$ followed by a β -decay to ^3He ; Morrison and Pine, 1955), and (ii) from decay of natural or anthropogenic tritium (^3H) (see next section).

Production of subsurface ^3He is likely responsible for observed $^3\text{He}/^4\text{He}$ ratios on the order of 10^{-7} to 10^{-8} found in crustal rocks and associated groundwaters. In contrast to crustal rocks the $^3\text{He}/^4\text{He}$ ratio of natural gases and waters from areas of active rifting, volcanism or extensional tectonics can get much higher than 10^{-7} (e.g., Ozima and Podosek, 1983). High helium ratios suggest that the fluids contain a dominant mantle component, which has a higher $^3\text{He}/^4\text{He}$ ratio of approximately 10^{-5} .

To summarize, the measured ^3He and ^4He concentrations in groundwater can be written as

$$^4\text{He}_{tot} = ^4\text{He}_{eq} + ^4\text{He}_{ex} + ^4\text{He}_{crust} + ^4\text{He}_{mantle} \quad [\text{cm}^3\text{STP/g}] \quad (2.24)$$

$$^3\text{He}_{tot} = ^3\text{He}_{eq} + ^3\text{He}_{ex} + ^3\text{He}_{crust} + ^3\text{He}_{mantle} + ^3\text{He}_{tri} \quad [\text{cm}^3\text{STP/g}] \quad (2.25)$$

where the subscript *tot* refers to the total concentration, *eq* to the concentration in solubility equilibrium with the atmosphere, *ex* to the He component originating from excess air, and the subscript *crust* and *mantle* to the He components derived from the crust or mantle, respectively. In contrast to ^4He , ^3He has a fifth source that comes from the decay of tritium. In Equation (2.25) this tritiogenic component is indicated by $^3\text{He}_{tri}$.

The equilibrium concentrations (subscript *eq*) are determined by the temperature T , salinity S , and pressure P conditions prevailing during recharge (section 2.2). Commonly, ^{20}Ne is used as an indicator of the atmospheric helium component. If it is assumed that ^{20}Ne has no sources other than the atmosphere, the ratio $^{20}\text{Ne}_{ex}/^4\text{He}_{ex}$ is equal to $(^{20}\text{Ne}/^4\text{He})_{air}$ (i.e. no degassing). Using this assumption the terrigenous ^4He component, which is defined as $^4\text{He}_{terr} = ^4\text{He}_{crust} + ^4\text{He}_{mantle}$, can be calculated as

$$^4\text{He}_{terr} = ^4\text{He}_{tot} - ^4\text{He}_{eq} - \left(^{20}\text{Ne}_{tot} - ^{20}\text{Ne}_{eq} \right) \cdot \left(\frac{^4\text{He}}{^{20}\text{Ne}} \right)_{air} \quad [\text{cm}^3\text{STP/g}] \quad (2.26)$$

Note that the non-atmospheric $^4\text{He}_{terr}$ is mainly of radiogenic origin and therefore also called radiogenic ^4He ($^4\text{He}_{rad}$).

The terrigenous ^3He can be calculated from the terrigenous ^4He , according to

$$^3\text{He}_{terr} = ^4\text{He}_{terr} \cdot \left(\frac{^3\text{He}}{^4\text{He}} \right)_{terr} = ^4\text{He}_{terr} \cdot R_{terr} \quad [\text{cm}^3\text{STP/g}] \quad (2.27)$$

where R_{terr} is the terrigenous $^3\text{He}/^4\text{He}$ ratio. In cases where no tritiogenic ^3He is present, i.e. old groundwaters, it is normally possible to determine the terrigenous helium ratio R_{terr} . Problems arise in younger groundwaters in which the terrigenous helium ratio is masked by tritiogenic ^3He . In some cases, it may be possible to determine the $^3\text{He}/^4\text{He}$ ratio of the terrigenous component (R_{terr}), from He measurements in a tritium free water mass underlying the water under investigation. If, however, only mantle helium or radiogenic helium are additionally present, it is easier to separate the different He

components because in such case reasonable estimates of the $^3\text{He}/^4\text{He}$ ratios of the added helium are available (see Table 2.5). Often it can be excluded that mantle helium is present and the radiogenic helium ratio of $2 \cdot 10^{-8}$ (Mamyrin and Tolstikhin, 1984) is assumed. An alternative way of obtaining information on additional helium sources is to study a $^3\text{He}/^4\text{He}$ ratio plot (Figure 2.7).

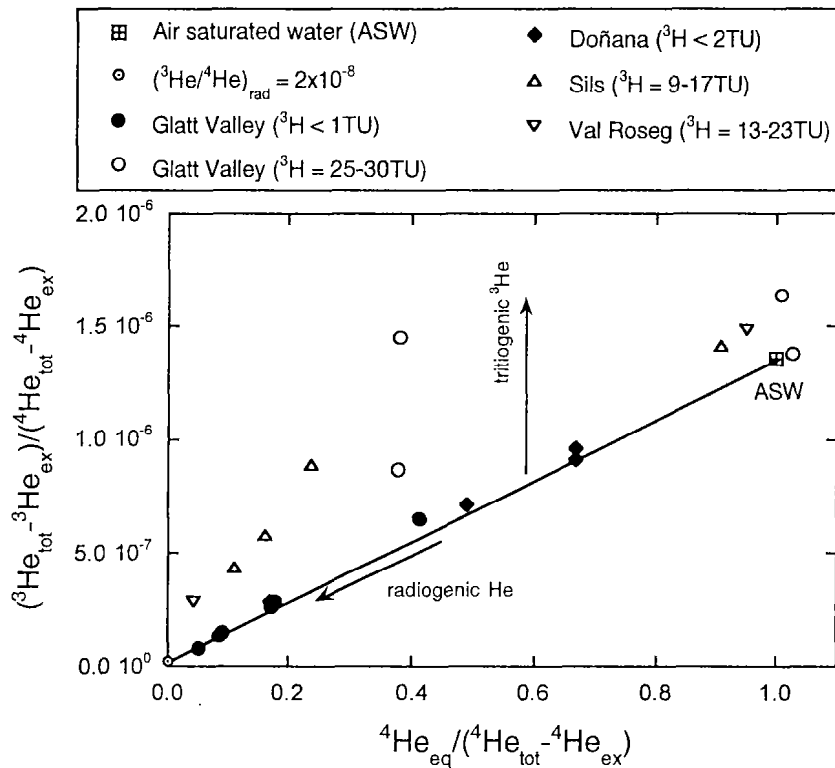
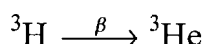


Figure 2.7: Measured $^3\text{He}/^4\text{He}$ ratio corrected for excess air versus the inverse of the excess air corrected He concentration ($^4\text{He}_{\text{tot}} - ^4\text{He}_{\text{ex}}$) normalized to the solubility equilibrium ($^4\text{He}_{\text{eq}}$). Helium data are from two Paleogroundwater systems (Glatt Valley aquifer, Switzerland (Beyerle et al., 1998b) and coastal aquifer in Doñana, Spain) and two alpine groundwaters in Switzerland (Sils and Val Roseg). Samples that contain only atmospheric and radiogenic He with a constant $^3\text{He}/^4\text{He}$ ratio of $R_{\text{terr}} = 2 \cdot 10^{-8}$ (Mamyrin and Tolstikhin, 1984) should fall on the plotted line. If tritogenic ^3He or mantle derived He is present, the data points lay above this line. The range of the measured tritium (^3H) concentration is given in brackets.

2.4.2 Tritium (^3H)

Tritium (^3H) is the radioactive isotope of H that decays by β -decay to ^3He (half-life: $T_{1/2} = 12.38$ years (Oliver et al., 1987):



$$\text{with decay constant: } \lambda = \ln(2) / T_{1/2} = 0.05599 \text{ yr}^{-1} = 1.774 \cdot 10^{-9} \text{ s}^{-1} \quad (2.28)$$

For modern water isolated from the atmosphere, ^3H is a major source of ^3He . For each ^3H that decays one ^3He atom is produced. The natural abundance of ^3H is usually expressed in Tritium Units (TU):

$$\begin{aligned} 1 \text{ TU} &= 1 \text{ } ^3\text{H} \text{ atoms per } 10^{18} \text{ H atoms} \\ &= 1.1100 \cdot 10^{-19} \text{ mol/g}_{\text{pure water}} = 66'846 \text{ atoms/g}_{\text{pure water}} \end{aligned} \quad (2.29)$$

Sometimes ^3H concentrations are also expressed in activities (IAEA, 1992):

$$1 \text{ Bq/L} = 8.47 \text{ TU}; \quad 1 \text{ pCi/L} = 0.313 \text{ TU} \quad (2.30)$$

The conversion from TU into $\text{cm}^3\text{STP/g}$ is given by

$$1 \text{ cm}^3\text{STP He} / \text{g}_{\text{water}} = \frac{4.0193 \cdot 10^{14}}{(1 - S/1000)} \text{ TU} \quad (2.31)$$

where S is the salinity of the water (in ‰). Since tritium is essential for the $^3\text{H}/^3\text{He}$ dating method (section 4.2.1), its properties will be discussed here in some detail.

Tritium is probably the single most important environmental isotope for the study of lakes, oceans and groundwater. It is produced naturally by the interaction of cosmic rays with nitrogen and oxygen, mainly in the upper atmosphere, and, after oxidation to HTO, takes part in the hydrological cycle. In the atmosphere the average production rate of natural ^3H is about $2500 \text{ } ^3\text{H} \text{ atoms m}^{-3} \text{ s}^{-1}$ (Craig and Lal, 1961; Rozanski et al., 1991), but varies with the geomagnetic latitude. Before significant amounts of ^3H were injected into the atmosphere through man's nuclear activities, precipitation had a natural background of around 5 TU (Kaufman and Libby, 1954; Craig and Lal, 1961; Lal and Peters, 1962; Roether, 1967). During the early 1960's, when the effects of atmospheric testing of nuclear weapons peaked, ^3H concentrations of over 2000 TU were measured. Since most of the nuclear weapons tests were performed in the

northern hemisphere, even today the ^3H distribution is strongly asymmetric between the northern and southern hemisphere (Figure 2.8). Today atmospheric background levels in the northern hemisphere are between about 5 and 30 TU, and in the southern hemisphere between 2 -10 TU (IAEA/WMO, 1998).

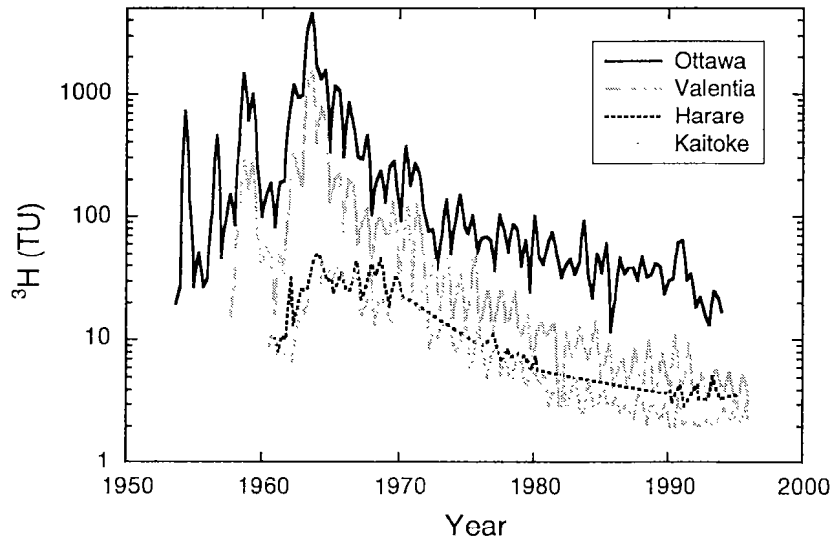


Figure 2.8: Tritium concentration in precipitation since 1950 at four IAEA stations (IAEA/WMO, 1998): Ottawa, Canada (northern hemisphere, continental); Valentia, Ireland (northern hemisphere, marine); Harare, Zimbabwe (southern hemisphere, continental); Kaitoke, New Zealand (southern hemisphere, marine).

In groundwater ^3H is a good indicator of the presence of or contamination by recently infiltrated water (younger than 50 years). Subsurface production of ^3H occurs mainly by the reaction $^6\text{Li} (n, \alpha) ^3\text{H}$ in the rock matrix and depends therefore largely on the Li content and on the neutron flux. The produced ^3H atom migrates from the site of origin and finally exchanges a H atom in a water molecule (Andrews et al., 1989). Since the produced ^3H decays to ^3He , the subsurface produced ^3H concentration in groundwater represents an approximate balance between production and decay. For example, Andrews et al. (1989) calculated a maximum ^3H concentration from in situ production of 0.7 TU in the Stripa groundwaters.

As mentioned before, the natural ^3H level prior to the bomb-peak is not well known. An aquifer that contains water which was infiltrated before 1950, offers the possibility to reconstruct the natural 'pre-bomb' ^3H concentration in past rainfall by measuring the in the mean time ingrowth tritiogenic ^3He ($^3\text{He}_{tri}$). In old groundwaters, tritiogenic ^3He

produced by decay of pre-bomb ^3H is masked by the other ^3He components according to Equation (2.25):

$$^3\text{He}_{tri} = ^3\text{He}_{tot} - ^3\text{He}_{eq} - ^3\text{He}_{ex} - ^3\text{He}_{terr} \quad [\text{cm}^3\text{STP/g}] \quad (2.32)$$

where $^3\text{He}_{terr}$ is the sum of $^3\text{He}_{crust}$ and $^3\text{He}_{mantle}$. Assuming that both the $R_{terr} = ^3\text{He}_{terr}/^4\text{He}_{terr}$ and the $^3\text{He}_{tri}$ is constant in each water sample j taken from an aquifer, the following balance equation can be defined:

$$^3\text{He}_{tri} = ^3\text{He}_{tot}^j - ^3\text{He}_{eq}^j - ^3\text{He}_{ex}^j - ^4\text{He}_{terr}^j \cdot R_{terr} \quad [\text{cm}^3\text{STP/g}] \quad (2.33)$$

In Equation (2.33) $^3\text{He}_{tot}^j$ is the measured ^3He concentration in sample j . Under the given assumption, the $^3\text{He}_{eq}^j$, $^3\text{He}_{ex}^j$, and $^4\text{He}_{terr}^j$ components of each sample can be calculated. In case of more than two samples, the equation system (2.33) is over-determined and can be solved by least squares method to find a optimal solution for the two unknowns R_{terr} and $^3\text{He}_{tri}$. The various ^3He components dissolved in the paleogroundwater of the Glatt Valley aquifer, northern Switzerland, is given in Figure 2.9.

Tritium concentrations in waters can be determined using low-level liquid-scintillation counting techniques. The lower ^3H levels in recent precipitation demand more precise analytical methods than in the 1970-1990 period. Modern analytic techniques, such as prior isotopic enrichment (Weiss et al., 1976) or the determination of ^3H by ^3He ingrowth (Clarke et al., 1976), allow ^3H detection as low as 0.1 to 0.005 TU (Bayer et al., 1989). Limitations in the use of ^3H alone, as a water mass tracer, arise from its radioactive nature and from dispersion of the bomb signal in the system investigated, leading to difficulties in interpreting the ^3H distributions as a measure of the residence time. Therefore ^3He is additionally measured to obtain water ages (see $^3\text{H}/^3\text{He}$ dating in section 4.2.1).

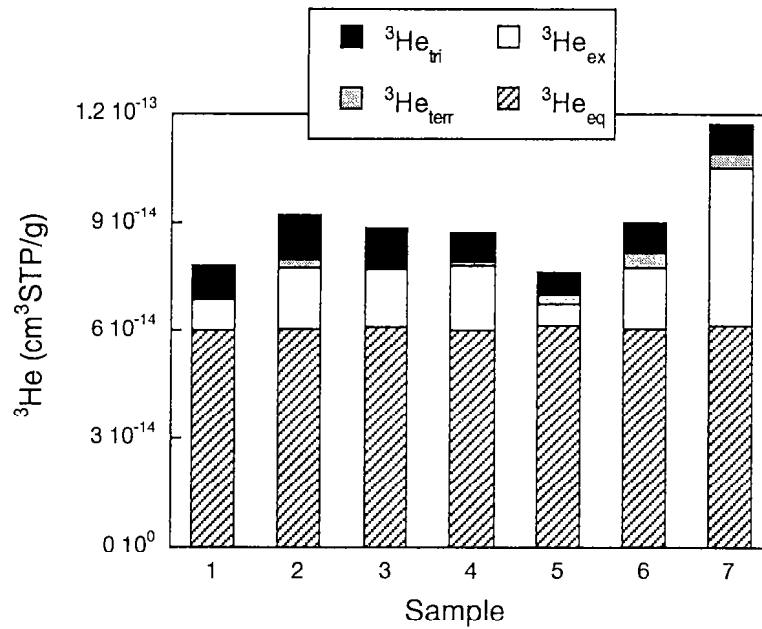


Figure 2.9: The composition of the measured ^3He ($^3\text{He}_{\text{tot}}$) in the paleogroundwater of the Glatt Valley aquifer. The sample numbers refer to the boreholes shown in Figure 6.1 (chapter 6). The various ^3He components are: $^3\text{He}_{\text{eq}}$: equilibrium concentration; $^3\text{He}_{\text{ex}}$: unfractionated excess air component; $^3\text{He}_{\text{terr}}$: terrigenic ^3He component; $^3\text{He}_{\text{tri}}$: tritiogenic ^3He component. The terrigenic ^3He and the tritiogenic ^3He components are derived from an optimizing process. On average the calculated tritiogenic ^3He concentration is $(9.4 \pm 2.0) \cdot 10^{-15} \text{ cm}^3 \text{STP/g}$ which corresponds to a pre-bomb tritium concentration of $3.8 \pm 0.8 \text{ TU}$.

2.4.3 Non-atmospheric Ne, Ar, Kr and Xe

Except for the $^3\text{He}/^4\text{He}$ ratio, the isotopic ratios of noble gases in groundwater are usually indistinguishable from atmospheric ratios. However, in very old groundwater the isotopic ratios can significantly differ from atmospheric ratios. With increasing residence times isotopic anomalies are detected first in Ar, after in Ne and eventually in Kr and Xe.

Elevated Ar concentrations in groundwater are caused by diffusion of ^{40}Ar from minerals and rocks containing considerable amounts of radiogenic ^{40}Ar (Table 2.6). ^{40}Ar accumulates in rocks as a β -decay product of ^{40}K . The radioactive isotope ^{40}K is a minor constituent of the natural potassium (0.0117%) and decays with a half-life of $1.26 \cdot 10^9$ yr. In 11% of its disintegrations, ^{40}K decays to ^{40}Ar . Because of the large quantities of atmospheric ^{40}Ar dissolved during groundwater infiltration ($4 \cdot 10^{-4}$ $\text{cm}^3\text{STP/g}$), the detection of any radiogenic ^{40}Ar added to the groundwater is often difficult (see section 4.2.2)

Even more difficult to identify are non-atmospheric excesses in ^{21}Ne and ^{22}Ne . Both Ne isotopes are produced in solid earth as a result of interactions between α particles from U and Th decay and light elements in the surrounding rocks (primarily ^{18}O , ^{19}F and ^{25}Mg) (Craig and Lupton, 1976; Kennedy et al., 1990). Typical radiogenic Ne isotope ratios are listed in Table 2.6. The radiogenic production ratio of $^{21}\text{Ne}/^{22}\text{Ne}$ is one order of magnitude higher than the atmospheric ratio. Therefore in groundwater a non-atmospheric ^{21}Ne excess can be detected first. Since only a minority of the produced α particles interact with light elements, the production rate of Ne isotopes is much smaller than that of the generating ^4He . Typical ^{21}Ne to ^4He production ratios are around $4 \cdot 10^{-8}$ (Craig and Lupton, 1976; Kennedy et al., 1990).

Table 2.6: Major sources for Ne and Ar isotopes (Mamyrin and Tolstikhin, 1984) compared to the atmospheric ratios (Ozima and Podosek, 1983).

Source	$^{20}\text{Ne}/^{22}\text{Ne}$	$^{21}\text{Ne}/^{22}\text{Ne}$	$^{40}\text{Ar}/^{36}\text{Ar}$	$^{38}\text{Ar}/^{36}\text{Ar}$
Primordial	12 - 13	0.03	10^{-14}	0.17 - 0.18
Radiogenic	0	0.3 - 1.0	10^7	1
Spallogenic	0.9	0.95	0.01	0.65
Atmosphere	9.8	0.03	295.5	0.19

Several isotopes of Xe (^{131}Xe , ^{132}Xe , ^{134}Xe , and ^{136}Xe) and Kr (^{83}Kr , ^{84}Kr , and ^{86}Kr) are formed as fission products in spontaneous fission of ^{238}U , ^{235}U , and ^{232}Th . Spontaneous fission half-lives are $1.9 \cdot 10^{17}$ yr for ^{235}U , $6.8 \cdot 10^{15}$ yr for ^{238}U , and $> 10^{21}$ yr for ^{232}Th (Marine, 1981). Thus only ^{238}U have significant fission yields for Xe and Kr. Measurable amounts of in situ produced fissionic (also called nucleogenic) Xe and Kr are theoretically expected on time scales of 10^8 to 10^{10} years (Stute, 1989). For all practical purposes, the isotopes of Kr and Xe dissolved in meteoric groundwater can be regarded as exclusively of atmospheric origin.

A mass spectrometric system for the analysis of noble gases and tritium from water samples

U. Beyerle¹, W. Aeschbach-Hertig¹, D. M. Imboden¹, H. Baur², T. Graf² and R. Kipfer¹

¹ Department of Environmental Physics, Swiss Federal Institute of Technology (ETH) and Swiss Federal Institute of Environmental Science and Technology (EAWAG), CH-8600 Dübendorf, Switzerland

² Isotope Geology, Department of Earth Sciences, Swiss Federal Institute of Technology (ETH), NO C61, CH-8092 Zürich, Switzerland

(submitted to *Environmental Science & Technology*)

Abstract

The design, setup and performance of a mass spectrometric system for the analysis of noble gases isotopes (³He, ⁴He, ²⁰Ne, ²¹Ne, ²²Ne, ³⁶Ar, ⁴⁰Ar, ⁸⁴Kr, ¹³⁶Xe) and tritium (³H) from water samples are described. The ³H concentration is measured indirectly by the ³He ingrowth from radioactive decay. First water samples are completely degassed. After purification and separation, the noble gases are measured in two non-commercial double-collector 90° magnetic sector spectrometers. We present here a new approach for the analysis of the heavy noble gas isotopes that enables, in principle, to measure Ar, Kr and Xe simultaneously. Typical precision for the measurements of ³H, He, Ne, Ar, Kr, and Xe concentrations are ±2.7%, ±0.3%, ±0.9%, ±0.3%, ±0.8%, and ±1.0% respectively. For the isotopic ratios ³He/⁴He, ²⁰Ne/²²Ne and ⁴⁰Ar/³⁶Ar the typical precision are ±0.7%, ±0.3%, and ±0.2%. These values express the reproducibility of the measurement of an internal freshwater standard and include the overall stability of the system, as well as of the extraction

procedure. To verify the method the noble gas concentration of air-saturated water samples, which were prepared under controlled conditions, are compared with noble gas solubility data. Additionally, the $^{40}\text{Ar}/^{36}\text{Ar}$ and $^{20}\text{Ne}/^{22}\text{Ne}$ fractionation during solution is estimated from 70 measured surface water samples.

3.1 Introduction

The noble gas isotopes of He, Ne, Ar, Kr, Xe and the hydrogen isotope tritium are widely used as environmental tracers to study the dynamics of natural water systems such as the ocean, lakes and groundwaters. Tritium (^3H) in combination with its decay product ^3He (half life $T_{1/2} = 12.38$ yr, Oliver et al., 1987) enables the determination of the water residence time or the 'water age'. The $^3\text{H}/^3\text{He}$ dating method is used in oceanography and limnology (e.g., Clarke et al., 1976; Torgersen et al., 1977) to study the circulation of water masses and large-scale mixing processes. Applied in groundwater systems, the $^3\text{H}/^3\text{He}$ water age is used to determine recharge rates, groundwater flow velocities and mixing ratios (e.g., Schlosser et al., 1988). In addition, radiogenic production of ^4He (from U and Th decay series) (Clarke and Kugler, 1973), of ^{40}Ar (from ^{40}K decay) (Mazor, 1977) or even of ^{21}Ne (from α -induced nuclear reactions with ^{18}O , ^{19}F) (Bottomley et al., 1984) in rocks and subsequent accumulation in groundwater offers the possibility to derive estimates of groundwater residence times up to millions of years.

Since noble gases are chemically inert under natural conditions, they are ideal tracers. In water the concentration of dissolved atmospheric noble gases is determined by the temperature and salinity of the water and the atmospheric pressure (Stute and Schlosser, 1993; Aeschbach-Hertig et al., 1999). Hence the noble gas concentration of a water body, which is isolated from the atmosphere, provides information about the conditions prevailing during gas exchange with the atmosphere. In old groundwater, the measured concentration of atmospheric noble gases are therefore used to deduce paleotemperatures back to the last glacial period (e.g., Andrews and Lee, 1979; Stute and Deák, 1989; Stute et al., 1995b; Beyerle et al., 1998b).

Mass spectrometric methods to determine the isotopic compositions of He, Ne and/or Ar in water are outlined by Clarke et al. (1976), Lynch and Kay (1981), Smith and Kennedy (1983), Lott and Jenkins (1984), Bayer et al. (1989), and Jean-Baptiste et al. (1992). In this paper a combined system is described for the measurement of ^3H (using the ^3He ingrowth method) and the most abundant isotopes of He, Ne, Ar, Kr and Xe in water samples. We present here a new approach for the analysis of the heavy noble gas isotopes that enables, in principle, the determination of Ar, Kr and Xe simultaneously. The precision and performance of the analysis is discussed. To verify the analytical technique noble gas concentrations of air-equilibrated water samples are compared with published solubility data.

3.2 Experimental Section

The determination of noble gas and ^3H concentrations in natural water samples requires several steps. The first step is to collect water samples in the field and transport them in appropriate containers to the lab. Here the sample is extracted and after purification and separation the noble gases are measured mass spectrometrically. After the noble gas measurement the sample is re-closed and a few month later the ^3He produced by decay of ^3H is analyzed.

3.2.1 Sampling

As noble gases are highly volatile it is extremely important to avoid gas exchange between the water sample and the atmosphere during sampling, transport or storage. Water samples from oceans or lakes can be taken with the aid of Niskin bottles (Figure 3.1). In case of supersaturated lake or sea water (e.g. high CO_2 concentrations), we also use an in situ sampling technique that allows under water sampling.

Since groundwater is commonly supersaturated with respect to noble gases (known as excess air phenomenon, Heaton and Vogel, 1981), it is essential to keep the

groundwater sufficiently under pressure during sampling. Therefore submersible pumps have to be used to avoid degassing.

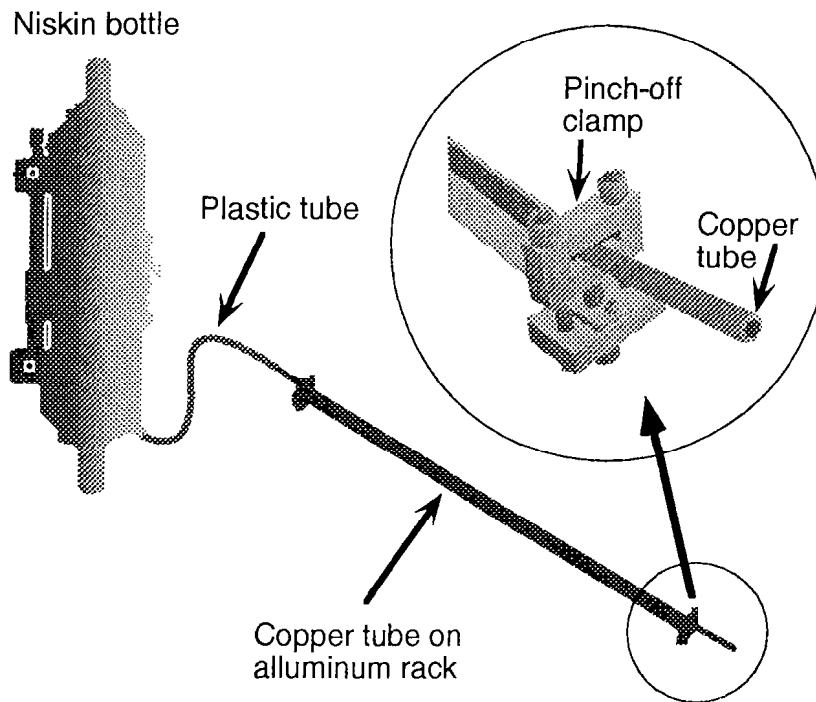


Figure 3.1: Setup for sampling of lake or sea water. One pinch-off clamp, which closes the copper tube, is shown zoomed. The water can be taken at different depths with the aid of Niskin bottles.

In any case the water has to be transferred as fast as possible to airtight containers. Usually about 45 g of water is filled in 1.2 m long copper tubes (internal diameter 7.7 mm) which are mounted on a sliding aluminum rack (Kipfer, 1991). This sliding aluminum rack enables the re-closure of the copper tube after the noble gas measurement for further tritium analysis. To avoid any air bubbles being generated or captured during sampling the copper tube is rinsed thoroughly. Afterwards, stainless steel pinch-off clamps at either side of the aluminum rack are closed to seal off the tube (Figure 3.1). The use of pure copper guarantees that the tube can be reopened in the laboratory without breaking. Being closed, the sample can be stored without any

significant gas loss or gain. Even for the most mobile He the maximum leakage rate to vacuum is smaller than 10^{-9} cm³STP yr⁻¹ (Kipfer, 1991; Aeschbach-Hertig, 1994), whereas the typical amount of He in the copper tube is on the order of $2 \cdot 10^{-6}$ cm³STP. For high precision ³H measurements about 1 kg of water is sampled in plastic bottles. In the lab, this water is transferred to a full metal stainless steel bottle (1000 cm³) with a piece of copper tube as a bottleneck for connection to the extraction line. After degassing the water completely (see procedure for copper tubes extraction, 3.2.2), the bottleneck is tightly closed using a clamp. Several months later the ³He, which is produced by the decay of ³H, is measured.

3.2.2 Gas extraction

In order to quantitatively extract the noble gases from the water sample, the copper tube is directly connected to the ultra high vacuum (UHV) extraction line. Figure 3.2 illustrates the setup of the extraction and purification line. The whole line is made of stainless steel tubes (diameter 19 mm) connected with commercial Varian ConFlat[®] flanges. Valves are either manually operated NUPRO (N) and all metal valves (VM) or pneumatically actuated (V) all-metal valves. The automatic valves are controlled by the two mass spectrometer computers. In order to clean the extraction line the whole system can be heated to 300°C.

The copper tube (CT) is connected to the extraction vessel (EX) by means of a fastening device which directly presses the front of the copper tube UHV-tight onto a metal cutting edge (Kipfer, 1991). Note that in contrast to the common extraction procedure (Bayer et al., 1989), our system does not use any kind of O-ring fitting. This design therefore completely avoids any air contamination during extraction. A cascade of pumps produces the UHV in the extraction vessel. First, a membrane pump (MP1) is used mainly to remove the water vapor from the system (final pressure of a few mbar). Second, a rotary pump (RP1), protected from water vapor by a liquid nitrogen cooled trap, produces a rough vacuum (final pressure $\approx 10^{-1}$ mbar).

Finally, a combination of a membrane (MP2) and turbomolecular pump (TP2) reduces the pressure to about 10^{-7} mbar.

After establishing UHV, the extraction line is separated from the vacuum pumps (close valves N4, V8, V8a). Then the pinch-off clamp (PC1) of the copper tube on the UHV-system side is opened and the sealed part of the copper tube is reopened by a special pair of pliers (Kipfer, 1991). Subsequently the water is transferred from the copper tube into the 500 cm^3 extraction vessel (EX). The extraction vessel is connected with the extraction line by flexible metal bellows MB (length 1 m). To enhance the removal of the gases from the water phase the extraction vessel is shaken mechanically to produce turbulence in the molecular boundary layer of the water and to enlarge the active surface area of gas exchange. The extracted gases and the water vapor are adsorbed at the all-metal trap (T1) and the zeolith ZEO1 (molecular sieve with 5 \AA pore diameter) of the extraction line that are at this time cooled by liquid nitrogen. Water vapor is adsorbed mainly on T1 (about 0.5 g during the whole extraction procedure). The adsorption of the condensable gases maintains a strong pressure gradient between the extraction vessel and the traps, including a continuous flow of water vapor and extracted gases. This flow is controlled by a capillary (C) (internal diameter 0.5 mm, length 2 cm), which reduces the amount of transported water vapor and increases the flow velocity in order to prevent back diffusion of non-condensable gases (such as He, Ne and CH_4). The pressure in the extraction line can be monitored by 3 Pirani cells (P1, P2, and P3), allowing the detection of large leaks and the control of the removal efficiency of condensable gases. All along, the capillary and the metal bellows are gently heated. Heating of the capillary (about 50°C) and of the metal bellows above room temperature (30°C) prevents condensation of water vapor and guarantees therefore a complete gas extraction. After 5 minutes, the gas extraction is completed and the valve just before the capillary (V8) closes the extraction line. For the He extraction, the efficiency of the system is higher than 99.995% (Aeschbach-Hertig, 1994).

Mass Spectrometric System

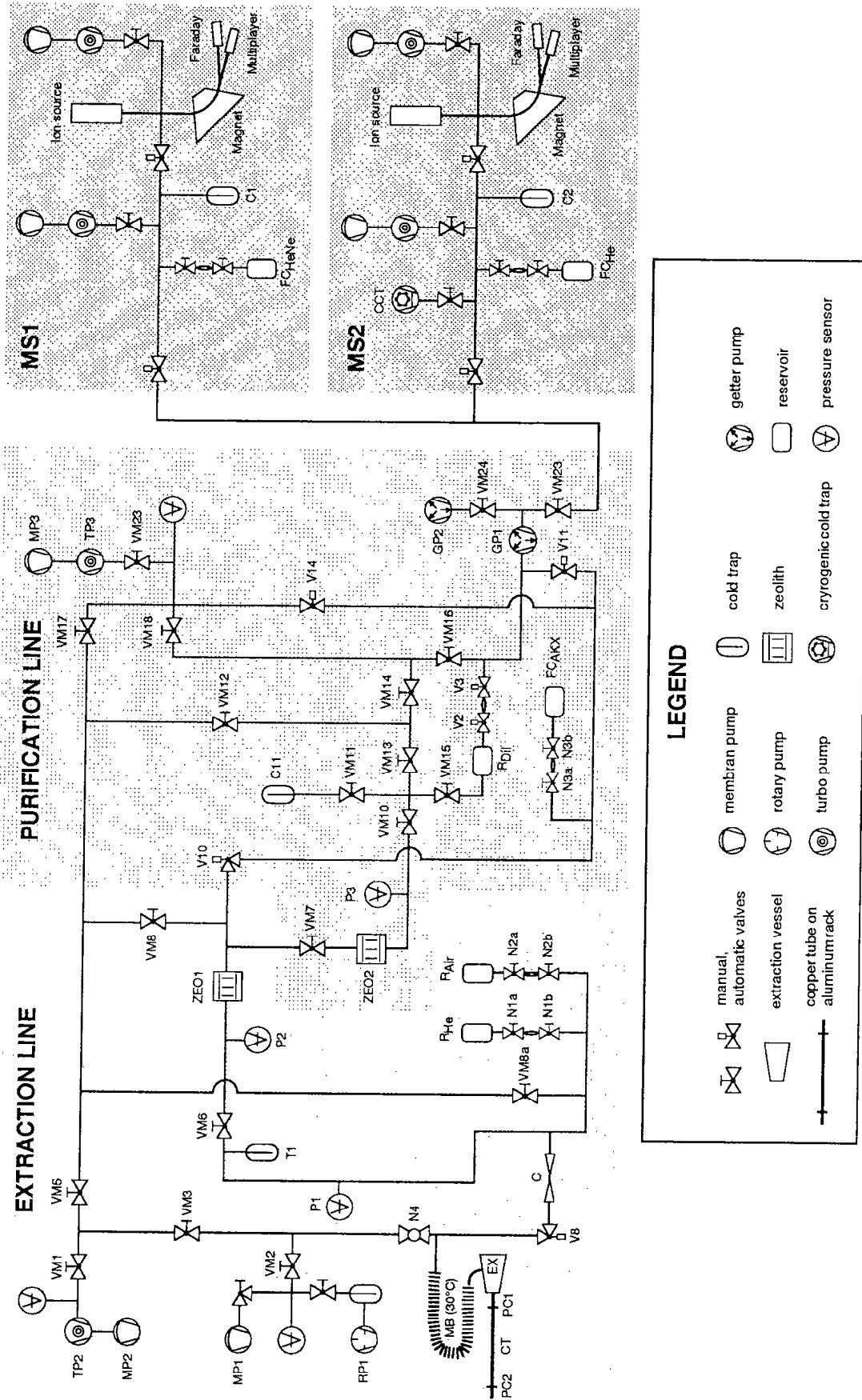


Figure 3.2: Schematic diagram of the extraction and purification line and the two mass spectrometers MS1 and MS2. Abbreviations see text.

3.2.3 He and Ne measurement

After extraction the gas remains exposed to the cold trap and the zeolith for 10 minutes to ensure complete adsorption of the condensable gases, whereas non condensable gases, mainly He and Ne, remain in the gas phase. Afterwards the extraction line is connected to the purification line (open V10, while VM7 remains closed). In the purification line all remaining active gases are caught in two getter pumps (GP1 = Zr-Ti bulk getter at 700°C and GP2 = NP 10 getter). The noble gases are unaffected by the two getters. To ensure complete pressure equilibrium between all involved parts of the extraction line and purification line, the cold traps (T1 and ZEO1) are bypassed (close VM5 and open line between VM8 and VM8a).

In a first step a minor split of the He and Ne phase (between V10 and VM23) is expanded to a non-commercial 90° magnetic sector spectrometer (MS1) equipped with the highly linear Baur-Signer source (Baur, 1980). In the spectrometer He and Ne are measured simultaneously. The noble gas isotopes ^4He , ^{20}Ne and ^{22}Ne are detected and measured using a Faraday cup and ^{21}Ne can be counted on an electron multiplier. The specifications of the MS1 are given in Table 3.1. The UHV before and in the spectrometer (about 10^{-9} mbar and 10^{-10} mbar, respectively) is established with two molecular turbo pumps each combined with a membrane pump. The pressure is monitored in various parts of the mass spectrometric system by pressure gauges.

In a second step the remaining He and Ne phase (behind V10) is admitted to the second mass spectrometer (MS2) for simultaneous measurement of ^4He and ^3He . To avoid Ne ion back-scattering on ^3He during the measurement it is necessary to separate He from Ne quantitatively. Therefore the He and Ne phase is transferred to a cryogenic cold trap at 14 K (CCT) containing a high porosity filter of sintered stainless steel (fineness: 1.5 μm) that adsorbs Ne quantitatively while He remains a free gas. The temperature of the CCT can be set by computer control and is stable within ± 0.1 K or better during Ne adsorption. After 20 minutes the He fraction is transferred to the spectrometer and the CCT is heated to 100 K to release Ne, which is pumped off.

The MS2 is an all-metal, statically operated 90° sector mass spectrometer equipped with a Baur-Signer source (Baur, 1980) and a double collector system (specifications

see Table 3.1). The MS2 is tuned for maximum linearity and not necessarily for maximum sensitivity. The $^4\text{He}^+$ ion current is integrated on a Faraday cup. The small $^3\text{He}^+$ ion beam is counted by an electron multiplier (16-stage, discrete Cu-Be dynode). The sensitivity, resolution and the background of the system are designed to permit He measurements down to 10^{-9} cm³STP for ^4He and 10^{-14} cm³STP for ^3He . The mass resolution (defined as the average mass \bar{m} divided by the mass difference δm , which just can be resolved) can be adjusted at the ion source and the multiplier collector and is set to about 750 allowing accurate separation of $^3\text{He}^+$ and HD^+ ion signals (Dunai and Touret, 1993).

3.2.4 Ar, Kr, Xe measurement

For the measurements of the heavy noble gases, the water which was transferred to the cold traps during the extraction (about 0.5 g) and all other condensable gases including Ar, Kr and Xe are released by external heating (180°C) of T1 and ZEO1. To remove water vapor the liberated gas phase is transferred to a charcoal trap cooled by liquid nitrogen (C11) by passing dynamically a second Zeolith (ZEO2) (open VM7, VM10 and VM11). This setup acts as a diffusion pump, transporting the gas from the warm T1 and ZEO1 through ZEO2 to the cold C11. The ZEO2, which is filled with 3 Å molecular sieve, is kept at room temperature (20°C) and adsorbs water vapor, but allowing the heavy noble gases to pass through be adsorbed on C11. To ensure complete gas transfer to C11, after 10 minutes the heated ZEO1 is directly connected to C11 by bypassing ZEO2 (open VM8, VM8a, VM12 and VM13).

Afterwards, the water free gas phase is removed by heating C11 to 180°C. Since less than 1% of the dried gas phase extracted from 45 g of water is needed for mass spectrometric analysis of the heavy noble gases, the dry gas phase is expanded into a large reservoir (R_{Dil} , 2000 cm³) by opening valve VM15. Out of R_{Dil} small splits (0.7 cm³) are taken for mass spectrometric analysis. The first small gas split, about 0.3% of the total heavier gas fraction passes by getters (GP1, GP2) that remove all reactive gases, and is then admitted to the first mass spectrometer (MS1) for simultaneous

analysis of Ar, Kr, and Xe. Note that in this first analysis the heavy noble gases are not separated from each other. The noble gas amount, for this step, is adjusted such that Ar can be measured on the Faraday cup, whereas Kr and Xe ions are counted by the electron multiplier of MS1.

Repeated measurements proved that commonly the heavy noble gases (Ar, Kr, and Xe) can be adequately measured simultaneously in the small gas aliquot and that there are basically no ^{40}Ar interferences on the Kr and Xe measurement. In particular, there is no significant increase of background due to ion back-scattering on mass 136 which is used for Xe counting. But even when the electron multiplier is set to maximum sensitivity, the ^{136}Xe count rate of an unseparated gas aliquot (<1,000 Hz) is too low to reach the desired overall precision of the Xe concentration measurement of about 1%. Therefore, Xe is reanalyzed in a second gas aliquot in which the Xe is separated from Ar and Kr by selective adsorption at an activated charcoal cold trap (C1) at -100°C . Later, Xe is released from C1 by heating to 180°C . Note that there is no requirement for complete separation between Xe and Kr. It has to be only guaranteed that Xe is trapped quantitatively. Due to the active transfer of Xe by trapping it on C1 next to MS1, the amount of Xe in the second Xe analysis is increased by a factor of 10, and hence the second ^{136}Xe analysis yields a count rate of more than 10,000 Hz and the counting error drops to 0.3%. The second Xe analysis including the separation requires 40 minutes. After Xe measurement the expansion reservoir R_{Dil} is heated (100°C) and pumped out. A complete analysis of all noble gases takes about 3 hours. If only He and Ne isotopes are measured, the procedure lasts for 1.5 hour.

Table 3.1: Specification of the two mass spectrometers used for noble gas measurements

Spectro- meter	Collector F= Faraday M = Multiplier	Radius (mm)	Mass resolution ⁽¹⁾ ($\bar{m}/\delta m$) (-)	Measured isotopes	Yield
MS1	F	115	~ 50	⁴ He, ²⁰ Ne, ²² Ne, ³⁶ Ar, ⁴⁰ Ar	$10^{-6} \text{ cm}^3 \text{STP} \approx 10^{-10} \text{ A}$
	M	120		²¹ Ne, ⁸⁴ Kr, ¹³⁶ Xe	$10^{-10} \text{ cm}^3 \text{STP} \approx 10^4 \text{ Hz}$
MS2	F	230	~ 750	⁴ He	$10^{-6} \text{ cm}^3 \text{STP} \approx 10^{-10} \text{ A}$
	M	210		³ He	$10^{-10} \text{ cm}^3 \text{STP} \approx 10^4 \text{ Hz}$

⁽¹⁾ The mass resolution is defined as the average mass \bar{m} divided by the mass difference δm of two neighboring resolvable ions.

3.2.5 Tritium measurement

After noble gas analysis, the degassed water sample is transferred back into the original copper tube. To re-close the sample, the length of the sliding aluminum rack holding the tube is reduced by about 3 cm and the copper tube is clamped again. Several months later, ³H is measured indirectly by measuring the ingrowth ³He that was produced by the decay of ³H during storage. The extraction, purification and measuring procedure is analogous to a He, Ne measurement, but simpler. Due to the fact that the extracted gas contains practically only ³He but no Ne, He needs not to be separated from Ne. After extraction both He isotopes are measured in mass spectrometer MS2. Usually a measurable amount of ⁴He indicates a contamination of air during storage or measurement and is therefore used for atmospheric correction. However, in samples with very high initial He concentrations ($>10^{-6} \text{ cm}^3 \text{STP/g}$) sometimes a measurable He residue remains in the water after the noble gas analysis, although the concentrations are reduced by a factor of at least 10^4 . In such cases the ³He/⁴He ratio measured during noble gas analysis can be used to correct for the remaining ³He which otherwise would distort the ³H measurement.

3.2.6 Calibration

Noble gas concentrations and isotopic compositions were calibrated against an air standard by peak height comparison. The well-defined air aliquots of about $0.6 \text{ cm}^3 \text{ STP}$ are taken from reservoir R_{Air} . This reservoir was filled with atmospheric air at a known temperature, pressure and humidity. The noble gas amounts of the air aliquot are calculated using the atmospheric abundances given by Ozima and Podosek (1983), and the $^3\text{He}/^4\text{He}$ ratio given by Clarke et al. (1976). Air aliquots, in the following called slow calibrations, are usually measured after every fifth sample and are prepared with exactly the same conditions as a water sample. Note that slow calibrations are processed either as dry air or wet air. In the later case water vapor from a previously completely degassed water sample is mixed with the air aliquot in order to simulate the real clean up procedures for a water sample.

To compensate for short-term sensitivity changes of the spectrometer, fast calibrations are always carried out immediately before each noble gas analysis. In case of the He and Ne measurement, the fast calibration gas contains either pure He (reservoir FC_{He}) or a mixture of He and Ne (reservoir FC_{HeNe}) and is directly injected into the spectrometer. In contrast, the Ar, Kr, and Xe fast calibration gas (reservoir FC_{AKX}) is the dried gas of a completely degassed water sample, which has been additionally enriched in Xe by a factor of four to increase the Xe count rate in the mass spectrometer. As the AKX fast calibration gas from reservoir FC_{AKX} still contains all atmospheric gases with the exception of water, the aliquot is first cleaned at the getter pumps (GP1 and GP2) before being admitted to the spectrometer MS1.

Each aliquot taken from the standard reservoirs (R_{Air} , FC_{He} , FC_{HeNe} and FC_{AKX}) reduces the total gas amount in the reservoir. Therefore the measured signal has to be corrected using the known individual dilution factors given by the volume of the reservoir divided by the sum of the volume of the reservoir and the volume of the pipette.

The ratios between slow calibration and fast calibration signals, both corrected for dilution, are a measure of the long-term stability of the analysis and are given as follows:

$$E_i = \frac{\overline{FS}_i}{CS_i} \quad [-] \quad (3.1)$$

where \overline{FS}_i is the average signal of the fast calibration measured before and after each slow calibration i , and CS_i the slow calibration signals. The gas volume dissolved in a sample j , SA_j , is calculated as

$$SA_j = \overline{E}_i \cdot CA \cdot \frac{SS_j}{\overline{FS}_j} \quad [\text{cm}^3\text{STP}] \quad (3.2)$$

where SS_j is the measured signal of the sample j , \overline{FS}_j the average signal of the fast calibrations measured before and after sample j , \overline{E}_i the long-term mean of the ratios between fast and slow calibrations and CA the volume of the slow calibration gas (cm^3STP). Dividing SA_j by the sample weight yields the noble gas concentration in $\text{cm}^3\text{STP/g}$.

The error of a single measurement in a spectrometer is given by the uncertainty associated with the regression algorithm applied to compensate for ion-pumping or memory effects during the analysis. In case of a small multiplier signal as for ^3He , this error is mainly determined by the counting statistic. In general, the error of a signal measured on a Faraday cup is much smaller than the error of a multiplier signal (Table 3.2). The total error of one measurement, including that associated with the gas extraction and purification, corresponds to the standard deviation of E_i (ratio between the slow and fast calibration, Equation 3.1) combined with the individual error of each signal. Compared to the long-term stability given by the reproducibility of E_i , the errors of the Faraday measurement are negligible, whereas the errors of the multiplier measurement are smaller but relevant (Table 3.2).

In the case of the ^3H measurement the analyzed gas consists almost of pure ^3He . Therefore it is calibrated only against a pure He standard with a known $^3\text{He}/^4\text{He}$ ratio (reservoir R_{He}). To avoid an increase of the ^3He background no fast calibrations are carried out between the individual ^3He measurements. Thus the concentration of ^3He in the sample is calculated directly by peak high comparison with the calibration gas.

Compared to the noble gas analysis, the tritiogenic ^3He signal of the tritium analysis is two orders of magnitude smaller (about 1 Hz instead of 100 Hz). Therefore the error due to counting statistic is larger (2 - 3%, Table 3.2). The detection limit using a standard water sample of 45g is about 0.1 TU. Using larger water samples (up to 2000g) the amount of ^3He , which is produced by the decay of tritium during storage, is much higher and the tritium concentration can therefore be measured down to about $2 \cdot 10^{-3}$ TU.

Table 3.2: Total error of an individual measurement compared to the typical errors of the signal measured in the spectrometer.

Isotope or ratio	Spectrometer	Collector F = Faraday M = Multiplier	Signal (standard sample)		Typical error of the signal (%)	Typical error of the measurement (%)
			(A)	(Hz)		
^4He	MS1	F	$5 \cdot 10^{-13}$	-	0.1	0.6
^{20}Ne		F	$5 \cdot 10^{-12}$	-	0.02	0.9
$^{20}\text{Ne}/^{22}\text{Ne}$		F	-	-	0.1	0.1
^{21}Ne		M	-	10^4	0.4	1.0
^{40}Ar		F	10^{-10}	-	0.1	0.8
$^{36}\text{Ar}/^{40}\text{Ar}$		F	-	-	0.1	0.1
^{84}Kr		M	-	$5 \cdot 10^4$	0.3	1.0
^{136}Xe		M	-	10^4	0.3	1.3
^4He	MS2	F	10^{-11}	-	0.01	0.5
^3He		M	-	100	0.3	0.5
$^3\text{He}_{\text{tri}}$		M	-	1	2-3	2-3

3.3 Results and Discussion

3.3.1 Standard water samples

In order to monitor the overall reproducibility of sampling, gas extraction, gas purification, gas separation and sample storage, it is useful to routinely measure aliquots of a water standard. The water standard consists of lake water from Lake Alpnach, Switzerland, and was taken in July 1995. Up to now, 24 standard water samples have been processed for noble gas determination. The heavy noble gas isotopes of Ar, Kr and Xe were analyzed in about half of these aliquots, whereas He and Ne isotopes were measured in every standard sample. Of the extracted standard water samples, 15 were taken for tritium analysis.

The results of all measured standard water samples are shown in Figures 3.3 and 3.4, and are summarized in Tables 3.3 to 3.5. As listed in Table 3.3, the standard deviations of the noble gas concentrations are equal to or even smaller than the total errors of the individual measurements, proving that the error calculation of the individual measurement includes all major error sources. Since there are no systematic trends in the measured noble gas concentrations over the last 3 years, any gas loss or gain during storage can be neglected. In contrast to the concentrations, the errors of the isotopic noble gas ratios seem to be slightly under estimated by the total measurement error (Table 3.4). A higher standard deviation of the measured $^3\text{He}/^4\text{He}$ ratio can be explained by the applied correction for the ^3He concentrations measured in the sample, which takes into account that ^3He is produced by in situ ^3H decay since sampling.

In general, lake waters can be expected to be in close equilibrium with the atmosphere during gas exchange. At equilibrium the concentration of each noble gas in water depends on its solubility and on its partial pressure in the gas phase. The noble gases solubilities are themselves functions of the water temperature and salinity. Assuming an atmospheric pressure of 0.949 atm at the altitude of Lake Alpnach (434 m), a salinity of 0.3‰ and saturated water vapor during gas exchange, the equilibrium temperature can be calculated from the measured noble gas concentration. In Table 3.3 the temperatures were derived with the solubility data of Weiss (1970b, 1971), Weiss and Kyser (1978) for He, Ne, Ar and Kr and of Clever

(1979b) for Xe. The equilibrium temperatures during gas exchange calculated from Ne, Ar, Kr and Xe concentrations are in good agreement with each other. But not with the water temperature of 4.5°C . Note that the calculated equilibrium temperature for Ar, Kr or Xe is almost independent of the used solubility data. In contrast, using the solubility of Clever (1979a) for Ne yields an equilibrium temperature of $(6.0 \pm 0.9)^{\circ}\text{C}$ instead of $(5.3 \pm 0.9)^{\circ}\text{C}$. The low He temperature is a result of a small He excess of $10^{-9} \text{ cm}^3\text{STP/g}$ that originates from radiogenic ^4He emanation from the lake bottom (Aeschbach-Hertig, 1994).

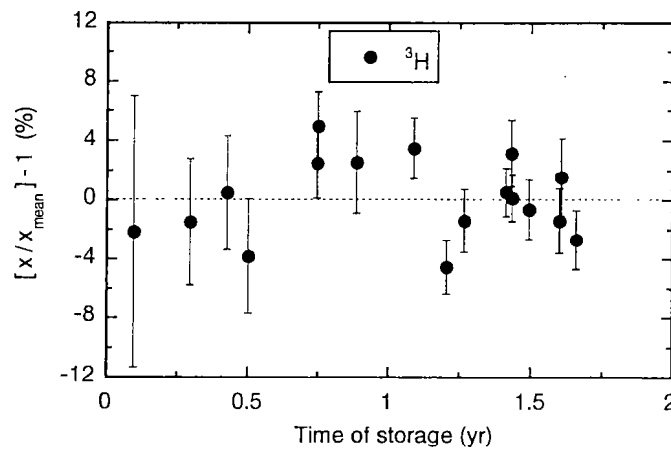


Figure 3.3: Tritium (^3H) concentrations measured in aliquots of the lab-internal freshwater standard normalized to the respective mean values plotted versus the storage time of the extracted sample. The error bars correspond to 1σ error of the individual measurement. With increasing time of storage this error becomes smaller due to a higher multiplier count rate of the tritiogenic ^3He .

Mass Spectrometric System

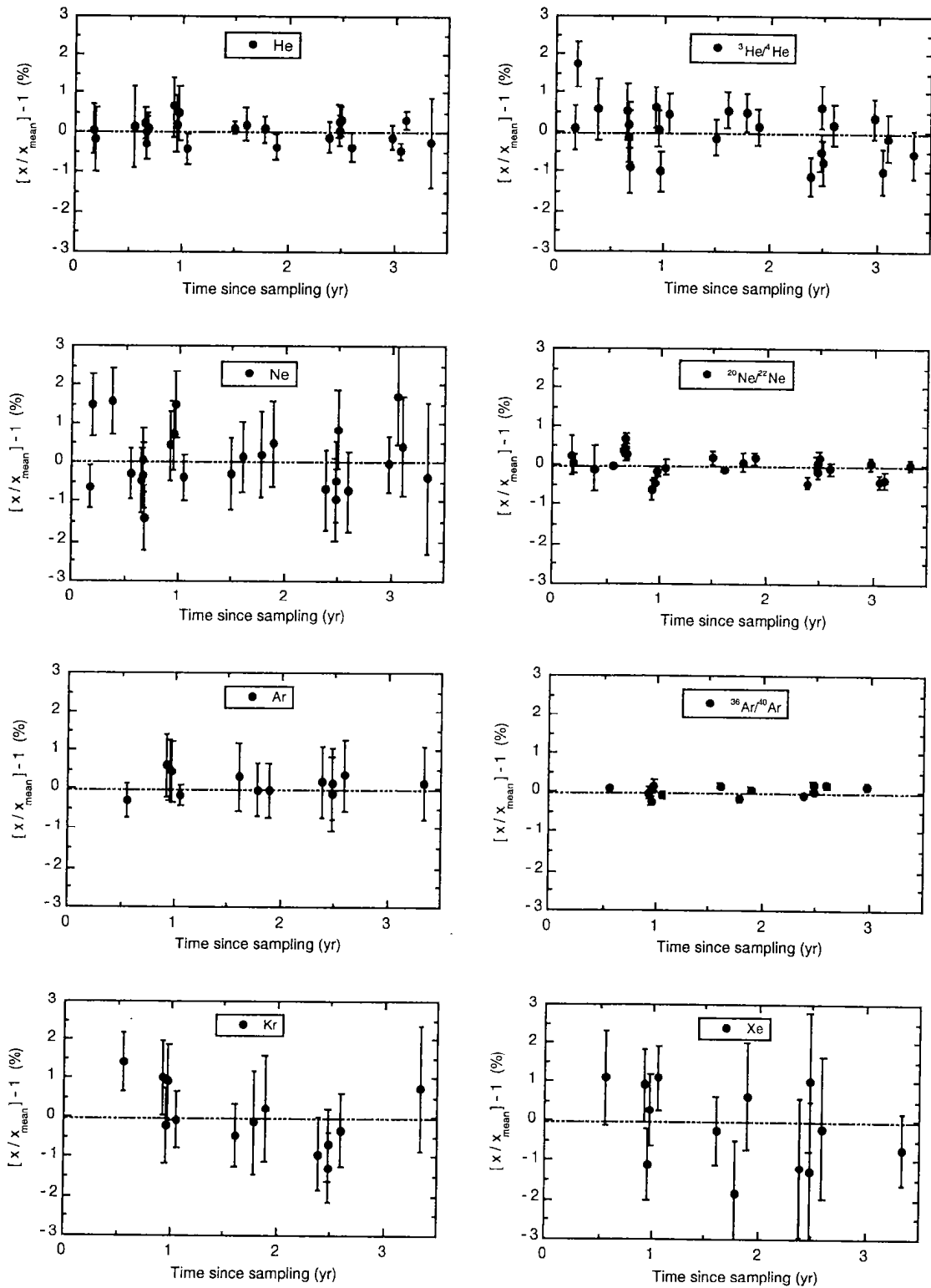


Figure 3.4: Isotopic ratios and concentrations of noble gases measured in aliquots of the lab-internal freshwater standard normalized to the respective mean values plotted versus the time since sampling. The aliquots were collected on 18th July 1995 in Lake Alp-nach at a depth of 29m. The error bars correspond to 1σ error of the individual measurement. The $^3\text{He}/^4\text{He}$ ratios are corrected to time of sampling.

Table 3.3: Average noble gas concentrations and corresponding standard deviations of the internal freshwater standard compared to the mean error of an individual measurement.

Noble gas	Average concentration (\pm standard deviation) (cm ³ STP/g)	Standard deviation (%)	Mean individual error of 1 σ (%)	Calculated equilibrium temperature (°C)
He ⁽¹⁾	$(4.594 \pm 0.035) \cdot 10^{-8}$	0.75	0.63	
He ⁽²⁾	$(4.575 \pm 0.023) \cdot 10^{-8}$	0.50	0.54	
He ⁽³⁾	$(4.585 \pm 0.013) \cdot 10^{-8}$	0.29	0.48	2.0 \pm 0.5
Ne	$(2.005 \pm 0.017) \cdot 10^{-7}$	0.84	0.95	5.3 \pm 0.9
Ar	$(4.080 \pm 0.011) \cdot 10^{-4}$	0.27	0.77	5.4 \pm 0.2
Kr	$(9.826 \pm 0.079) \cdot 10^{-8}$	0.81	1.01	5.6 \pm 0.3
Xe	$(1.456 \pm 0.015) \cdot 10^{-8}$	1.04	1.26	5.8 \pm 0.3

⁽¹⁾ measured in spectrometer MS1

⁽²⁾ measured in spectrometer MS2

⁽³⁾ weighted average and weighted error of the two He concentrations measured on MS1 and MS2

Table 3.4: Average noble gas ratios and corresponding standard deviations of the internal freshwater standard compared to the mean error of an individual measurement.

Isotopic ratio	Atmospheric ratio (-)	Average ratio (\pm standard deviation) (-)	Standard deviation (%)	Mean individual error of 1 σ (%)
³ He/ ⁴ He	$1.384 \cdot 10^{-6}$ ⁽¹⁾	$(1.383 \pm 0.009) \cdot 10^{-6}$ ⁽⁴⁾	0.68	0.55
²⁰ Ne/ ²² Ne	9.80 ⁽²⁾	9.792 \pm 0.029	0.30	0.19
⁴⁰ Ar/ ³⁶ Ar	295.5 ⁽³⁾	295.93 \pm 0.44	0.15	0.09

⁽¹⁾ Clarke et al. (1976)

⁽²⁾ Ozima and Podosek (1983)

⁽³⁾ Steiger and Jäger (1977)

⁽⁴⁾ The ³He/⁴He ratios are corrected to time of sampling.

Table 3.5: Average tritium concentrations and corresponding standard deviations of the internal freshwater standard compared to the mean error of an individual measurement.

Tritium	Average concentration (\pm standard deviation) (TU)	Standard deviation (%)	Mean individual error of 1σ (%)
^3H	18.2 ± 0.5	2.7	2.9

3.3.2 Equilibrated samples

To verify the overall analytical procedure, water was equilibrated with atmospheric air in climate controlled rooms at various temperatures. To this end three open containers (30 dm^3) containing fresh water were placed in temperature stabilized rooms at different temperatures for at least 7 days (samples C1 - C3 in Table 3.6). The water was gently stirred to accelerate and facilitate gas exchange but avoiding any occurrence of bubbles. Samples were taken at the bottom outlet of the containers using standard copper tubes. Both water temperature and total ambient atmospheric pressure were monitored. Even though temperature became stable within the precision of the measurement ($\pm 0.1 \text{ }^\circ\text{C}$), the pressure varied typically by a few mbar over the time of exposure. All pressure readings of the last 7 days prior to sampling were averaged for further calculations (standard deviation $< 3\%$). A few measurements of electrical conductivity showed salinity to be $0.36 \pm 0.1 \text{ } \text{‰}$. This small value hardly affect the noble gas equilibrium concentrations. The uncertainties regarding the conditions during gas exchange have only a small effect on the noble gas equilibrium concentration. Depending on the noble gas, the expected equilibrium concentration varies between 0.3% (He) and 0.5% (Xe). Measured concentrations of the artificially equilibrated samples are listed in Table 3.6.

Table 3.6: Measured concentrations of artificially equilibrated water samples.

Sample	Sampling conditions			Concentrations					
	T (°C)	P (atm)	S (%)	$^3\text{He}\cdot 10^{14}$	$\text{He}\cdot 10^8$	$\text{Ne}\cdot 10^7$	$\text{Ar}\cdot 10^4$	$\text{Kr}\cdot 10^8$	$\text{Xe}\cdot 10^8$
C1	3.8	0.948	0.36	6.28±0.03	4.72±0.02	2.05±0.02	4.27±0.04	10.36±0.09	1.57±0.03
C2	14.5	0.959	0.36	6.08±0.03	4.54±0.02	1.86±0.02	3.36±0.03	7.66±0.10	1.07±0.02
C3	29.4	0.956	0.36	5.85±0.03	4.28±0.02	1.65±0.02	2.51±0.02	5.33±0.06	0.70±0.01

In Figure 3.5 the measured concentrations are compared with three sets of solubility data:

- (i) the *Weiss solubilities*: the data of Weiss (1970b, 1971), and Weiss and Kyser (1978) for He, Ne, Ar, and Kr;
- (ii) the *Clever solubilities*: the data of Clever (1979a, 1980) combined with Smith and Kennedy (1983) for salinity correction;
- (iii) the *Benson solubilities*: the data of Benson and Krause (1976) combined with Smith and Kennedy (1983).

Note that in each set the ^3He equilibrium concentration was calculated with the temperature dependent $^3\text{He}/^4\text{He}$ ratio in water given by Benson and Krause (1980a). Except He all noble gases are in agreement with the solubility data (Figure 3.5). We assume that the He partial pressure in the climate controlled rooms, located below ground level and vented only artificially, is slightly enhanced relative to air, due to the presence of radiogenic ^4He . Indeed, according to the Benson solubilities (Benson and Krause, 1976, 1980a) the measured ^3He concentrations are in equilibrium with the atmosphere.

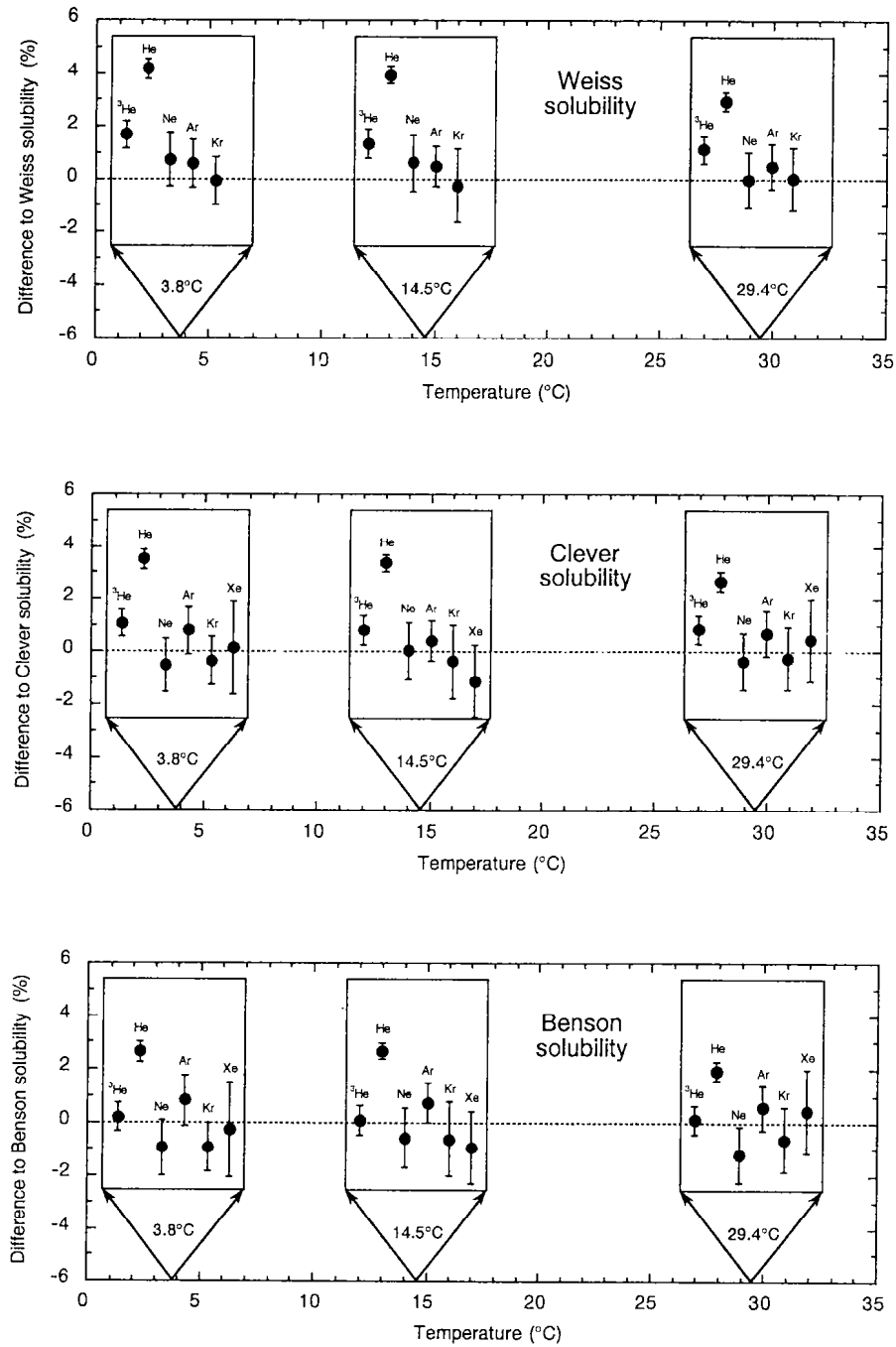


Figure 3.5: Measured noble gas concentrations of artificially equilibrated water samples at 3.8, 14.5 and 29.4 °C compared with three sets of solubility data (definition of sets see text). The difference is plotted in percent relative to the solubility data.

3.3.3 Isotopic fractionation during solution

The solubility of noble gases is mainly dependent on their individual atomic mass. Light noble gases are less soluble than heavier noble gases. This fractionation also theoretically influences the solubility of the different isotopes of one noble gas. For He, the relative difference between isotopic ratios in solution and air at equilibrium is defined as (Benson and Krause, 1980a)

$$\delta^3He_{eq}(\%) = \delta(^3He/^4He)_{eq}(\%) = \frac{R_{eq} - R_{air}}{R_{air}} \cdot 100 = \left(\frac{R_{eq}}{R_{air}} - 1 \right) \cdot 100 \quad (3.3)$$

where R_{air} and R_{eq} are the $^3He/^4He$ ratios in air and in solution, respectively. The δ^3He value measured by Benson and Krause (1980a) varies between -1.8 and -1.5% for water temperatures between 0°C and 40°C.

Aside from the helium isotopes 3He and 4He , hardly any information is available for noble gas isotope fractionation in equilibrated water. Up to now we have processed about 70 samples of surface waters (mainly of rivers and lakes). These data allow to estimate the isotopic fractionation for Ne and Ar. The measured isotopic fractionation factors $\delta^{20}Ne = \delta(^{20}Ne/^22Ne)$ and $\delta^{36}Ar = \delta(^{36}Ar/^40Ar)$ are shown as a stack histogram plot in Figure 3.6. As indicated by our data, fractionation of Ne and Ar isotopes is much smaller than for He isotopes (per mill instead of per cent). Nonetheless, these factors are in agreement with the fractionation of oxygen ($^{32}O_2/^34O_2$) of about -0.8‰ given by Benson and Krause (1980b). A slightly higher fractionation for Ne and Ar isotopes (compared to O_2 isotopes) can be explained by the larger relative mass difference of the two involved isotopes.

Mass Spectrometric System

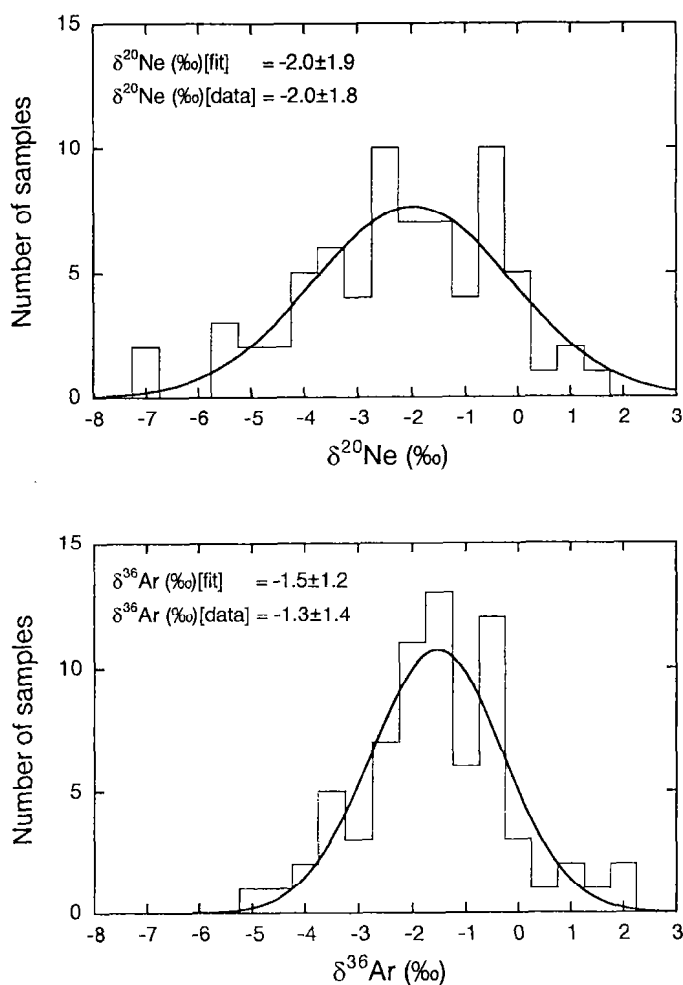


Figure 3.6: Stack histograms of the relative isotopic fractionation factor of $^{20}\text{Ne}/^{22}\text{Ne}$ and $^{36}\text{Ar}/^{40}\text{Ar}$ isotopes of 70 measured surface water samples. The data are distributed around a mean of $(-2.0 \pm 1.8)\text{‰}$ and $(-1.3 \pm 1.4)\text{‰}$, respectively. Both distributions are approximated with a Gaussian function: $(-2.0 \pm 1.9)\text{‰}$ and $(-1.5 \pm 1.2)\text{‰}$.

In conclusion, the system presented here for the measurement of noble gases and tritium in water samples yields coherent results and offers a powerful tool for the study of natural water systems. In the near future, we plan to lower the detection limit of the mass spectrometer by higher sensitivity $^3\text{He}/^4\text{He}$ mass spectrometry. This improvement will reduce significantly the waiting period between the noble gas and tritium analysis, which is at the moment at least 3 months.

Recharge conditions and groundwater age deduced from noble gas concentrations

As outlined in chapter 2, noble gases dissolved in groundwater can have an atmospheric (equilibrium, excess air) and a non-atmospheric (radiogenic, tritiogenic) origin. This chapter focuses on the interpretation of the different noble gas components with regard to their application in groundwater studies.

The atmospheric noble gas component is determined by the conditions prevailing at the last gas exchange with the atmosphere, such as water temperature and salinity, atmospheric pressure, and excess air. Usually it is possible to find reasonable values for the salinity and the atmospheric pressure. Therefore the amount of excess air and the temperature at recharge can be deduced from the atmospheric noble gas concentrations by least squares fitting (section 4.1.3). First, the principle of using paleogroundwater as an archive of past climate (section 4.1.1), and the link between the noble gas temperature and the temperature of the atmosphere are discussed (section 4.1.2). Finally, the potential of the least squares fitting method to estimate the altitude of the recharge area is illustrated with a few examples in section 4.1.4.

In Section 4.2 the non-atmospheric noble gas components are used to derive the typical scale of the groundwater residence time. First, section 4.2.1 puts emphasis on the $^3\text{H}/^3\text{He}$ dating method (groundwater age < 50 years). It is shown how the tritiogenic ^3He component can be separated from all other ^3He components. Second, the estimation of the residence time (up to several millions of years) with radiogenic noble gases ^4He , ^{21}Ne and ^{40}Ar is outlined (section 4.2.2).

During groundwater flow, the noble gas concentrations are influenced by dispersion and possibly by mixing. In section 4.3.1 the effect of groundwater mixing on the

noble gas temperature and on the $^3\text{H}/^3\text{He}$ water age is discussed. In section 4.3.2, theoretical considerations are outlined about how groundwater dispersion affects a temperature signal recorded by noble gas concentrations in a groundwater system.

4.1 Interpretation of atmospheric noble gas concentrations

4.1.1 The principle of the noble gas thermometer

Since the fundamental work of Mazor (1972) noble gas measurements in groundwater have been used in several studies to derive paleotemperatures during the last glacial period (e.g. Bath et al., 1979; Rudolph et al., 1984; Stute et al., 1992a; Andrews et al., 1994; Stute et al., 1995a; Stute et al., 1995b). The principle of the noble gas thermometer is that the solubility of noble gases in water is temperature dependent. Therefore old groundwaters contain dissolved atmospheric noble gases in concentrations that are mainly defined by the ambient temperature prevailing at the time of recharge. If the residence time of the groundwater is known, e.g. by means of groundwater dating, temperatures calculated from the observed noble gas concentrations can provide a relevant paleotemperature record (Figure 4.1). Because of the physical relation between noble gas concentration and temperature known as Henry's law, this 'noble gas thermometer method' can be used to directly reconstruct paleotemperatures. In contrast, other techniques of paleoclimatic reconstruction are, for example, based on the isotopic composition of the water molecule in all kind of well dated environmental archives (groundwaters, lake/ocean sediments, and ice cores); further on the width of tree rings; or on the types of pollen in dated paleosoils or sediment cores.

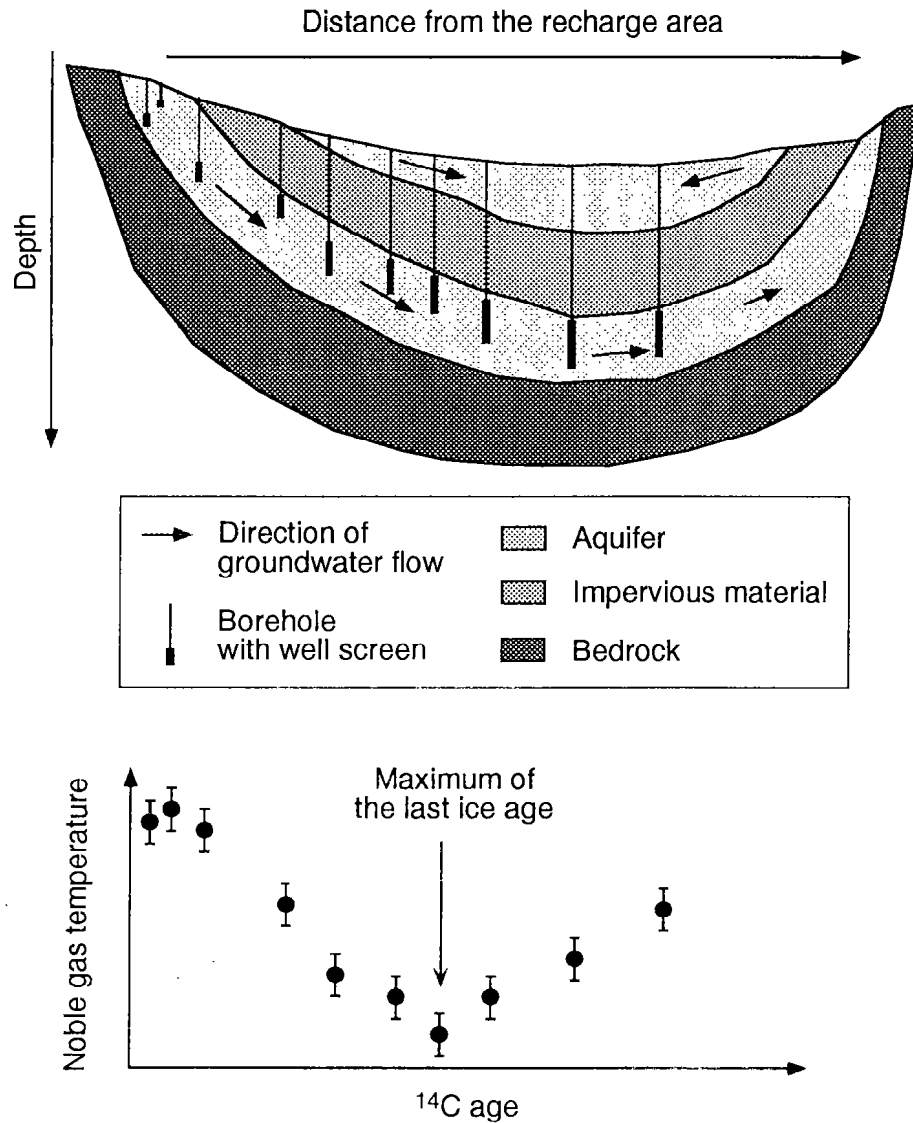


Figure 4.1: (Top) Paleogroundwater as an archive of past climate. The confined paleogroundwater system is separated from upper shallow groundwater by poorly permeable sediments. Groundwater flows from the recharge area (left) to the discharge area (right). (Bottom) The concentrations of dissolved noble gases allow the temperature at which the groundwater infiltrated to be reconstructed. If the groundwater can be reasonably dated, for example with ¹⁴C, the coupling of the age scale with the calculated noble gas temperature provides a relevant paleotemperature record. (Figure adapted from M. Stute, pers. comm.)

4.1.2 Impact of ground and air temperature on noble gas temperature

The calculation of the noble gas temperature is outlined in the next section. First some theoretical considerations are done to explain the relation between noble gas temperature and the atmospheric temperature.

For most recharge areas the groundwater temperature at the water table reflects the prevailing ground temperature. Exceptions can occur in cases where the infiltrated water has not sufficient time to equilibrate with the soil (e.g., very high infiltration rates or fast infiltration such as in karstic areas). Daily variations in atmospheric temperature penetrate only to a depth of about 50cm to 1m into the ground (as an example see Figure 4.2). Since groundwater tables lie commonly deeper than one meter below the soil surface daily temperature variations can be neglected.

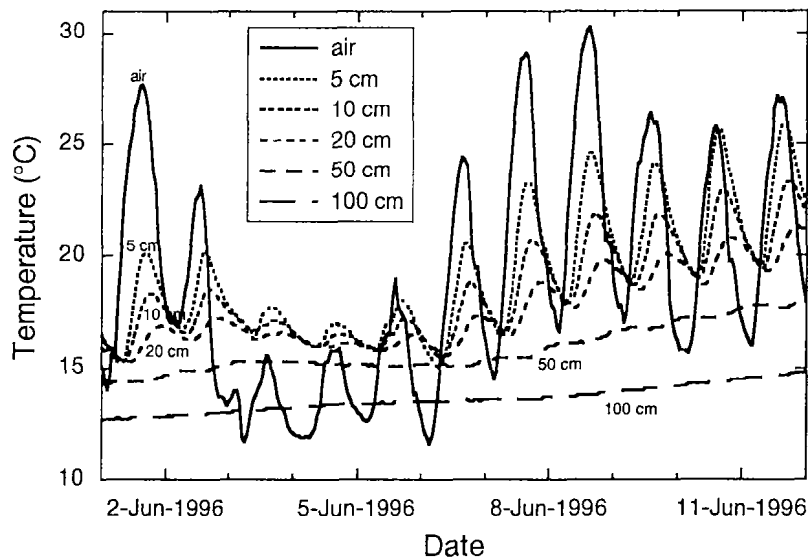


Figure 4.2: Air and soil temperatures during the beginning of June 1996 at the meteorological station in Zürich, Switzerland. The soil temperature is measured at different depths (5cm, 10cm, 20cm, 50cm and 100cm) below ground level. Daily fluctuations of the atmospheric temperature penetrate at maximum to a depth of 50cm and are completely attenuated at 1m. Due to the attenuation of the annual temperature signal, the ground temperature in summer decreasing with depth, whereas in winter ground temperatures are normally higher than air temperatures.

Seasonal fluctuation of the ground temperature oscillates around the mean ground temperature and decreases exponentially with depth (e.g. Matthess, 1982). The soil temperature T_s , as a function of time and depth in relation to the annual amplitude T_a , can be described according to Stute and Sonntag (1992)

$$T_s(z, t) = T_s(z=0) + T_a \cdot \exp\left(-\frac{z}{\bar{z}}\right) \cdot \sin\left(\omega t - \frac{z}{\bar{z}} + \phi\right) + \frac{\Delta T}{\Delta z} z \quad [^\circ\text{C}] \quad (4.1)$$

where \bar{z} is the average penetration depth of the seasonal temperature variation, ω is $(1\text{yr}/2\pi)^{-1}$, ϕ is the phase shift in relation to the atmospheric forcing and $\Delta T/\Delta z$ is the geothermal gradient ($\approx 3^\circ\text{C}/100\text{m}$). Typical values for Europe are $\phi \approx 2/3\pi$ and $\bar{z} \approx 2.5\text{m}$ (Stute and Sonntag, 1992). Assuming 10°C for T_s and T_a , the amplitude of the temperature oscillation at a depth of 5m is about 1.4°C (Figure 4.3).

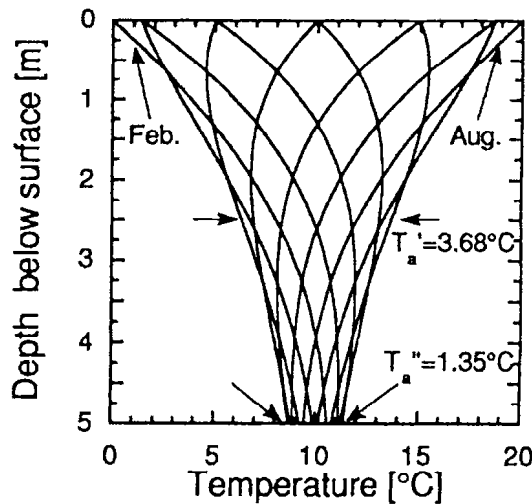


Figure 4.3: Simulated annual variation of the monthly averaged ground temperature profile as a function of depth below surface for a typical soil. The following parameters were used: $T_s = T_a = 10^\circ\text{C}$, $\bar{z} = 2.5\text{m}$. At 2.5m and 5m depth, the amplitude of the temperature oscillation is reduced to e^{-1} (3.68°C) and e^{-2} (1.35°C), respectively. Figure is taken from Stute and Schlosser (1993).

Although the penetration of the seasonal variations depends on the soil cover (e.g., open land has a lower penetration than forest, Matthess, 1982), below 10-15m seasonal variations are usually no longer detectable. In contrast, in recharge areas where the water table is close to the surface, the calculated noble gas temperatures show seasonal fluctuations (see chapter 5). But due to dispersion these oscillations

will be smoothed out along the groundwater flow. The impact of dispersion is discussed in more detail in section 4.3.2.

Besides the ground temperature fluctuation, variation in the precipitation might have an impact on the recorded noble gas temperature. In a first order approximation, the average noble gas temperature should somehow be weighted with the infiltration rate and is therefore not equal to the average ground temperature. However, if temperature variations are insignificant at the water table, the noble gas temperature will be not affected by a variable infiltration rate. Stute and Schlosser (1993) have shown that the difference between mean annual ground temperature and average noble gas temperature depends on (i) the variation of the infiltration rate, (ii) the depth below the water table, and (iii) the properties of the groundwater flow (flow velocity and dispersion). Although these parameters can only be approximated, the offset between the mean annual ground temperature and the recorded recharge temperature can hardly exceed 1-2°C (Stute and Schlosser, 1993).

Noble gas temperatures are usually compared to the mean atmospheric temperature in the recharge area. It is often assumed that the mean ground temperature is equal to the mean air temperature. A comparison of mean annual soil and air temperatures at selected sites in the United States is given by Smith et al. (1964). In most areas of the United States, the mean annual air temperature is a consistently good indication of the mean annual soil temperature although the latter is in general a little higher (about 1°C). In dry climate regions this effect is even more pronounced (Smith et al., 1964). In contrast, some data from western Europe show soil temperatures to be lower than the air temperatures (Smith et al., 1964). This relation has been attributed to the cold rains and/or to evaporation, but the reduction of solar radiation by the cloud cover may also be an important factor. Smith et al. (1964) observed that in areas where the mean annual air temperature is low, the difference between soil and air temperature tends to grow in direction of warmer soil temperatures. At higher altitudes the insulating effect of snow cover is likely responsible for warmer soil temperatures. Theoretically, any kind of cover can potentially influence the mean soil temperature, but hardly any data show any significant effects (Smith et al., 1964).

In practice, the noble gas temperature of a recent groundwater is often equal to or not distinguishable from the mean annual atmospheric temperature in the recharge area

(Stute and Sonntag, 1992). Even if there are some deviations from the mean air or ground temperature, the absolute difference between two noble gas temperatures (e.g. recent climate and last glacial period) is well defined assuming similar infiltration regimes and soil covers. However, in some special cases deviation of the noble gas temperature from annual mean temperature cannot be exclusively interpreted in terms of atmospheric temperature changes. For example, if climate change has a dramatic effect on the depth of the water table (drier or more humid climate), the geothermal gradient has to be taken into account. Or, noble gas temperatures may be affected by a change of the period when groundwater predominantly infiltrates (e.g., preferentially precipitation in summer instead of winter, or occasionally ice or snow cover).

4.1.3 Calculation of noble gas temperature and excess air

In the following, the theoretical concepts for the reconstruction of recharge conditions, especially temperature, from measured noble gas concentrations in groundwater are presented. For more details the reader is referred to Aeschbach-Hertig et al. (1999).

As outlined in chapter 2, the initial concentration of atmospheric noble gases ($i = \text{He, Ne, Ar, Kr, and Xe}$) in groundwater, that involves all relevant components and processes (equilibrium, excess air, and degassing) is given as

$$C_i^{init} = C_i^{eq}(T, S, P) + A \cdot z_i \cdot \exp\left(-R \frac{D_i}{D_{Ne}}\right) \quad [\text{cm}^3 \text{STP/g}] \quad (4.2)$$

In Equation (4.2) C_i^{eq} is the equilibrium concentration as a function of the ambient temperature T , the salinity S and the pressure P (section 2.2), z_i is the volume fraction of gas i in dry air (Equation 2.17, Table 2.1) and D_i is the molecular diffusion coefficient of the noble gas i (Table 2.3).

Relative to equilibrium component the measured concentration is often elevated due to the presence of a certain amount of excess air A (in $\text{cm}^3\text{STP}_{\text{Luft}}/\text{g}_{\text{water}}$), which can maybe fractionated because of partial re-equilibration being described by the dimensionless re-equilibration parameter R (see Equation 2.20). Note that this re-equilibration is assumed to happen immediately after groundwater infiltration close to the water table where the hydraulic pressure is still too small to prevent degassing.

In addition to noble gases derived from the atmosphere, some noble gas isotopes can originate from other sources as discussed in section 2.4. Therefore Equation (4.2) can be applied for He only if the measured He concentration can be split in an atmospheric and non atmospheric component. Unfortunately in paleogroundwaters the radiogenic ^4He component often exceeds the atmospheric equilibrium concentration by many orders of magnitude. Hence, ^4He cannot be directly used for the determination of recharge temperatures, but it can be interpreted in terms of groundwater residence time (section 4.2.2). It should be noted that the difference between the measured He concentration and the result of Equation (4.2) evaluated yields the best estimate of the non-atmospheric He component. ^3He is rarely an alternative to ^4He , because non-atmospheric ^3He can originate from nucleogenic production in the crust, from a migration of mantle gases characterized by a high $^3\text{He}/^4\text{He}$ ratio, or from tritium decay. However, providing that any tritiogenic ^3He can be excluded and that the terrigenic $^3\text{He}/^4\text{He}$ ratio can be reasonably determined, the measured ^3He and ^4He concentrations can help to decide whether or how the excess air component is fractionated. Radiogenic ^{40}Ar produced by decay of ^{40}K is usually masked by the large atmospheric Ar concentration in natural waters. If nevertheless the $^{40}\text{Ar}/^{36}\text{Ar}$ ratio significantly exceeds the atmospheric value, ^{36}Ar can be used to calculate the atmospheric Ar component. The accumulation of other non-atmospheric noble gases is normally not relevant compared to the large amounts of initially dissolved atmospheric noble gases (see section 2.4.3).

As an example of the initial noble gas concentrations described by Equation (4.2), a hypothetical groundwater sample that equilibrated at $T = 10^\circ\text{C}$ and $P = 1$ atm and has a contribution of excess air of $A = 3 \cdot 10^{-3} \text{ cm}^3\text{STP/g}$ ($\Delta N_e = 27\%$) and $S = R = 0$ was calculated with the *Weiss solubilities* (section 2.2). In order to investigate both the sensitivity of the concentrations with respect to the parameters and the correlations among the parameters controlling noble gas dissolution, the relative changes of the

concentrations for standard changes of these parameters were calculated (Table 4.1). Obviously, the dependence of noble gas concentrations on the parameters follows some systematic trends. The effects of T and S increase with molar mass of the gas, whereas the effect of excess air decreases reflecting the fact that the solubilities strongly increase with the molar mass. Degassing also affects preferentially the light noble gases, particularly He, because of their higher diffusivities. Pressure has a uniform effect relative to equilibrium concentrations, but in the presence of an excess air component it is relatively more important for the heavy noble gases. From Table 4.1 it can easily be seen which parameter combinations are well identifiable, because they have very different patterns of effects (e.g., T and A), and which are hard to separate, because they have almost identical effects (e.g., S and P), which can compensate each other. Note that these findings are general and do not depend on the choice of noble gas solubilities.

Table 4.1: Concentration changes induced by specified small changes of the parameters, relative to a hypothetical groundwater (temperature $T = 10^\circ\text{C}$, salinity $S = 0\text{‰}$, pressure $P = 1$ atm, amount of excess air $A = 3 \cdot 10^{-3}$ cm³STP/g, and re-equilibration parameter $R = 0$)

Initial concentration	He (cm ³ STP/g)	Ne (cm ³ STP/g)	Ar (cm ³ STP/g)	Kr (cm ³ STP/g)	Xe (cm ³ STP/g)
C_i^{init}	$6.217 \cdot 10^{-8}$	$2.563 \cdot 10^{-7}$	$4.141 \cdot 10^{-4}$	$9.445 \cdot 10^{-8}$	$1.344 \cdot 10^{-8}$
<i>(Weiss solubilities)</i>					
Parameter changes	ΔHe (%)	ΔNe (%)	ΔAr (%)	ΔKr (%)	ΔXe (%)
$\Delta T = 1^\circ\text{C}$	-0.32	-0.74	-2.12	-2.71	-3.35
$\Delta S = 1\text{‰}$	-0.42	-0.48	-0.67	-0.72	-0.77
$\Delta P = 0.01$ atm	0.76	0.80	0.94	0.98	0.99
$\Delta A = 10^{-4}$ cm ³ STP/g	0.84	0.71	0.23	0.12	0.06
$\Delta R = 0.1$	-4.44	-2.03	-0.42	-0.14	-0.06

The non-linear system of equation (4.2) contains five unknown parameters (T : temperature, S : salinity, P : pressure, A : amount of excess air, R : re-equilibration parameter) and one equation for each of the four or five applicable noble gases. Because of the errors of the measured concentrations, it is not advisable to look for exact solutions of the equations, but for parameter combinations that provide model predictions which agree with the measured data within experimental error. If some parameters are either known or prescribed, such that the number of free parameters becomes smaller than the number of applicable measured gases, the system (4.2) is over-determined and can be solved by a least squares method.

Different conceptual sub-models can be derived from Equation (4.2). For instance, in surface waters it appears reasonable to set A and R zero, thus reducing the model to atmospheric equilibrium. In groundwaters, at least A (i.e. unfractionated excess air) has to be included. Most often, S and P are well known (i.e. small salinity during infiltration and known altitude of the recharge area), and the recharge temperature T is searched for. In principle, it is also possible to derive estimates of the other environmental parameters S , P , A and R .

In the following the method described by Aeschbach-Hertig et al. (1999) to solve the equation system (4.2) for any subset of up to three of the five model parameters is outlined. The parameters are determined such that the sum of the weighted squared deviations between the modeled and measured concentrations is minimized. The goal function to be minimized is:

$$\chi^2 = \sum_i \frac{(C_i - C_i^{\text{mod}})^2}{\sigma_i^2} \quad [-] \quad (4.3)$$

where C_i^{mod} are the modeled, C_i the measured concentrations, and σ_i their experimental 1σ -errors.

Standard methods of least squares fitting can be applied to solve the minimization problem (4.3). The used code is based on the mathematical software MATLAB[®] and the Levenberg-Marquardt method (Press et al., 1986) to minimize χ^2 . It includes tools for statistical and graphical analysis of the output data. Since there were no restrictions of the range of possible parameter values implemented, solutions with

unphysical values (e.g., negative values of any parameter) should be discarded, and a different conceptual model should be used.

The presented approach to derive environmental parameters from noble gas concentrations in waters is quite different from the traditional approach to determine recharge temperatures from noble gases in groundwaters (e.g., Stute and Schlosser, 1993). The latter method uses the temperature as fit target, i.e., it looks for parameter values of A and R (P and S are basically prescribed) such that the spread of the temperatures calculated individually from Ne, Ar, Kr, and Xe is minimized. The measured concentrations are corrected for (fractionated) excess air and a temperature is calculated from the corrected concentration of each noble gas. This process is iteratively repeated with varying amounts of excess air until optimum agreement between the four temperatures is reached. The noble gas temperature is taken as the mean, its error as the standard deviation of the individual temperatures. In contrast, the approach described here treats all physical parameters in the same way, rather than focusing on temperature alone.

The new approach has a number of advantages compared to the traditional method. First, the contribution of each noble gas to the goal function is weighted with the individual experimental errors. In the traditional approach, the experimental errors are not considered, and the temperature derived from each noble gas species has equal weight. However, because the sensitivity to temperature increases with molecular weight, the temperatures derived from the heavy noble gases should have higher weights if all gases were determined with the same precision. Because of the different weighting, the temperatures derived from the two approaches differ slightly but not systematically. As an example the noble gas temperature of 42 groundwater samples from the Linsental aquifer (see chapter 5) were calculated with both methods and are plotted in Figure 4.4.

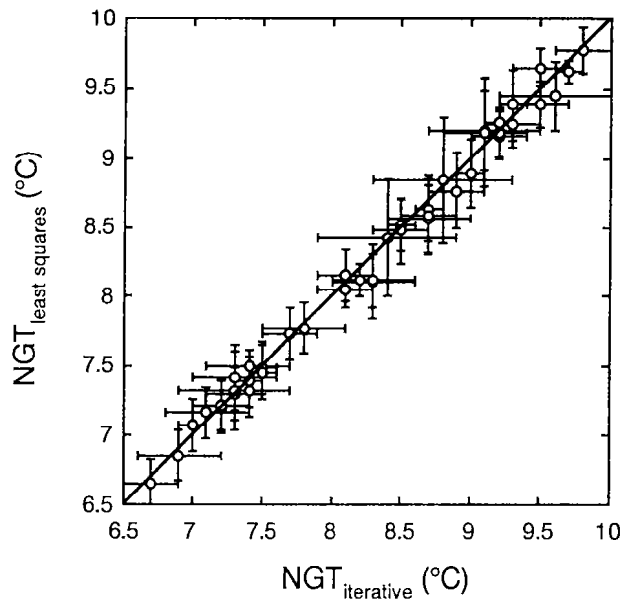


Figure 4.4: Noble gas temperatures (NGT) of 42 groundwater samples from the Linsental aquifer calculated with the iterative method of Stute and Schlosser (1993) ($\text{NGT}_{\text{iterative}}$) versus noble gas temperatures calculated with the least squares method of Aeschbach-Hertig et al. (1999) ($\text{NGT}_{\text{least squares}}$). However, the noble temperatures and the corresponding errors are slightly different, the deviation is not systematically.

A second advantage is that the experimental errors can be used to judge the quality of the fit, i.e. the validity of the conceptual model that was adopted to describe the data. The decision whether or not additional parameters such as excess air or re-equilibration have to be invoked to consistently explain the experimental data is based on the χ^2 -test. If the minimum χ^2 found for a particular model is so high that the probability of obtaining a χ^2 equal to or larger than this value by chance is lower than some cut-off value, the model has to be rejected. Commonly models with probability $p < 0.05$ have to be rejected with respect to statistics. This cut-off value is equivalent to the requirement that the modeled concentrations lie within the 2σ -error of the measured values. If a model has to be rejected, a different model, possibly with an additional parameter, should be applied.

The third advantage of this approach is that confidence intervals for the derived parameters can be calculated and the correlation between the parameters can be studied. In the theory of least squares fitting, uncertainties of the estimated parameters are derived from the covariance matrix (Press et al., 1986). These errors

correspond to a rigorous propagation of the experimental uncertainties, if the latter are independent and normally distributed. If this condition can be not fulfilled, the errors may be propagated numerically by a Monte Carlo simulation. In the Monte Carlo calculations, a prescribed number of artificial data sets are randomly generated from each measured set of concentrations, according to the experimental errors and their distribution. For each generated data set, the optimal parameter values are calculated. Finally, the distribution of the so calculated parameters is analyzed. In case that the experimental errors are normally distributed, the theoretical (from covariance analysis) and numerical (from Monte Carlo) error estimates of the parameters should be the same (Press et al., 1986).

For more details about the error calculation the reader is referred to Aeschbach-Hertig et al. (1999).

Besides the uncertainties of the parameters, also their mutual correlations can be obtained from the covariance matrix. High correlations between two or more parameters occur when a change in one parameter can be approximately compensated by corresponding changes in the others. Such ill-defined parameter sets are the combination of temperature T and excess air A with an additional parameter either S or P . For each variation of T , there is a corresponding value for P or S which keeps the change of χ^2 small, because S and P are strongly correlate. As listed in Table 4.1, increasing temperature have almost the same effect on the noble gas solubility as increasing salinity or decreasing pressure. Thus, for groundwaters it is essential to have a good control on S and P , if the temperature is to be determined with reasonable accuracy. Fortunately, this is usually no problem. On the other hand, if salinity or pressure shall be determined, then T should be known.

At best, recharge temperatures in groundwater can be determine with a precision of 0.2 - 0.3°C (see Figure 4.2 and chapter 5). If it is necessary to assume a fractionation of the excess air in order to achieve a good fit, noble gas temperatures are worse defined and the errors increase to about 1 - 3°C (Aeschbach-Hertig et al., 1999). In cases in which the noble gas pattern is slightly disturbed and no model provide a very good fit, errors of calculated noble gas temperatures can be in the order of about 1°C.

4.1.4 Determination of the recharge altitude

In this section, the potential of the least squares method for the determination of the recharge altitude is discussed. In contrast to the determination of the recharge temperature T , the pressure P is the goal parameter. As an example 5 samples from 3 different alpine sites in Switzerland were taken (Table 4.2). Two samples from a shallow aquifer in the alpine valley Engadin close to the village Sils were taken at an altitude of about 1800m (SI1 and SI2). Two samples were obtained from a shallow aquifer in the Val Roseg, at an altitude of about 2000m in a distance of two kilometers from a glacier (VR1 and VR2). One sample was taken from a thermal spring near Bad Ragaz, at an altitude of about 700m (BRT).

Table 4.2: Observed conditions at sampling and measured noble gas concentrations of selected alpine groundwater samples.

Sample ⁽¹⁾	sampling conditions				noble gas concentrations				
	T (°C)	P (atm)	H (m)	S (‰)	He · 10 ⁸ (cm ³ STP/g)	Ne · 10 ⁷ (cm ³ STP/g)	Ar · 10 ⁴ (cm ³ STP/g)	Kr · 10 ⁸ (cm ³ STP/g)	Xe · 10 ⁹ (cm ³ STP/g)
SI1	3	0.805	1800	0	25.1 ± 0.1	2.12 ± 0.02	3.97 ± 0.03	9.45 ± 0.13	1.40 ± 0.02
SI2	3	0.805	1800	0	36.1 ± 0.1	2.12 ± 0.02	3.95 ± 0.03	9.34 ± 0.12	1.38 ± 0.02
BRT	36	0.920	690	0	1197 ± 10	2.06 ± 0.02	3.49 ± 0.03 ⁽²⁾	7.81 ± 0.07	1.14 ± 0.02
VR1	2	0.786	2000	0	5.20 ± 0.02	2.13 ± 0.02	3.92 ± 0.04	9.25 ± 0.09	1.37 ± 0.02
VR2	4.5	0.786	2000	0	90.0 ± 0.3	2.36 ± 0.02	4.04 ± 0.04	9.24 ± 0.09	1.34 ± 0.02

⁽¹⁾ Sample names: SI = Sils; BRT = Bad Ragaz, thermal spring; VR = Val Roseg.

⁽²⁾ The atmospheric Ar of sample BRT was calculated from ³⁶Ar, due to the presence of radiogenic ⁴⁰Ar.

In all cases, the water may have infiltrated at altitudes substantially higher than at the place of sampling. Therefore, we have to treat the pressure as a free parameter, and a logical approach would be to fit the data with temperature, pressure and excess air as free parameters, although we know that it is badly defined due to the strong correlation between temperature T and pressure P . Indeed, quite erratic results and large errors are obtained for the pressure P and the altitude H , respectively (Table 4.3).

Table 4.3: Fit results with *Weiss solubilities* (definition see section 2.2) for alpine groundwater samples of Table 4.2. Temperature T , Pressure P , and excess air A are the free parameters. The altitude H was calculated from the pressure P using Equation 2.14.

Sample	$He_{terr}^{(1)}$ (cm ³ STP/g)	χ^2	$p^{(2)}$	T (°C)	$A \cdot 10^4$ (cm ³ STP/g)	P (atm)	H (m)	$r_{TP}^{(3)}$	$r_{TA}^{(3)}$	$r_{PA}^{(3)}$
SI1	$20.2 \cdot 10^8$	0.01	0.92	5 ± 2	13 ± 5	0.886 ± 0.056	1000 ± 520	0.993	-0.938	-0.962
SI2	$31.2 \cdot 10^8$	0.10	0.75	6 ± 2	12 ± 5	0.906 ± 0.057	820 ± 530	0.993	-0.940	-0.963
BRT	$1192 \cdot 10^8$	1.34	0.25	9 ± 3	22 ± 7	0.822 ± 0.081	1630 ± 820	0.995	-0.963	-0.977
VR1	$0.22 \cdot 10^8$	0.28	0.59	6 ± 2	15 ± 6	0.882 ± 0.073	1040 ± 690	0.995	-0.965	-0.978
VR2	$84.4 \cdot 10^8$	0.72	0.40	10 ± 3	20 ± 7	0.986 ± 0.083	120 ± 700	0.995	-0.965	-0.979

⁽¹⁾ Terrigenous (non-atmospheric) He component given by the difference between measured and modeled He concentration.

⁽²⁾ Probability: a good fit provides a $p \geq 0.05$.

⁽³⁾ Correlation coefficient between two parameters (e.g. r_{TP} : correlation between parameters T and P)

In this discussion, P and H are always related by Equation (2.14) with $H_0 = 8300\text{m}$. The Sils samples (SI1 and SI2) give relatively uniform altitudes between 800 and 1000m. The individual error of the altitudes is about $\pm 500\text{m}$. Obviously, these altitudes are too low, since the samples were taken at 1800m. For the Val Roseg samples (VR1 and VR2), the altitude can be estimated with an uncertainty of $\pm 700\text{m}$, but the results scatter greatly, between 100 and 1000m. The thermal water from Bad Ragaz yields an altitude of $1600 \pm 800\text{m}$, and a temperature of $9.3 \pm 2.7^\circ\text{C}$. However, mean annual temperatures at 1600m altitude in the Swiss Alps are only about 3°C , thus the altitude and temperature results are inconsistent.

Hence, we tried to determine the recharge altitude by looking for pairs of temperature T and altitude H that are consistent with the local meteorological relationship between air temperature and altitude. From the meteorological data given by Schüepp (1981), the following approximate relation was derived:

$$T_{air} = 11.5 - 0.005 \cdot H \quad [^\circ\text{C}] \quad (4.4)$$

where T_{air} is the air temperature in $^\circ\text{C}$ at the altitude of H (in meters above sea level). For this approach, a series of altitudes between 0 and 3000m were prescribed and a

model with only temperature T and excess air A as free parameters was then solved for each altitude. The results are nearly straight lines in the T-H plain (Figure 4.5).

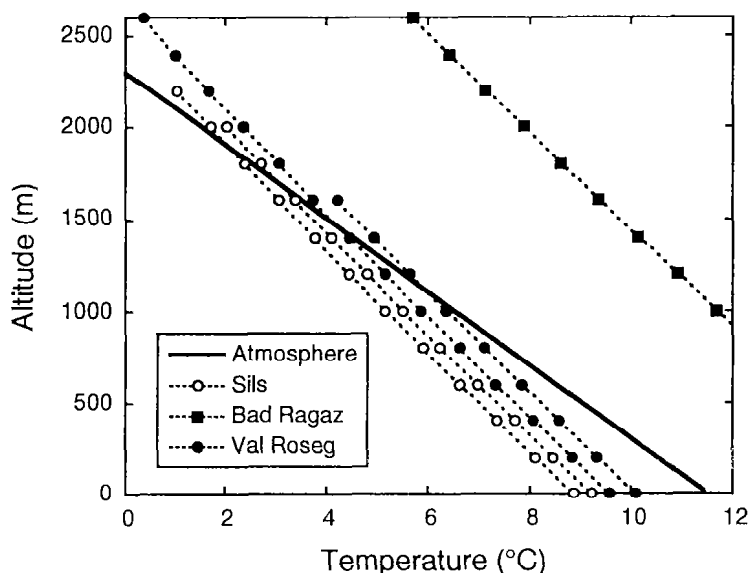


Figure 4.5: Noble gas temperatures of alpine groundwaters in dependence of the assumed recharge altitude. The results of temperature and excess air (T and A) fits for a series of prescribed altitudes are shown as points. The points obtained from each sample are connected by lines, illustrating the pressure dependence of the calculated noble gas temperatures. Only results from statistically significant and physically reasonable T and A fits are shown ($p \geq 0.05$, $A \geq 0$). The bold line represents Equation (4.4), the local relationship between mean annual air temperature and geographical altitude. If the recharge temperature were equal to the mean annual air temperature, the intersection of each sample line with the bold line would indicate the recharge altitude. This appears to be approximately true for the Sils samples (SI1 and SI2), whereas the other samples must have infiltrated at temperatures higher than the mean annual air temperature.

Consistent T-H pairs are those which intersect representing the atmospheric condition (Equation 4.4). Unfortunately, the lines intersect at a small angle and the solutions are therefore not precisely defined. For the two Sils samples there are intersections close to the sampling altitude of 1800m. These samples may therefore be interpreted as

water that infiltrated locally at the mean annual temperature of about 2.5°C. For the samples from Val Roseg, the intersections lie at too low altitudes. Or, since we know that recharge must have taken place at altitudes higher than 2000m, they indicate noble gas temperatures above the local mean annual air temperature. In fact, this is not so surprising, since according to Equation (4.4) mean annual temperatures at these altitudes are close to the freezing point. Thus, recharge can only take place during the warm season. As outline in section 4.1.2, in cold regions with long periods of snow cover, ground temperatures can be several degrees above the mean annual air temperatures.

These arguments appear insufficient to explain the comparatively high noble gas temperature of the thermal water from Bad Ragaz. Nevertheless, this water probably infiltrated as meteoric water at high altitude and later picked up heat (spring temperature is 36°C) and radiogenic gases during deep circulation. It has by far the highest amount of radiogenic He of the samples used in this study and it is the only sample with significant radiogenic ^{40}Ar ($^{40}\text{Ar}/^{36}\text{Ar} = 300 \pm 1$). However, the calculation of the recharge altitude is completely impossible for this sample.

To summarize, the determination of recharge altitude is hampered by two independent problems. First, the model parameters temperature T and pressure P (i.e. altitude) are badly identifiable, especially if excess air is present. Second, the relationship between the two model parameters resembles strongly the meteorological temperature-altitude relation, thus limiting the use of the latter as an additional constraint. The only way to obtain well defined altitude estimates is to prescribe the recharge temperature, if it can be accurately estimated, for example from the groundwater temperature at sampling. Because in such case the temperature can be taken as a known parameter and only the pressure P and the excess air component A has to be treated as free parameters.

4.2 Groundwater dating

The groundwater systems investigated in this work have residence times extending from a few days to several hundred thousand years. This wide range of residence times calls for dating methods that use different hydrological tracers. Moreover, only the combination of multiple tracer methods allows a detailed investigation of transport and mixing properties of groundwater.

In the last 50 years, abundant information on isotopes in groundwater has been obtained, and their widespread application to hydrogeological research has recently increased. Quite a few of these isotopes can be used to date groundwaters and to estimate their residence times. The tracers that are commonly used in hydrology for dating are summarized in Table 4.4.

Table 4.4: Tracers used in groundwater studies for dating.

Tracer	Half-life ($T_{1/2}$)	Dating range	Main source ⁽¹⁾	Major problem
^{222}Rn	3.8 d	~ 20 d	S	determination of in situ production
^3H	12.38 yr	~ 50 yr	M, (A)	atmospheric input function of ^3H into the aquifer
^3He ⁽²⁾	stable	~ 50 yr	A, M, (S)	separation of the tritiogenic ^3He component
^{85}Kr	10.72 yr	~ 50 yr	M	atmospheric input function of ^{85}Kr
CFCs ⁽³⁾	~ stable ⁽⁴⁾	~ 50 yr	M	not always stable, contamination, input function
^{39}Ar	269 yr	~ 10^3 yr	A, S	in situ production in the aquifer
^{14}C	5730 yr	~ 40,000	A, (M)	complex carbon geochemistry
^{81}Kr	229,000 yr	~ 10^6 yr	A	detection
^{36}Cl	301,000 yr	~ 10^6 yr	A, S	chloride geochemistry, in situ production
^{129}I	$15.7 \cdot 10^6$ yr	$> 5 \cdot 10^7$ yr	A, S	in situ production
^4He	stable	> 10 yr ⁽⁵⁾	A, S	determination of the accumulation rate
^{40}Ar	stable	$> 10^5$ yr ⁽⁵⁾	A, S	determination of the accumulation rate, small excess
^{21}Ne	stable	$> 10^7$ yr ⁽⁵⁾	A, S	determination of the accumulation rate, very small excess

⁽¹⁾ Source: A = atmosphere (natural), M = man-made (anthropogenic), S = subsurface

⁽²⁾ in combination with ^3H

⁽³⁾ CFC = chlorofluorocarbons as CFC-11 (CFCl_3), CFC-12 (CF_2Cl_2) and CFC-113 ($\text{C}_2\text{F}_3\text{Cl}_3$).

⁽⁴⁾ CFC-11 is not stable under anoxic conditions (Cook and Solomon, 1995; Hofer and Imboden, 1998).

⁽⁵⁾ Isotopes, which are continuously accumulated during groundwater flow, enable, in principle, to date water masses with infinite ages. However, the upper limitation of these dating tools is in the range of several million years. The lower limitation is given by the analytical error (section 4.2.2).

The dating methods are based on the radioactive decay, on a continuously accumulation of isotopes during groundwater flow, and on time dependent atmospheric concentrations (i.e., variable input function). For young groundwaters ^3H , ^3He , ^{85}Kr and CFCs are well established dating tools (Cook and Solomon, 1997). In old groundwaters they are valuable indicators of any contamination or admixing of younger groundwater. The $^3\text{H}/^3\text{He}$ dating method will be discussed in more detail in the next section.

The most useful age indicator for groundwater with ages of several hundred years is ^{39}Ar (e.g., Loosli and Oeschger, 1978; Forster et al., 1992). However, caution has to be taken in calculating groundwater ages, because ^{39}Ar is also produced in situ in rocks and minerals by $^{39}\text{K} (n, p) ^{39}\text{Ar}$ reactions. Nevertheless, a simultaneous measurement of ^{37}Ar (half-life: $T_{1/2} = 34.8$ days) provides an estimate for ^{39}Ar underground production (Loosli et al., 1991).

To interpret noble gas temperatures in terms of a paleoclimate record it is absolutely important that the groundwater can be reasonable dated. The ^{14}C method is the only well established dating tool for groundwater on time scales between several hundreds to about 40,000 years. Dating of groundwater with ^{14}C is complicated by the complex hydrochemistry of carbon that can alter the initial atmospheric ^{14}C content. In order to derive reliable ^{14}C ages, the geochemical evolution of groundwater has to be taken into account and correction models have to be applied (Ingerson and Pearson, 1964; Fontes and Garnier, 1979). Studies comparing different correction models (e.g., Phillips et al., 1989) imply that an error of at least ± 2000 years has to be assigned to ^{14}C ages of groundwater. For low ^{14}C concentrations corresponding to ages on the order of 30,000 years and higher, contamination with modern carbon and the limited accuracy of ^{14}C measurement gain importance, resulting in an increase of the errors to several thousand years. New tracers such as ^{36}Cl (e.g., Andrews and Fontes, 1992; Purdy et al., 1996) and ^{81}Kr (e.g., Lehmann et al., 1985) might extend the time scale for groundwater dating beyond the range of ^{14}C .

In contrast to the above mentioned methods, radiogenic ^4He , ^{40}Ar and ^{21}Ne offer, in principle, the possibility to date groundwater up to several million years. However, the accumulation rates of these isotopes in groundwater are strongly dependent on the aquifer rocks and the surrounding geological settings. The determination of the

respective accumulation rates is not at all straight forward (especially for ^{40}Ar and ^{21}Ne). In several studies radiogenic ^4He provided reasonable estimates of residence times. Confidence in the calculated ^4He ages can be gained, if ^4He ages are calibrated with ^{14}C ages (e.g., Torgersen and Clarke, 1985). Dating methods using the accumulation of radiogenic noble gases will be discussed in section 4.2.2.

4.2.1 $^3\text{H}/^3\text{He}$ -dating method

Assuming closed system behavior (i.e. no mixing, etc) the tritium concentration of a water parcel decreases by radioactive decay according to following equation:

$$^3\text{H}(t) = ^3\text{H}(t_0) \cdot e^{-\lambda(t-t_0)} \quad [\text{TU}] \quad (4.5)$$

where $^3\text{H}(t)$ is the tritium concentration at time t and $^3\text{H}(t_0)$ is the initial tritium concentration at time t_0 . The decay constant of tritium λ is given by $\lambda = \ln(2)/T_{1/2} = 0.05599 \text{ yr}^{-1}$ (see Equation 2.28) with $T_{1/2}$ being the half-life of tritium ($T_{1/2} = 12.38$ years, Oliver et al., 1987). As soon as the water parcel is isolated from the atmosphere (i.e. no gas exchange with the atmosphere) the ^3He concentration increases as the ^3H concentration decreases, according to

$$\begin{aligned} ^3\text{He}_{\text{tri}}(t) &= ^3\text{H}(t_0) - ^3\text{H}(t) = ^3\text{H}(t_0) \cdot (1 - e^{-\lambda(t-t_0)}) \\ &= ^3\text{H}(t) \cdot (e^{\lambda(t-t_0)} - 1) \quad [\text{TU}] \end{aligned} \quad (4.6)$$

where $^3\text{He}_{\text{tri}}(t)$, is the tritiogenic ^3He concentration at time t . The $^3\text{He}_{\text{tri}}$ is defined as the fraction of the total ^3He being produced solely by ^3H decay. In case that $^3\text{He}_{\text{tri}}$ is measured in $\text{cm}^3\text{STP/g}$ and ^3H in TU, $^3\text{He}_{\text{tri}}$ concentration has to be converted from $\text{cm}^3\text{STP/g}$ to TU by multiplying by $4.0193 \cdot 10^{14} / (1-S/1000)$ where S is the salinity in ‰ of the water sample.

From the ^3H and $^3\text{He}_{\text{tri}}$ concentration, the $^3\text{H}/^3\text{He}$ age $\tau = t - t_0$ of a closed, homogeneous body of water can be calculated using Equation (4.6) (Tolstikhin, 1969):

$$\tau = \frac{1}{\lambda} \cdot \ln \left(1 + \frac{^3\text{He}_{\text{tri}} [\text{TU}]}{^3\text{H} [\text{TU}]} \right) \quad [\text{yr}] \quad (4.7)$$

where ^3H and $^3\text{He}_{\text{tri}}$ are the ^3H and ^3He concentrations of the water sample at the time t of sampling expressed in equal units, e.g. TU.

Note that the $^3\text{H}/^3\text{He}$ age defined in Equation (4.7) is independent of the initial ^3H concentration $^3\text{H}(t_0)$ of the water parcel. This is the major advantage of the method because it circumvents problems due to the input of ^3H to a water system which is usually only vaguely known. It has to be further noted that the $^3\text{H}/^3\text{He}$ water age is an apparent age and can only be taken as the true age of the water if ^3He sources other than ^3H decay can be corrected for (see below), and if mixing of waters with different $^3\text{H}/^3\text{He}$ concentrations can be excluded or can be quantified (see also section 4.3.1).

According to Eq (2.25), the $^3\text{He}_{tri}$ of a groundwater sample can be calculated as the difference of the total measured ^3He ($^3\text{He}_{tot}$) and all other non-tritiogenic ^3He components (e.g., Schlosser, 1992):

$$^3\text{He}_{tri} = ^3\text{He}_{tot} - ^3\text{He}_{eq} - ^3\text{He}_{ex} - ^3\text{He}_{crust} - ^3\text{He}_{mantle} \quad [\text{cm}^3\text{STP/g}] \quad (4.8)$$

The origin of the different ^3He components with regard to the $^3\text{H}/^3\text{He}$ dating method is outlined in Figure 4.6.

The non-tritiogenic components of Equation 4.8 can be deduced as follows (see also section 2.4.1 and 2.4.2):

$^3\text{He}_{eq}$: The equilibrium concentration is a function of the water temperature T , the salinity S , and the atmospheric pressure P prevailing during recharge (section 2.2). The best measure of the infiltrated water temperature is the calculated noble gas temperature (section 4.1). In cases where only He and Ne isotopes were analyzed, the in situ water temperature of the sample or the mean annual temperature of the recharge area can be taken to estimate the recharge temperature. Note that in groundwaters the in situ salinity may be quite high, but relevant for the solution of atmospheric noble gases is the salinity at the time of infiltration, which is usually close to zero. From the altitude of the presumed recharge area, the atmospheric pressure P can be derived using the barometric Equation (2.14).

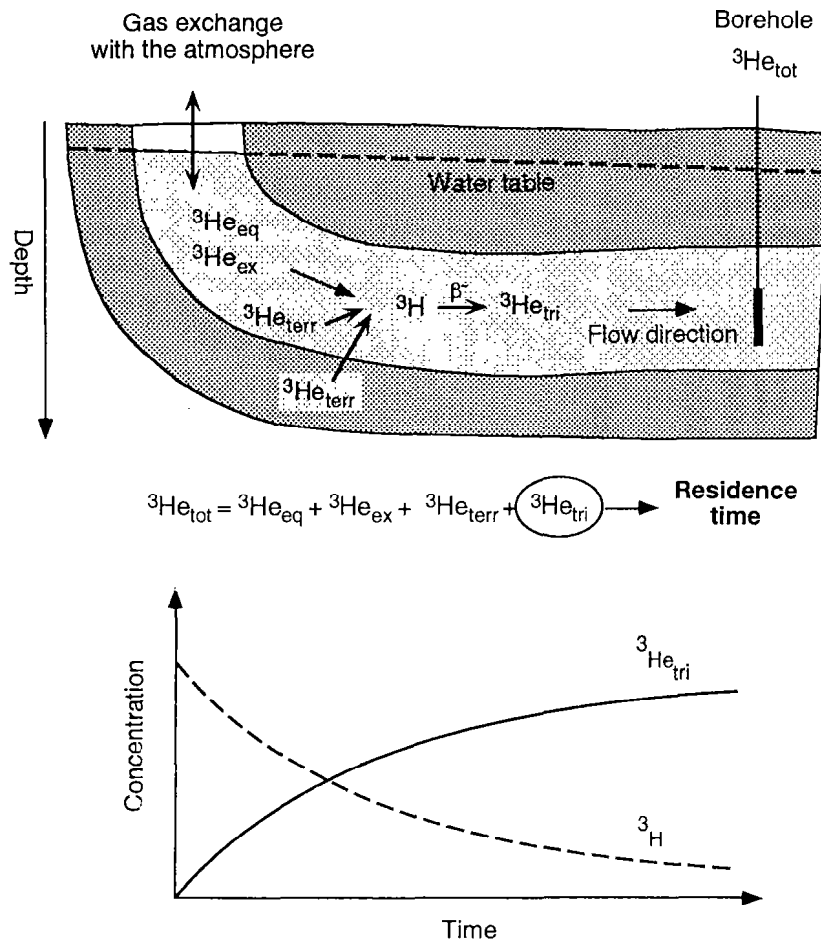


Figure 4.6: With increasing residence time of the water the ^3H concentration decreases whereas the $^3\text{He}_{\text{tri}}$ concentration increases. If the tritiogenic ^3He component ($^3\text{He}_{\text{tri}}$) can be determined from the measured ^3He concentration by correcting for the different non-tritiogenic ^3He components ($^3\text{He}_{\text{eq}}$: equilibrium, $^3\text{He}_{\text{ex}}$: excess air, and $^3\text{He}_{\text{terr}}$: terrigenic ^3He component), the so-called $^3\text{H}/^3\text{He}$ age can be calculated according to Eq (4.7).

$^3\text{He}_{\text{ex}}$: The excess air component can be best calculated by multiplying the fitted excess air parameter A by the volume fraction of ^3He in dry air. In case of an unfractionated excess air, the ^{20}Ne concentration is normally a good enough measure to derive the atmospheric excess of ^3He :

$$^3\text{He}_{\text{ex}} = (^3\text{He}/^{20}\text{Ne})_{\text{air}} \cdot (^{20}\text{Ne}_{\text{tot}} - ^{20}\text{Ne}_{\text{eq}})$$
 Caution has to be taken when degassing significantly influences the noble gas concentrations. If degassing is not considered, the calculated $^3\text{He}_{\text{ex}}$ would be overestimated resulting in a smaller $^3\text{He}_{\text{tri}}$ and $^3\text{He}/^3\text{He}$ age.

${}^3\text{He}_{terr}$: The difficult part of the ${}^3\text{He}_{tri}$ calculation is often the determination of the terrigenous ${}^3\text{He}$ component (defined by ${}^3\text{He}_{terr} = {}^3\text{He}_{crust} + {}^3\text{He}_{mantle}$). In principle, the ${}^3\text{He}_{terr}$ concentration can be calculated from the ${}^4\text{He}_{terr}$ (Equation 2.27), if the corresponding ${}^3\text{He}/{}^4\text{He}$ ratio R_{terr} is known, which is for single water sample often not the case. Sometimes the R_{terr} can be deduced from samples with high content of ${}^4\text{He}_{terr}$ (e.g., Aeschbach-Hertig et al., 1998; see also section 2.4.1). However, if the radiogenic ${}^4\text{He}$ is small and no ${}^3\text{He}$ from the mantle is present, the contribution of the ${}^3\text{He}_{terr}$ component to the measured ${}^3\text{He}$ is small or even negligible.

Assuming that the excess air component consists of unfractionated atmospheric air the tritiogenic ${}^3\text{He}$ can be calculated as

$${}^3\text{He}_{tri} = {}^4\text{He}_{tot} \cdot R_{tot} - {}^4\text{He}_{eq} \cdot R_{eq} - ({}^{20}\text{Ne}_{tot} - {}^{20}\text{Ne}_{eq}) \cdot \left(\frac{{}^3\text{He}}{{}^{20}\text{Ne}} \right)_{air} - {}^4\text{He}_{terr} \cdot R_{terr} \quad [\text{cm}^3\text{STP/g}] \quad (4.9)$$

where R_{tot} is the measured ${}^3\text{He}/{}^4\text{He}$ ratio of the water sample and R_{eq} the ${}^3\text{He}/{}^4\text{He}$ ratio in atmospheric equilibrium (see section 2.2.1). If all terrigenous He components can be excluded, ${}^4\text{He}$ is used to correct for excess air:

$${}^3\text{He}_{tri} = {}^4\text{He}_{tot} \cdot R_{tot} - {}^4\text{He}_{eq} \cdot R_{eq} - ({}^4\text{He}_{tot} - {}^4\text{He}_{eq}) \cdot R_{air} \quad [\text{cm}^3\text{STP/g}] \quad (4.10)$$

where R_{air} is the atmospheric ${}^3\text{He}/{}^4\text{He}$ ratio. As Equation (4.10) has no Ne related terms the error of the calculated ${}^3\text{He}_{tri}$ concentration is smaller than the error resulting from Equation (4.9). Consequently, in cases where no terrigenous He components are present in the groundwater the ${}^3\text{H}/{}^3\text{He}$ age can be normally determined with higher precision.

In general, the age resolution of the ${}^3\text{H}/{}^3\text{He}$ method is given by the analytical precision and the applied corrections. On the basis of analytical precision of $\pm 0.5\%$ for the ${}^3\text{He}/{}^4\text{He}$ ratio, of $\pm 1\%$ for He and Ne concentrations and of $\pm 2\%$ for ${}^3\text{H}$ concentrations, the lower limit of the ${}^3\text{He}/{}^4\text{He}$ dating method is calculated and plotted in Figure 4.7. The resulting age resolution depends mainly on the analytical precision of the ${}^3\text{He}/{}^4\text{He}$ ratio, on the ${}^3\text{H}$ concentration, and on the applied correction for excess air (i.e. with or without terrigenous He). For groundwaters with ${}^3\text{H}$ concentrations of

about 20 TU and no significant terrigenous He, the lowest detectable $^3\text{H}/^3\text{He}$ groundwater age is about 50 days.

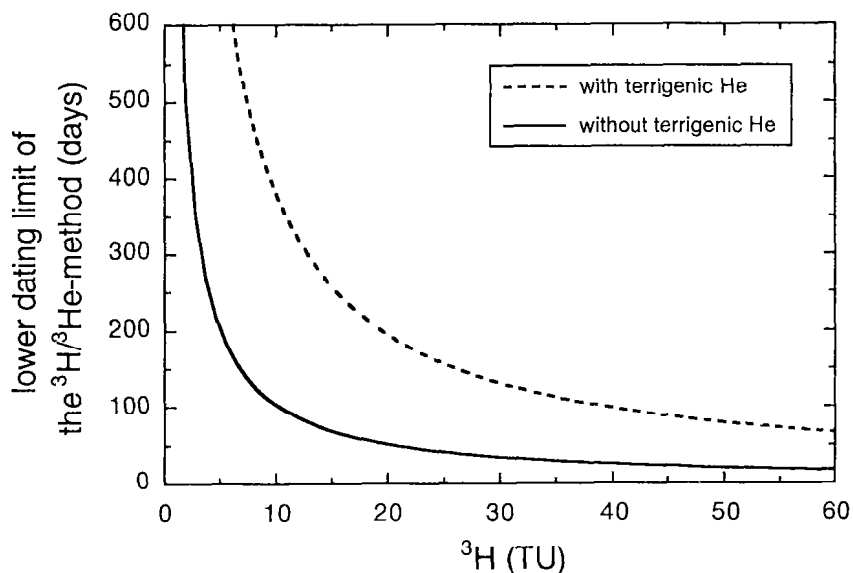


Figure 4.7: Lower limit of the $^3\text{H}/^3\text{He}$ method as a function of the tritium (^3H) concentration of water samples. Dashed line: Ne is used for excess air correction. Solid line: No terrigenous ^4He is present and He is used for excess air correction. The following assumptions were used: typical analytical precision ($\pm 0.5\%$ for $^3\text{He}/^4\text{He}$ ratios, $\pm 1\%$ for noble gas and $\pm 2\%$ for ^3H concentrations); groundwater was infiltrated at 10°C with an excess air component of $20\% \Delta\text{Ne}$.

4.2.2 Accumulation of radiogenic noble gases

Besides the radioactive isotopes ^{14}C (half-life: $T_{1/2} = 5730$ yr), ^{81}Kr (229,000 yr) and ^{36}Cl (301,000 yr), the stable noble gas isotopes ^4He , ^{21}Ne and ^{40}Ar have the potential to be used for dating very old groundwater. The production of these radiogenic noble gas isotopes is controlled by very long-lived nuclides in mineral and rocks, as for example ^{238}U (half-life $4.47 \cdot 10^9$ yr), ^{232}Th ($1.4 \cdot 10^{10}$ yr), and ^{40}K ($1.28 \cdot 10^9$ yr). In contrast to ^4He and ^{40}Ar , which are produced directly by the decay of U, Th, or K, ^{21}Ne is produced indirectly by interactions between light elements in the rock (e.g. ^{18}O) and α particles from the decay of U and Th. Groundwater ages using ^4He , ^{21}Ne or ^{40}Ar are based on the assumption that the radiogenic noble gases accumulate continuously during groundwater flow. The radiogenic noble gases are expected either to diffuse out of minerals within the aquifer (in situ production) or to emanate from deeper strata into the aquifer. To derive 'more realistic' ages it is sometimes additionally assumed that lighter isotopes, in particular ^4He , can escape from groundwater by molecular diffusion.

To start one can calculate accumulation rates in a closed volume of rock (i.e. in situ production) based on given production rates depending on the geochemical composition of the rock. The production P_i rates for radiogenic noble gases ($i = ^4\text{He}$, ^{21}Ne , and ^{40}Ar) in rocks can be calculated as (e.g., Craig and Lupton, 1976; Lehmann and Loosli, 1991)

$$\begin{aligned} P_{^4\text{He}} &= 2.355 \cdot 10^{-13} \cdot U^* \\ &= 1.2 \cdot 10^{-13} \cdot U + 2.9 \cdot 10^{-14} \cdot Th \end{aligned} \quad [\text{cm}^3\text{STP}/(\text{g}_{\text{rock}} \cdot \text{yr})] \quad (4.11)$$

$$\begin{aligned} P_{^{21}\text{Ne}} &= 6.7 \cdot 10^{-21} \cdot U^* \\ &= 3.4 \cdot 10^{-21} \cdot U + 8.2 \cdot 10^{-22} \cdot Th \end{aligned} \quad [\text{cm}^3\text{STP}/(\text{g}_{\text{rock}} \cdot \text{yr})] \quad (4.12)$$

$$\text{with } U^* = U \cdot \left(1 + 0.123 \cdot \left(\frac{Th}{U} - 4 \right) \right)$$

$$P_{^{40}\text{Ar}} = 4 \cdot 10^{-18} \cdot K \quad [\text{cm}^3\text{STP}/(\text{g}_{\text{rock}} \cdot \text{yr})] \quad (4.13)$$

where U , Th and K are the concentrations in ppm ($\mu\text{g/g}$) of the respective elements in rock. Because of the indirect produced ^{21}Ne , Equation (4.12) is only valuable for the production rate of ^{21}Ne in a silicate rock containing 45% oxygen (Craig and Lupton, 1976).

Assuming that the aquifer consists of rock completely saturated with water, the corresponding accumulation rate A_i in water is given as

$$A_i = \frac{P_i}{\theta'} \cdot \frac{\rho_{rock}}{\rho_{water}} \cdot \Lambda_i \quad [\text{cm}^3\text{STP}/(\text{g}_{water}\cdot\text{yr})] \quad (4.14)$$

where ρ_{rock} is the rock density (g/cm^3) and Λ_i the transport efficiency of the noble gas i from rock to water (number between 0 and 1). It can be reasonably assumed that the water density ρ_{water} is equal to $1 \text{ g}/\text{cm}^3$. In Equation (4.14) θ' is the volume ratio between pore volume and matrix space ($\text{cm}^3_{water}/\text{cm}^3_{rock}$). This ratio is related to the porosity θ of the aquifer, which is defined as the ratio between pore volume and total volume ($\text{cm}^3_{water}/\text{cm}^3_{total}$), as follows:

$$\theta' = \frac{\theta}{1-\theta} \quad [\text{cm}^3_{water}/\text{cm}^3_{rock}] \quad (4.15)$$

Inserting Equation (4.15) in Equation (4.14) yields:

$$A_i = P_i \cdot \frac{1-\theta}{\theta} \cdot \frac{\rho_{rock}}{\rho_{water}} \cdot \Lambda_i \quad [\text{cm}^3\text{STP}/(\text{g}_{water}\cdot\text{yr})] \quad (4.16)$$

The transfer factor Λ_i mainly depends on the grain size and it is often assumed to be equal to 1. Such complete transfer of radiogenic noble gases from the rock matrix into water may be justified for ^4He but it appears unrealistic in particular for ^{40}Ar because the well established K-Ar rock dating method, which only works if most radiogenic ^{40}Ar is trapped in the minerals.

In case only in situ production adds radiogenic noble gases, the groundwater ages τ_i can be calculated as

$$\tau_i = \frac{C_i^{rad}}{A_i} \quad [\text{yr}] \quad (4.17)$$

where $C_i^{rad} = C_i^{tot} - C_i^{init}$ is the non-atmospheric radiogenic concentration (in $\text{cm}^3\text{STP}/\text{g}_{water}$) defined as the difference between the measured noble gas

concentration C_i^{tot} and the calculated initial atmospheric concentration C_i^{init} in groundwater as given in Equation (4.2).

To summarize, the use of in situ accumulation rates for calculating groundwater ages requires a detailed knowledge of the aquifer matter and characteristics, such as the porosity, the concentrations and spatial distributions of the radioelements (U, Th and K) and as well as information about the transport efficiency of the radiogenic noble gases from rock to water. In many cases, detailed spatial information on these parameters is not available and overall estimations have to be assumed. Examples of accumulation rates assuming only in situ production are given in Table 4.5 and shown in Figure 4.8. Taken into account an analytical error between 1‰ and 1%, the lower limits of groundwater dating are about $1 \cdot 10^2$ years for ^4He , $10^4 \cdot 10^6$ years for ^{40}Ar , and more than 10^7 years for ^{21}Ne .

Table 4.5: Examples of in situ accumulation rates of ^4He , ^{40}Ar , and ^{21}Ne in groundwater compared to the initial noble gas concentration C_i^{init} .

Rock type	[U]	[Th]	[K]	ρ_{rock}	Porosity θ	Accumulation rate in water ⁽³⁾		
	(ppm)	(ppm)	(ppm)	(g/cm ³)	(-)	(cm ³ STP / (g _{water} ·yr))		
						^4He	^{40}Ar	^{21}Ne
Muschelkalk ⁽¹⁾	2	1	5000	2.2	0.1	$5.6 \cdot 10^{-12}$	$4.1 \cdot 10^{-13}$	-
Crystalline ⁽¹⁾	4	18	40000	2.6	0.01	$2.6 \cdot 10^{-10}$	$4.1 \cdot 10^{-11}$	-
Korallenoolith ⁽²⁾	3	7	?	1.9	0.2	$4.3 \cdot 10^{-12}$	-	$1.2 \cdot 10^{-19}$
Assumption						Concentration (cm ³ STP / g _{water})		
Initial conc. C_i^{init}	$(T = 10^\circ\text{C}, P = 1 \text{ atm}, \Delta Ne = 20\%)$					$6.5 \cdot 10^{-8}$	$4.1 \cdot 10^{-4}$	$6.5 \cdot 10^{-10}$

⁽¹⁾ Lehmann and Loosli (1991)

⁽²⁾ Weise et al. (1992)

⁽³⁾ The transport efficiencies Λ_i of the noble gases from rock to water are assumed to be equal to 1.

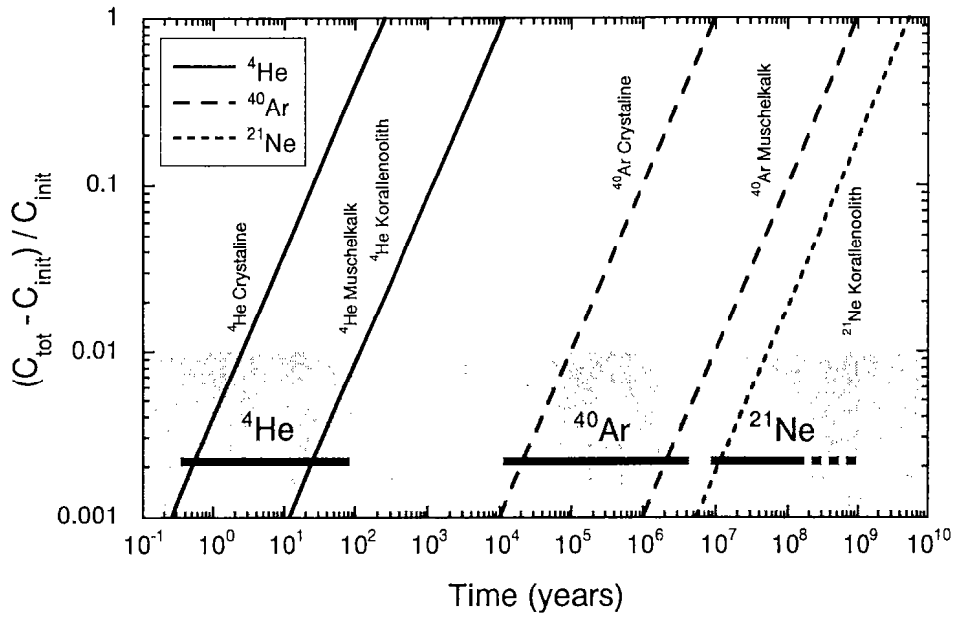


Figure 4.8: Accumulation of the noble gas isotopes ^4He , ^{40}Ar and ^{21}Ne in groundwater relative to the initial concentration as a function of time assuming only in situ production. C_{mit} is the initial concentration of the noble gas (^4He , ^{40}Ar , or ^{21}Ne) in groundwater (recharge temperature $T = 10^\circ\text{C}$, atmospheric pressure $P = 1 \text{ atm}$, and excess air $\Delta\text{Ne} = 20\%$). C_{tot} is the measured noble gas concentration as a function of time. Properties of the different aquifers are given in Table 4.5.

As pointed out by several authors (e.g., Andrews, 1985; Torgersen and Clarke, 1985; Lehmann and Loosli, 1991) model ages based on in situ production alone tend to overestimate water residence times. As it is demonstrated when cross calibration with ^{14}C , ^{36}Cl ages or reliable hydrodynamic model ages is possible. The overestimation of the residence time is explained by the fact that transport from deeper strata of the radiogenic noble gas isotopes is not taken into account.

Higher accumulation rates as expected from in situ production are most apparent for the very mobile He. And in most cases, they exceed the in situ accumulation rates by orders of magnitude. As it is often impossible to describe the physical transport of noble gases through a complex geological environment to the investigated aquifer, conceptual models for the accumulation of He are presented in the following.

The most simple model relates the residence time τ of water in an aquifer to the external flux F (in $\text{cm}^3\text{STP}/(\text{cm}^2\cdot\text{yr})$) of ^4He into the aquifer at the lower aquifer boundary and to the measured non-atmospheric excess of ^4He ($^4\text{He}_{rad}$). The residence time τ can be written as

$$\tau = \frac{{}^4\text{He}_{rad} \cdot d \cdot \theta \cdot \rho_{water}}{F} \quad [\text{yr}] \quad (4.18)$$

with d being the thickness of the aquifer (in cm), θ the porosity and ρ_{water} the water density ($\rho_{water} \approx 1 \text{ g/cm}^3$). This model treats the aquifer as a ideal trap for He. No diffusive loss at the upper boundary is considered and the in situ production inside the aquifer is neglected. As demonstrated by Torgersen and Clarke (1985) for the Jurassic-aquifer (J-aquifer) of the Great Artesian Basin in Australia, the external flux of ^4He into the confined sandstone aquifer can be estimated from the in situ production rate in the underlying crystalline basement. Therefore the authors assume a steady state, in which for every He atom produced in the upper crust, one He atom is released through the upper boundary into the aquifer. This presumed steady state He flux is known in the literature as the whole crustal He flux. Whether this whole crustal flux is really existing or not, is matter of controversial and ongoing discussions. Table 4.6 shows some examples for calculated He fluxes.

Table 4.6: He fluxes from different sites.

He flux $\text{cm}^3\text{STP}/(\text{cm}^2\cdot\text{yr})^{(1)}$	Study site	Reference
$3.6 \cdot 10^{-6}$	Great Artesian Basin, Australia	Torgersen and Clarke (1985)
$3.3 \cdot 10^{-6}$	calculated from global He budget	O'Nions and Oxburgh (1983)
$1.5 \cdot 10^{-5} - 3.3 \cdot 10^{-5}$	Lake Baikal	Hohmann et. al. (1998)
$1.3 \cdot 10^{-6} - 5.6 \cdot 10^{-6}$	various lakes in Switzerland	Aeschbach-Hertig (1994)
$\sim 8 \cdot 10^{-7}$	Linsental aquifer, Switzerland (thickness $d = 20\text{m}$, $\theta = 0.2$)	chapter 5

⁽¹⁾ Conversion: $10^{10} \text{ atoms}/(\text{m}^2\cdot\text{s})$ is equal to $1.175 \cdot 10^{-6} \text{ cm}^3\text{STP}/(\text{cm}^2\cdot\text{yr})$, see Equation (2.3).

Andrews et al. (1985) used a different approach, a diffusion model, to calculate a flux of ^4He towards the surface. In this model the crust is considered as a thick layer of rock with a uniform radioelement content and a constant diffusion coefficient D_{crust} . The He concentration $c(z, t)$ in the crust is a function of the time t and the distance z below the surface and can be approximated by

$$c(z, t) = G \cdot t \cdot \left[1 - \exp\left(-\frac{2z}{\sqrt{D_{crust} \cdot t \cdot \pi}}\right) \right] \quad [\text{cm}^3\text{STP}/\text{cm}^3] \quad (4.19)$$

where G is the rate of production of He per unit volume of the crust expressed in $\text{cm}^3\text{STP}/(\text{cm}^3 \cdot \text{yr})$. The flux F at the surface ($z = 0$) is obtained by

$$F = 2 \cdot G \sqrt{\frac{D_{crust} \cdot t}{\pi}} \quad [\text{cm}^3\text{STP}/\text{cm}^2 \cdot \text{yr}] \quad (4.20)$$

Assuming that the crust consists of rock with a density ρ_{rock} and a porosity θ_{rock} , the He production rate G in the crust can be calculated from the production rate $P_{^4\text{He}}$ in rocks (Equation 4.11):

$$G = P_{^4\text{He}} \cdot \rho_{rock} \cdot (1 - \theta_{rock}) \quad [\text{cm}^3\text{STP}/(\text{cm}^3 \cdot \text{yr})] \quad (4.21)$$

However, it is more difficult to choose values for the diffusion coefficient D_{crust} , and the total time t , for the build-up of a concentration profile. The maximum of the latter is given by the age of the crustal rock (several 100 millions years). Further, the determination of the diffusion coefficient in the crust can be approximated assuming that the crust is a porous media and that its pore space is completely saturated with water.

It is obvious that the effective diffusion coefficient D_{eff} of He in porous media is smaller than the one in pure water, D . In fact, there are several different empirical approaches for the relation between D_{eff} and D (e.g., Helfferich, 1966; Parkomenko, 1967; Greenkorn and Kessler, 1972; Greenkorn, 1983; Balderer and Lehmann, 1991; see also Figure 4.9). As for example, according to Helfferich (1966), the effective diffusion coefficient falls in a relatively wide range

$$D_{eff} = n \cdot D \quad \text{where } n = \frac{\theta}{2} \quad \text{to} \quad n = \left(\frac{\theta}{2 - \theta}\right)^2 \quad (4.22)$$

In Equation (4.22) the correction factor n depends on the porosity θ . In most cases D_{eff} is also a function of the tortuosity (Greenkorn and Kessler, 1972). However, in practice, only the direct experimental determination of D_{eff} leads to reliable results.

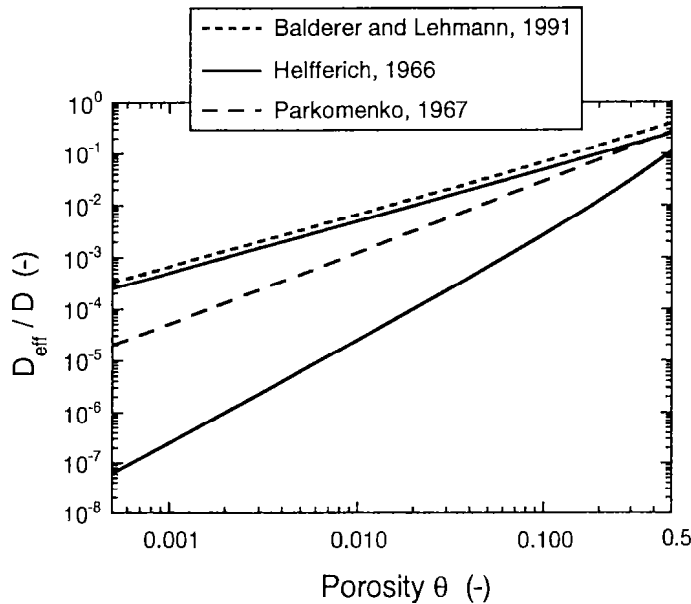


Figure 4.9: The ratio between the effective diffusion coefficient D_{eff} in a porous media and the diffusion coefficient D in pure water in function of the porosity θ .

Assuming a He accumulation in the crust during the last 1,000 million years, a porosity of $\theta = 0.01$, a U, Th content as in crystalline rocks of northern Switzerland (Lehmann and Loosli, 1991) and the highest effective diffusion coefficient of Figure 4.9, the ^4He flux F according to Equation (4.20) is about $3 \cdot 10^{-7} \text{ cm}^3 \text{STP}/(\text{cm}^2 \cdot \text{yr})$. This value is one order of magnitude smaller than any fluxes listed in Table 4.6. As a consequence, Lehmann and Loosli (1991) argued that diffusion is not effective enough to transport He through crystalline rocks, and that rather He is transported advectively by water circulation in the upper most part of the continental crust.

A completely different model, which explains elevated He concentrations in alluvial aquifers is proposed by Solomon et al. (1996). They suggested that the ^4He is released from small grains inside the aquifer which act as He reservoirs. Since the aquifer material has been recently eroded from crustal rocks, in which the ^4He had

accumulated over long time scales, the He release of the eroded grains is much higher than one would expect by only in situ production.

At present a generally accepted model for the accumulation of radiogenic ^4He in groundwaters is still missing. Consequently, the accumulation rate of radiogenic noble gases can be only determined with confidence in those cases in which cross-calibration with other dating methods is possible (see for example chapter 5).

Similar approaches, as for ^4He , can also be postulated for the transport of radiogenic ^{40}Ar from neighboring rock strata outside the aquifer. Since the molecular weight of ^{40}Ar is 10 times larger than the one of He, the diffusion through the crust is much less effective. However, it seems that at least in some cases the accumulation of ^{40}Ar can not be explained by assuming in situ production alone (Lehmann and Loosli, 1991).

Basically ^{21}Ne exhibits the same difficulties when using for groundwater dating as ^4He and ^{40}Ar . An additional source of uncertainty is the determination of the efficiency of the $^{18}\text{O}(\alpha,n)^{21}\text{Ne}$ reaction which is represented by the factor $6.7 \cdot 10^{-21}$ in Equation (4.12). Furthermore, as the in situ production in rocks of ^{21}Ne is very low, ^{21}Ne excess are only detectable in groundwaters which have an age of at least 10^7 years. As a consequence of these and other limitations (Weise et al., 1992), ^{21}Ne is hardly used for quantitative groundwater dating.

As an example for the accumulation of radiogenic ^4He and ^{40}Ar , noble gas data from the Great Artesian Basin (GAB) in Australia are discussed in the following. The Great Artesian Basin of Australia is the world's largest confined groundwater system and occupies 1.7 Million km^2 of the Australian continent extending from northeast Queensland to South Australia (Habermehl, 1980). The basin consists of a at least two layered confined aquifer system of continental sandstones, the upper K-aquifer and lower J-aquifer. The potentiometric surface is above ground level in most areas of the basin and therefore most boreholes are artesian. Samples, which are plotted in Figure 4.10, were taken in the southwestern part of the GAB out of the J-aquifer. In this part, recharge to the J-aquifer occurs in the northeastern margin of the basin and the groundwater flows toward the southwest. Estimated flow velocities are about 0.4

m/yr. For an easier sampling and to avoid degassing during sampling, samples were drawn only from artesian boreholes.

In the GAB the accumulation rate of He observed by Torgersen and Clarke (1985) is about $2.9 \cdot 10^{-10}$ cm³STP/(g·yr). Compared with the expected ⁴He in situ production of $4 \cdot 10^{-12}$ cm³STP/(g·yr) (Table 4.7), the observed accumulation rate is two orders of magnitude larger. Therefore Torgersen and Clarke (1985) concluded that the He concentration is elevated due to an external He flux into the GAB. The corresponding flux at the lower boundary of the aquifer is $3.5 \cdot 10^{-6}$ cm³STP/(cm²·yr) assuming an average aquifer thickness of 600m and a porosity of 20% (Table 4.7). Furthermore, Torgersen and Clarke (1985) suggested that this flux is equal to a steady-state flux of the whole crust.

Table 4.7. Accumulation of ⁴⁰Ar and ⁴He in the Great Artesian Basin due to in situ production and due to external fluxes.

Aquifer properties: $\theta = 20\%$, $\rho_{rock} = 2.6$ cm ³ /g ⁽²⁾ , thickness $d = 600$ m [U] = 1.7ppm ⁽¹⁾ , [Th] = 6.1ppm ⁽¹⁾ , [K] = 1.5% ⁽²⁾ , Initial concentration: recharge temp. $T = 22^\circ\text{C}$, excess air $\Delta Ne = 50\%$, altitude $H = 330$ m						
Initial conc.	Accumulation rate due to	External flux	Concentration after 400,000yr			
C_{init}	in situ ⁽³⁾	flux	F	in situ	flux	
cm ³ STP/g	cm ³ STP/(g·yr)	cm ³ STP/(cm ² ·yr)	cm ³ STP/g	cm ³ STP/g	cm ³ STP/g	cm ³ STP/g
⁴ He	$6.8 \cdot 10^{-8}$	$4.0 \cdot 10^{-12}$	$2.9 \cdot 10^{-10(1)}$	$3.5 \cdot 10^{-6}$	$1.7 \cdot 10^{-6}$	$1.2 \cdot 10^{-4}$
⁴⁰ Ar	$3.3 \cdot 10^{-4}$	$6.2 \cdot 10^{-13}$	$6.6 \cdot 10^{-11}$	$8.0 \cdot 10^{-7(2)}$	$3.3 \cdot 10^{-4}$	$3.6 \cdot 10^{-4}$
⁴⁰ Ar/ ³⁶ Ar	295.5	-	-		295.7	319.2

⁽¹⁾ Torgersen and Clarke (1985)

⁽²⁾ Torgersen et al. (1989)

⁽³⁾ The accumulation rate was calculated using Equations (4.11), (4.13), and (4.16) assuming that all the produced ⁴He and ⁴⁰Ar are released to the fluid phase (i.e. $\Lambda_i = 1$).

As calculated from preliminary ⁸¹Kr data, the residence time of four groundwater samples shown in Figure 4.10 are between 200 - 400 kyr. A ⁴He accumulation rate, which is equal to the one observed by Torgersen and Clarke (1985), yields

groundwater residence times that have the same order of magnitude than the calculated ^{81}Kr ages. This finding supports the idea of an external He flux.

In Figure 4.10 the radiogenic ^4He is plotted against the $^{40}\text{Ar}/^{36}\text{Ar}$ ratio. Any accumulation of ^{40}Ar leads to an increase of the $^{40}\text{Ar}/^{36}\text{Ar}$ ratio, because ^{36}Ar in groundwater is almost exclusively of atmospheric origin. Although the data show a significant correlation between radiogenic ^4He and an elevated $^{40}\text{Ar}/^{36}\text{Ar}$ ratio, the accumulation rate of ^{40}Ar is too high compared to in situ production alone and too low compared to the whole crustal ^{40}Ar flux of Torgersen et al. (1989) (compare Figure 4.10 with Table 4.7).

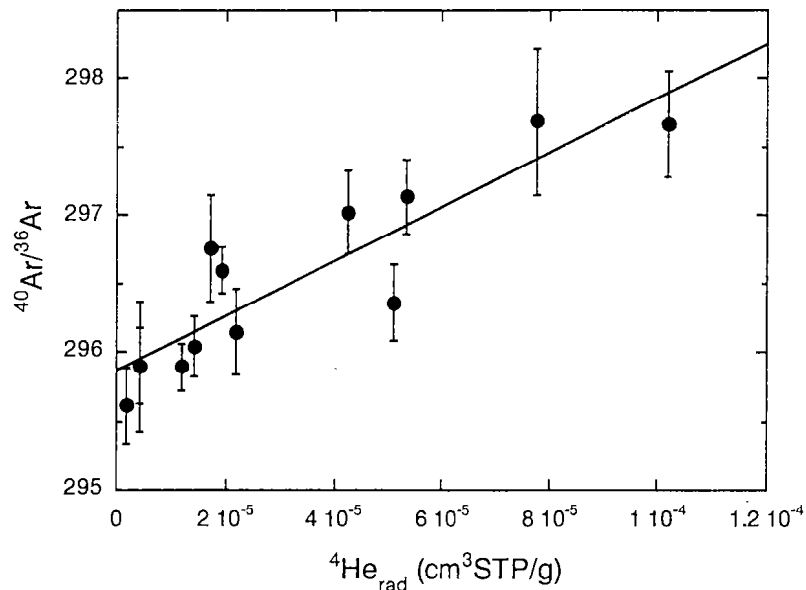


Figure 4.10: $^4\text{He}_{\text{rad}}$ versus $^{40}\text{Ar}/^{36}\text{Ar}$ ratio in the Great Artesian Basin, Australia. A linear fit through the data yields a radiogenic $^4\text{He}/^{40}\text{Ar}$ ratio of about 50.

Both the $^4\text{He}/^{40}\text{Ar}$ production ratio assuming only in situ production and the $^4\text{He}/^{40}\text{Ar}$ production ratio suggested by Torgersen are between 5-6, which is in agreement with the production ratio in crustal rocks (Mamyrin and Tolstikhin, 1984). However, the $^4\text{He}/^{40}\text{Ar}$ production ratio deduced from Figure 4.10 is in the order of 50. We therefore conclude that the release of ^{40}Ar into the aquifer is much less effective than the release of ^4He .

4.3 Effect of binary mixing and dispersion

After leaving the zone near the water table, groundwater is isolated from the atmosphere and migrates to the discharge area, following the hydraulic gradient. Usually it is assumed that water flow can be described by Darcy's law. The Darcy velocity or the Darcy flux q defines a specified discharge through an area and has the dimension of a velocity:

$$q = -K \frac{dh}{dx} \quad [\text{m/s}] \quad (4.23)$$

In Equation (4.23), h is called the hydraulic head (in m) and dh/dx is the hydraulic gradient in x -direction. The parameter K (m/s) is known as the hydraulic conductivity. Sometimes the conductivity of a porous media is expressed with the permeability κ :

$$\kappa = \frac{\nu_w}{g} K \quad [\text{m}^2] \quad (4.24)$$

where ν_w is the kinematic viscosity of the groundwater ($\nu_w = 1.3 \cdot 10^{-6} \text{ m}^2/\text{s}$, water at 10°C) and g the acceleration of gravity (9.81 m/s^2). The effective velocity of the groundwater v_x is related to the Darcy velocity by the porosity θ :

$$v_x = \frac{q}{\theta} \quad [\text{m/s}] \quad (4.25)$$

Darcy's law only describes the advective part of the groundwater flow. In reality, there are at least two additional processes: molecular diffusion and hydrodynamic dispersion. Both processes tend to smooth concentration gradients. In moving groundwater dispersion is normally much more pronounced than molecular diffusion. In addition to dispersion and diffusion, mixing of different groundwaters can change the concentrations of noble gases in the investigated groundwater. As a consequence, in studies using noble gas isotopes as environmental tracers the influence of dispersion and mixing should be estimated and if possible corrected for.

4.3.1 Mixing

Mixing of different groundwater masses can potentially occur between adjacent aquifers. However, a further source of mixed groundwater of different age and origin are leaky well casing or wells with large open intervals. A careful study of chemical parameters (e.g., chloride) and isotopic age indicators (e.g., ^3H , ^{39}Ar) of the groundwater flow system provides the basis for evaluating whether an aquifer is disturbed by mixing. A good indication of mixed groundwaters are 'forbidden' combinations of age indicators as for example low ^{14}C concentration and significant ^3H content in the same groundwater sample. An example of a two component mixture between groundwaters of different ages is given in chapter 6.

In the next paragraph the impact of mixing on the calculated noble gas temperature is discussed, followed by some remarks about how mixing of groundwaters can affect $^3\text{H}/^3\text{He}$ dating.

As the solubility-temperature curves of noble gases are concave from above (Figure 2.1), mixing of waters that equilibrated at different temperatures produces apparent supersaturation relative to the temperature of the mixture. The effect is greatest for the heavier gases, it is minimal for He and Ne, and it is more pronounced at low temperatures. In principle, it should be possible to determine mixing ratios from the measured noble gas concentrations using the five atmospheric noble gases. However, in practice, mixing cannot be resolved as long as the effect is strongly masked by other unknown parameters such as excess air, degassing or altitude effects. Consequently, the identification of mixed groundwater samples has been done by other hydrological tracers or by a precise analysis of the chemical composition and evolution of the groundwater. As a first approximation it can be reasonably assumed that the noble gas temperature of a groundwater sample representing a binary mixture of water masses recharged at different temperatures, is equal to the average of the recharge temperatures of the two samples. This approximation is less valid for larger temperature differences between the two end-members (Figure 4.11).

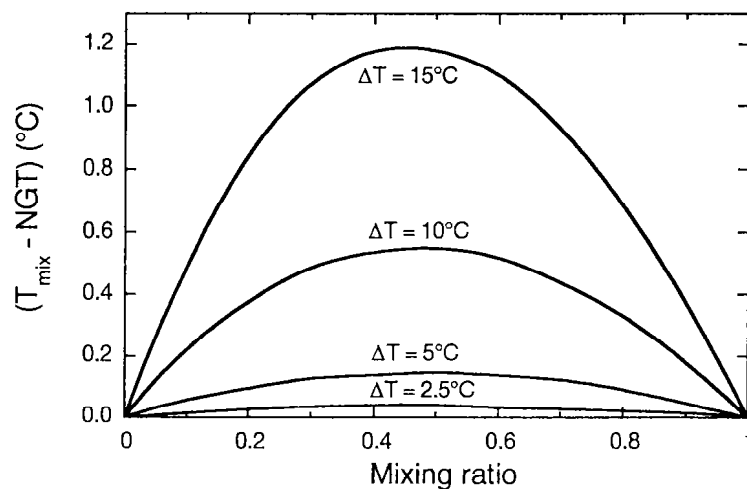


Figure 4.11: The impact of mixing two groundwater samples on the calculated noble gas temperature with a temperature difference of ΔT . T_{mix} defines the water temperature of the mixture and NGT is the noble gas temperature calculated from the mixed noble gas concentrations. The mixing ratio plotted on the x-axis refers to a water mass ($T = 10^\circ\text{C}$, excess air $A = 2 \cdot 10^{-3} \text{ cm}^3\text{STP/g}$) mixed with another water mass ($T = 10^\circ\text{C} + \Delta T$, excess air $A = 2 \cdot 10^{-3} \text{ cm}^3\text{STP/g}$).

Because of the radioactive decay of ^3H , the $^3\text{H}/^3\text{He}$ age is also non-linear with respect to mixing (Schlosser, 1992; Jenkins and Clarke, 1976). To illustrate this problem two mixing lines are drawn in a plot of isochrons calculated from Equation (4.7) (A-B and C-D in Figure 4.12). In both cases, the $^3\text{H}/^3\text{He}$ age of the mixture is weighted in favor of the water mass with the higher tritium concentration (Figure 4.12). Note that the non-linearity is normally less pronounced the smaller the age difference between the two mixing end-members is.

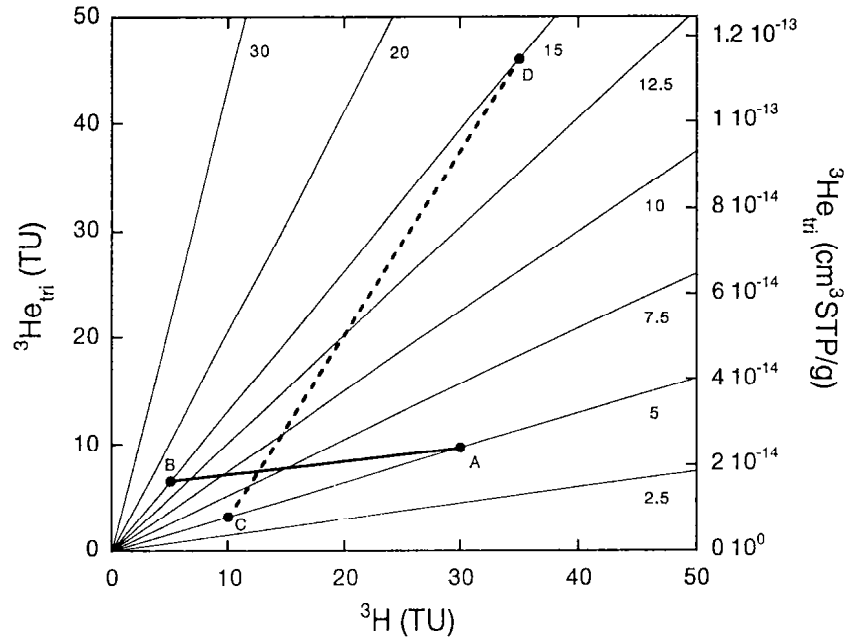


Figure 4.12: $^3\text{H}/^3\text{He}$ isochrons in years (thin solid lines). The $^3\text{H}/^3\text{He}$ age of the water mixtures along the lines A-B and C-D show non-linear behavior (see Figure 4.11).

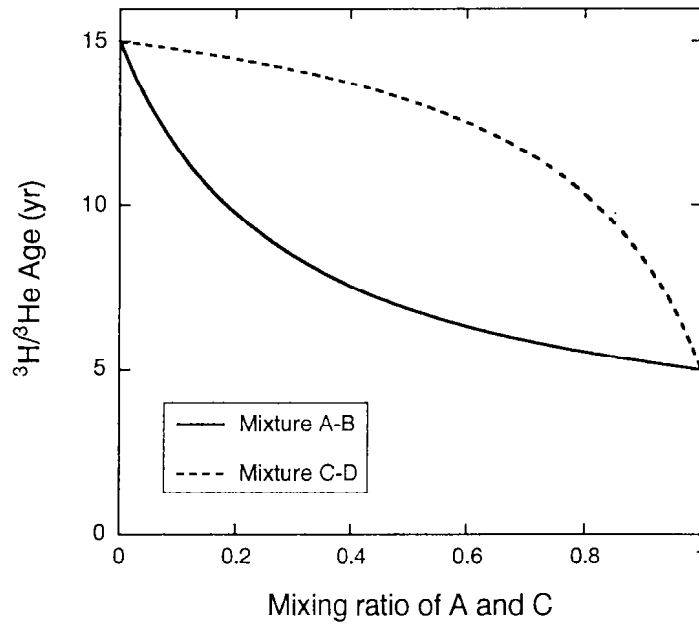


Figure 4.13: Non-linearity of the $^3\text{H}/^3\text{He}$ age with respect to the mixture along the line A-B and C-D shown in Figure 4.10. In both cases, the $^3\text{H}/^3\text{He}$ age of the mixture is weighted in favor of the water mass with the higher ^3H concentration. Figure 4.10 and Figure 4.11 are adapted from Jenkins and Clarke (1976).

4.3.2 Dispersion

Transport of a dissolved noble gas (concentration C) in a confined aquifer can be described by a one-dimensional dispersion/advection equation, if gas exchange with the atmosphere can be excluded:

$$\frac{\partial C}{\partial t} = D_x \frac{\partial^2 C}{\partial x^2} - v_x \frac{\partial C}{\partial x} + Q \quad [\text{cm}^3\text{STP}/(\text{g}\cdot\text{s})] \quad (4.26)$$

where v_x is the flow velocity of the groundwater. In the following it is assumed that groundwater flows with a constant velocity to the discharge area. In Equation (4.26) D_x is the dispersion coefficient and Q is any non-atmospheric production source for the noble gas. It is assumed that the porous medium is homogeneous and isotropic, that the medium is saturated, that the flow is steady-state, and that Darcy's law applies. Dispersion in groundwater is mainly caused by variations in the microscopic velocity within each pore channel and from one channel to another. The longitudinal dispersion coefficient D_x is related to the dispersivity or dispersion length α_x , the average linear velocity v_x and the diffusion coefficient D_{eff} (see Equation 4.22):

$$D_x = \alpha_x \cdot v_x + D_{eff} \quad [\text{m}^2/\text{s}] \quad (4.27)$$

Usually the contribution of molecular diffusion to the dispersion coefficient D_x is much smaller than the one of longitudinal dispersion (i.e., $D_{eff} \ll \alpha_x \cdot v_x$). The longitudinal dispersivity α_x has the dimension of a length and is characteristic for the observed aquifer.

Although the differential Equation (4.26) is linear and looks rather simple, explicit analytical solutions can only be derived for special cases. However, the sizes of certain non-dimensional numbers determine the shape of the solution in time and space. The following non-dimensional coordinates are introduced:

$$\xi = \frac{x}{x_0}, \quad \zeta = \frac{t}{t_0} \quad [-] \quad (4.28)$$

where x_0 and t_0 are the characteristic reference scales in space and time, such as

$$t_0 = \frac{x_0}{v_x} \quad [\text{s}] \quad (4.29)$$

Assuming no sink or source of noble gases in groundwater ($Q = 0$) Equation (4.26) can be transformed into a non-dimensional form

$$\frac{\partial C}{\partial \zeta} = \frac{D_x}{x_0 v_x} \cdot \frac{\partial^2 C}{\partial \xi^2} - \frac{\partial C}{\partial \xi} \quad [-] \quad (4.30)$$

The reciprocal value of the factor $D_x/(x_0 \cdot v_x)$ is called the Peclet number Pe and describes the relative importance of advection versus dispersive transport for a given distance x_0 from the recharge area :

$$Pe = \frac{x_0 \cdot v_x}{D_x} \quad [-] \quad (4.31)$$

Assuming that the molecular diffusion is negligible compared to dispersion (i.e. $D_x \approx \alpha_x \cdot v_x$) Equation (4.31) reduces to

$$Pe = \frac{x_0}{\alpha_x} \quad [-] \quad (4.32)$$

In practice and dealing with natural systems, it is hardly possible to determine the longitudinal dispersivity. A critical review of dispersivity observation from 59 different field sites is given by Gelhar et al. (1992). Overall, this data indicate a trend to systematic increase of the longitudinal dispersivity with observation scale (Figure 4.14). Although it is not appropriate to represent the longitudinal dispersivity data of Gelhar et al. (1992) by a single line, a simple linear regression through the data leads to the following rough estimation:

$$\alpha_x \approx \frac{x_0}{Pe} \quad [m] \quad \text{with } Pe \approx 10..100 \quad (4.33)$$

Note that the Peclet number does not depend on the flow regime at all (i.e. independent of v_x).

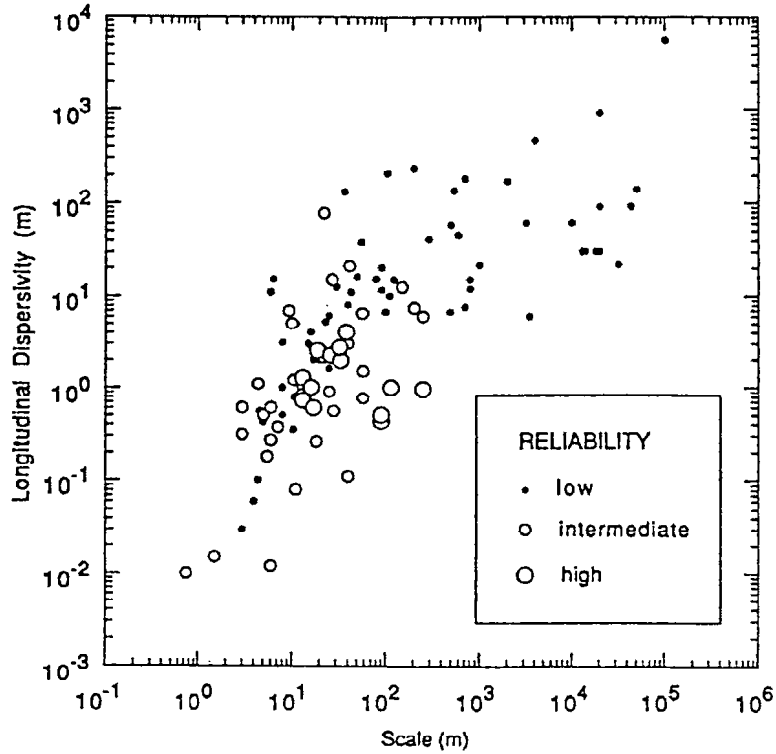


Figure 4.14: Longitudinal dispersivity α_x versus scale of observation x_0 classified by reliability. The data are from 59 filed sites characterized by widely different geologic materials (Gelhar et al., 1992).

In a first order approach, a climate signal produces periodic fluctuations of the dissolved noble gas concentration in groundwater, in particular in case of the temperature sensitive heavy noble gas species (Ar, Kr, and Xe). The typical periods T are between a day (diurnal fluctuations) and several thousand years in case of paleoclimatic oscillations. The fluctuations propagate into the aquifer by diffusion and advection. In addition to the Peclet number Pe , the non-dimensional attenuation number Ω (Roberts and Valochi, 1981) is given as

$$\Omega = \frac{\omega \cdot x_0}{v_x} = \frac{2\pi \cdot x_0}{T \cdot v_x} \quad [-] \quad (4.34)$$

The attenuation number Ω determines how far the external fluctuations are felt within the aquifer and how the phase shifts relative to the phase of the original signal.

Supposing that the noble gas concentration at the time of infiltration oscillates around a mean concentration C_0 with a amplitude of C_1 :

$$C^{init}(t) = C_0 + C_1 \cdot \sin(\omega t) \quad [\text{cm}^3\text{STP/g}] \quad (4.35)$$

The solution of advection/dispersion Equation (4.26) assuming no sink or sources ($Q = 0$) can be written in the form

$$C(x, t) = C_0 + C_1 \cdot \exp(-ax) \cdot \sin(\omega t - bx) \quad [\text{cm}^3\text{STP/g}] \quad (4.36)$$

The coefficients a and b describe the attenuation of the fluctuation and its corresponding phase shift. The non-dimensional expression of Equation (4.36) is (Roberts and Valochi, 1981):

$$\frac{C(\xi, \zeta)}{C_0} = 1 + \frac{C_1}{C_0} \cdot \exp(-\alpha\xi) \cdot \sin(\Omega\zeta - \beta\xi) \quad [-] \quad (4.37)$$

where the non-dimensional space and time coordinates, ξ and ζ , are define in Equation (4.28) and $\alpha = a \cdot x_0$ and $\beta = b \cdot x_0$. The non-dimensional attenuation coefficients α and β depend only on Pe and Ω as follows

$$\alpha = \frac{\text{Pe}}{2} \left(\sqrt{0.5 + 0.5 \sqrt{1 + \left[\frac{4\Omega}{\text{Pe}}\right]^2}} - 1 \right) \quad [-] \quad (4.38)$$

$$\beta = \frac{\text{Pe}}{2} \sqrt{0.5 \sqrt{1 + \left[\frac{4\Omega}{\text{Pe}}\right]^2} - 0.5} \quad [-] \quad (4.39)$$

To estimate the attenuation it is normally sufficient to use the following approximation of α and β :

$$\Omega \ll \text{Pe}: \quad \alpha = \frac{\Omega^2}{\text{Pe}}, \quad \beta = \Omega \quad [-] \quad (4.40)$$

$$\Omega \gg \text{Pe}: \quad \alpha = \beta = \sqrt{\frac{\text{Pe} \cdot \Omega}{2}} \quad [-] \quad (4.41)$$

According to Equation (4.37) the sinusoidal variation at the location $x = x_0$ is attenuated by the factor $\exp(-\xi \cdot \alpha)$ with $\xi = x/x_0 = 1$. For example, an attenuation factor

of $\exp(-\alpha) = 0.96$ corresponds to a reduction of the initial climate signal by 4%. The phase shift is equal to $-\beta/2\pi$ (in numbers of periods). For climate studies, however, the important factor is the attenuation of the signal.

In Figure 4.15 the attenuation factor $\exp(-\alpha)$ is plotted in function of the period T of a climate signal. As examples three different aquifers were chosen:

- (i) the shallow Linsental aquifer (either young samples (age ≈ 200 days) taken from high boreholes or older samples (age ≈ 3 years) taken from deep boreholes)
- (ii) the Glatt Valley aquifer with a horizontal extension of 10 km and a mean groundwater flow velocity of 0.4 m/yr, which corresponds to a maximum residence time of 25 kyr.
- (ii) the Great Artesian Basin in Australia, with a horizontal extension of 150 km (in the southwestern part) and a mean groundwater flow velocity of 0.4 m/yr, which corresponds to a maximum residence time of 375 kyr.

Table 4.8: Some examples of aquifers with different properties. Their potential as climate archives is shown in Figure 4.15.

		Linsental		Glatt Valley	Great Artesian Basin
		young samples	old samples		
Extension	x_0	200 m	1 km	10 km	150 km
Velocity	v_x	1 m/d	1 m/d	0.4 m/yr	0.4 m/yr
Longitudinal dispersivity	α_r	20 m	20 m	100 m	1.5 km
Time scale	$t_0 = x_0/v_x$	200 d	2.7 yr	25 kyr	375 kyr
Peclet number	$Pe = x_0/\alpha_r$	10	50	100	100

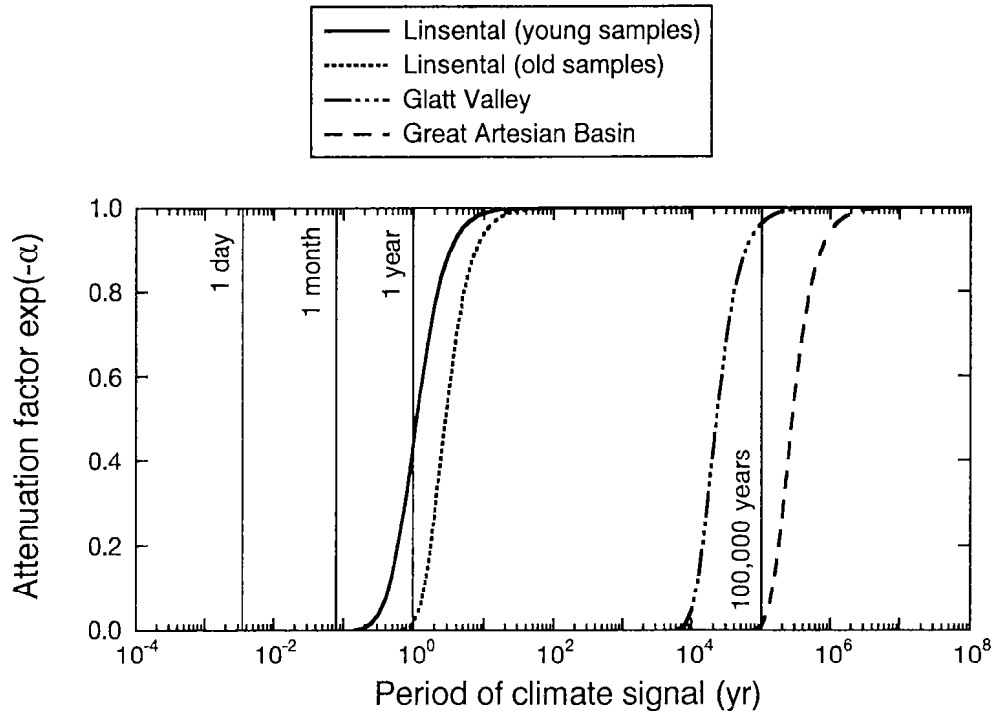


Figure 4.15: Attenuation factor $\exp(-\alpha)$ in function of the period T of a climate signal. The properties of the four examples are listed in Table 4.8. If the attenuation factor $\exp(-\alpha)$ is equal to 1, the climate signal is totally recorded in the aquifer. Yearly variations in the noble gas temperature are only detectable in the young samples of the Linsental aquifer (age ≈ 200 d). In contrast, the old samples (age ≈ 3 yr) should show no seasonal variations. The period of 100,000 years belongs to a typically paleoclimate oscillation. This signal is almost completely recorded in the Paleogroundwater of the Glatt Valley aquifer, whereas in the Great Artesian Basin the same signal is smoothed out.

In all four examples, daily variation of the temperature will be smoothed out completely. Note that daily variations are normally already attenuated by the soil and do not even penetrate to the water table (see section 4.1.2). In the Linsental aquifer the water age found in the shallow borehole is about 200 days on average (see chapter 5, Figure 5.3). It is known that the river mainly feeds the aquifer. The mean diurnal temperature of the river varies between 2°C in winter and 15°C in summer. With the assumption of Table 4.8 this amplitude would be reduced to about 45% after 200 days. In fact, there is a variation in the calculated noble gas temperature of the shallow boreholes in the order of 3°C (chapter 5, Table 5.1). In contrast to the shallow part of the Linsental aquifer, the samples taken from the deep boreholes show only a minimal variation in the noble gas temperature of $\pm 0.4^{\circ}\text{C}$, which is close

to the error of the noble gas method of $\pm 0.2^\circ\text{C}$. This finding is in good agreement with the estimation of Figure 4.15, which yields a reduction of the initial amplitude to 0.3°C (2% of 13°C) after 2.7 years.

The last two examples are paleogroundwaters, which record paleoclimate changes on much larger scales than the shallow Linsental aquifer (the Glatt Valley aquifer (GVA) in northern Switzerland (chapter 6), and the Great Artesian Basin (GAB) in Australia (Beyerle et al., 1998a). As shown in Figure 4.15, the amplitude of a typical interglacial-glacial climate signal with a period of 100,000 years (e.g., Rohling et al., 1998) is hardly reduced in the Glatt Valley aquifer. In contrast to the GVA, the same signal should be nearly smoothed out after 400 kyr in the Great Artesian Basin. Indeed, noble gas data from the Great Artesian Basin in Australia show an almost complete attenuation of the atmospheric Xenon concentrations after 200 kyr (Figure 4.16).

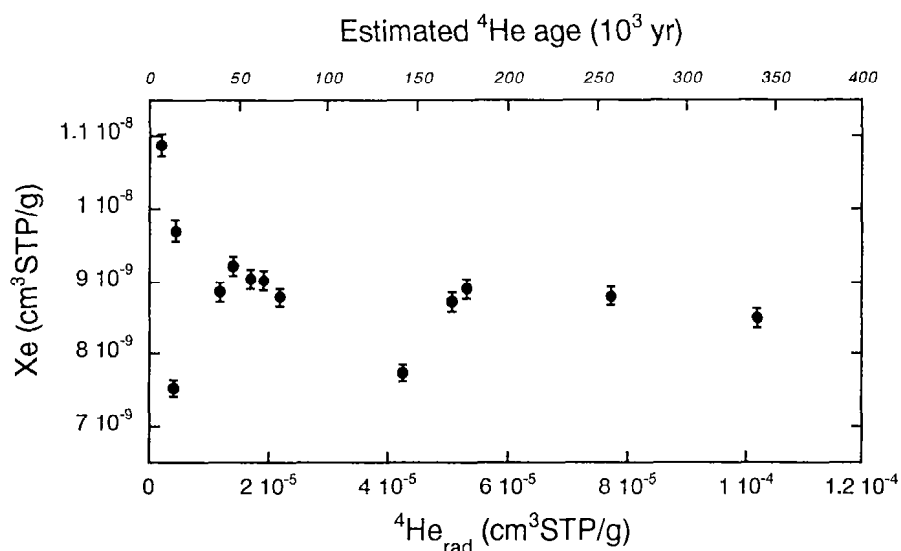


Figure 4.16: Xe concentration versus radiogenic ^4He of the Great Artesian Basin, Australia. The age that is plotted on the upper x-axis is estimated using the accumulation rate of a constant flux from outside of the aquifer (Tab. 4.6). The Xe concentration, which is most sensitive to temperature variations in the recharge area, becomes almost constant with increasing groundwater age.

Similar conclusion can be drawn if the advection/dispersion Equation (4.26) is solved numerically for different sets of parameters and boundary conditions. An example of such modeling is given in chapter 6 for the Glatt Valley Aquifer. Furthermore, Stute and Schlosser (1993) has shown how a $\delta^{18}\text{O}$ signal as recorded by benthic foraminifera obtained from deep sea cores (e.g., Shackleton et al., 1983) would be recorded in groundwater (Figure 4.17). As outlined before, the smoothing of the signal is mainly a function of the relative importance of dispersion and advection.

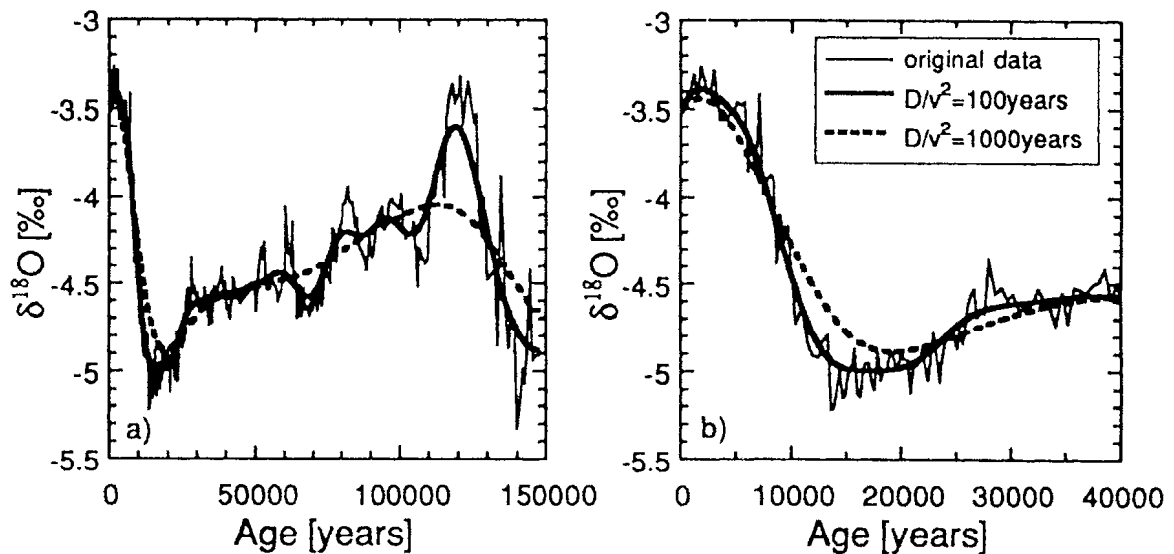


Figure 4.17: Smoothing of high frequency fluctuations of a climate signal by dispersion in a groundwater flow system as a function of $D_x/v_x^2 = \alpha_x/v_x$ for time scales of 150,000 years (left) and 40,000 years (right). The two Figures are taken from Stute and Schlosser (1993).

Infiltration of river water to a shallow aquifer investigated with $^3\text{H}/^3\text{He}$, noble gases and CFCs

U. Beyerle¹, W. Aeschbach-Hertig¹, M. Hofer¹, D. M. Imboden¹, H. Baur², and R. Kipfer¹

¹ Department of Environmental Physics, Swiss Federal Institute of Technology (ETH) and Swiss Federal Institute of Environmental Science and Technology (EAWAG), CH-8600 Dübendorf, Switzerland

² Isotope Geology, Department of Earth Sciences, Swiss Federal Institute of Technology (ETH), NO C61, CH-8092 Zürich Switzerland

(printed in *Journal of Hydrology* (1999) **220**, 169-185)

Abstract

Noble gas isotopes (^3He , ^4He , Ne, Ar, Kr, Xe), tritium (^3H), chlorofluorocarbons (CFCs) and dissolved oxygen (O_2) were seasonally measured in a small groundwater system recharged by infiltration of river water at Linsental, north-eastern Switzerland. All Groundwater samples contained an excess of atmospheric noble gases ('excess air') usually with an elemental composition equal to air. The concentrations of atmospheric noble gases in the groundwater were used to calculate the excess air component and the water temperature at recharge. The noble gas temperatures (NGTs) in the boreholes close to the river vary seasonally, however, the average NGT of all samples lies close to the mean annual temperature of the river water. Groundwater ages were calculated using the tritium/helium-3 ($^3\text{H}/^3\text{He}$) dating method. The water ages of the samples obtained near the river depend on the amount of recently infiltrated river water and are young during times of active river discharge. In contrast, the mean water age of about 3 years of the deep aquifer remained

nearly constant over the sampling period. The observed CFC-11 (CFCl_3) and CFC-12 (CF_2Cl_2) concentrations are significantly higher than the atmospheric equilibrium concentrations and therefore CFCs do not provide any direct information on the residence time of the groundwater. Nevertheless, the CFC excess in the groundwater shows a linear increase with the $^3\text{H}/^3\text{He}$ age. Additionally, both accumulation of radiogenic He ($^4\text{He}_{\text{rad}}$) and O_2 consumption are strongly correlated with residence time. All these correlations can be interpreted either in terms of mixing of recently infiltrated river water with older groundwater or in terms of accumulation/consumption rates.

5.1 Introduction

Young groundwater is commonly used for drinking water, e.g. over 80% of Switzerland's potable water resources come from groundwater (Hartmann and Michel, 1992). In alpine and prealpine countries a significant amount of this young groundwater is recharged by infiltration of river water. However, the knowledge about the time scale on which a particular groundwater is renewed is often poor. This situation may lead to mis-management and encourages the over-utilization of the groundwater as fresh water resource. Furthermore, if residence times are unknown, it is difficult to evaluate the potential effects of contamination and to develop strategies to protect the quality of the groundwater. Consequently, knowledge of the mean residence time and recharge dynamics of an aquifer is central for the protection and sustainability of groundwater resources.

The present study is part of a larger interdisciplinary research program which evaluates the possible impacts of a planned natural renaturalisation of the Swiss prealpine river Töss (Figure 5.1). Along its flow, the river Töss infiltrates through the riverbed and feeds the groundwater into the adjacent alluvial aquifer which provides drinking water for about 100,000 people. During the last century, the river Töss was canalized, but in recent years the effects of this canalization and of a potential renaturalisation of the river Töss have been discussed in detail.

In case of renaturalisation, the river bed could potentially move closer to the pumping stations leading to lower groundwater residence times which may have a negative effect on the drinking water quality. To develop objective criteria to decide on the planned renaturalisation, a series of hydrogeologic, flow-modeling, biological and isotopic studies have been initiated in a part of the Töss Valley called Linsental.

The main focus of this contribution is to determine the spatial and temporal variability of the mean groundwater residence times and to differentiate between recently infiltrated river water and older groundwater. To reach these objectives, the following tracers were used: (1) tritium (^3H) in combination with its decay product tritiogenic ^3He ($^3\text{He}_{\text{tri}}$); (2) dissolved chlorofluorocarbons (CFC-11, CFC-12); (3) dissolved oxygen (O_2), (4) radiogenic ^4He ($^4\text{He}_{\text{rad}}$), and (5) dissolved atmospheric noble gases.

The $^3\text{H}/^3\text{He}$ dating method offers a direct measure for the time since groundwater had its last gas exchange with the atmosphere (Tolstikhin and Kamenskiy, 1969; Schlosser et al., 1988) and provides quantitative groundwater residence times. Furthermore, excess in CFCs, deficits in O_2 and accumulation of $^4\text{He}_{\text{rad}}$ were established as qualitative indicators for older groundwater in the Linsental aquifer. All these indicators and the tritiogenic ^3He are based either on an excess or a lack of dissolved gases compared to the initial concentration in groundwater. This initial concentration can be derived from the concentrations of the atmospheric noble gases Ne, Ar, Kr, and Xe dissolved in groundwater.

5.2 Study area

The Töss valley is located 20 km north-east of Zürich, Switzerland. Its formation has been attributed to the fluvial erosion of the former glacial deposits through lateral migration of the river to the Upper Fresh Water Molasse bedrock. Subsequently, the bedrock was overlain with reconstituted Quaternary gravels from fluvial deposition forming the Töss Valley aquifer (Kempf et al., 1986). The Töss Valley aquifer is more than 40 km long with its lower boundary being the low permeable molasse bedrock.

The Linsental aquifer is in the lower reach of the Töss Valley and has a maximum thickness of 25 m and an average width of 200 m (Figures 5.1 and 5.2). Spatially the aquifer is highly heterogeneous with a range of hydraulic conductivities of 10^{-2} m/s in gravels to 10^{-5} m/s in clay lenses. Generally, the mean vertical hydraulic conductivity (K_V) in an alluvial aquifer is an order of magnitude smaller than the horizontal hydraulic conductivity (K_H) (Bouwer, 1978). This anisotropy can be attributed to the fluvial depositional history of the river. From field observations and pumping tests, the K_H of the gravels was found to fall in the range of 10^{-2} - 10^{-3} m/s (Kempf et al., 1986). Assuming a porosity between 0.2 and 0.3, which is typical for fluvial deposits, and a mean hydraulic gradient of the Linsental aquifer of about 10 m/km (Figure 5.1) the horizontal groundwater velocity can be estimated to be on the order of 10 to 100 m/d.

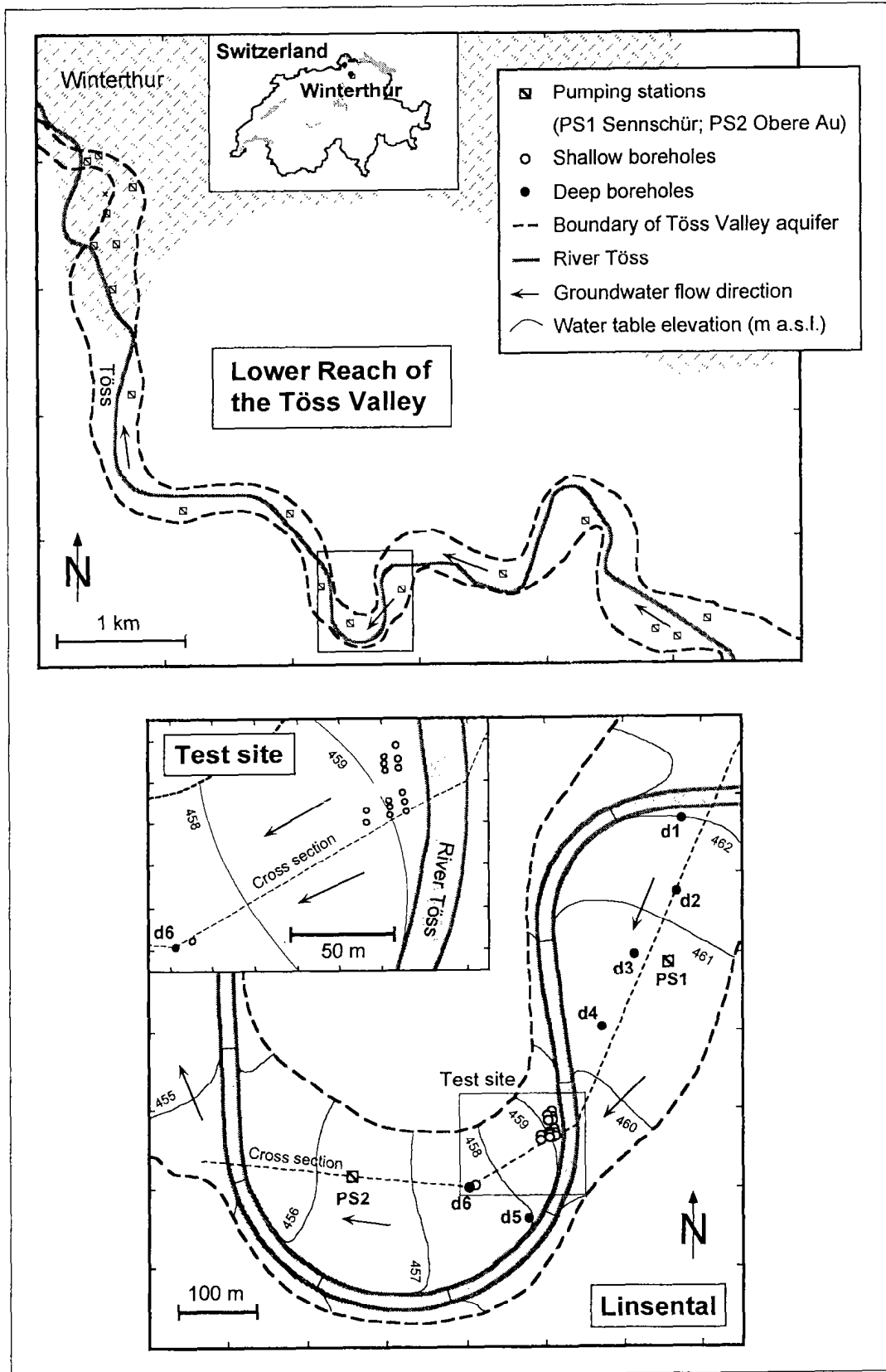


Figure 5.1: Schematic map of the Linsental (bottom), a part of the Töss Valley (top), Switzerland, close to the city of Winterthur. The thin dashed line indicates the position of the vertical cross section (shown in Figure 5.2).

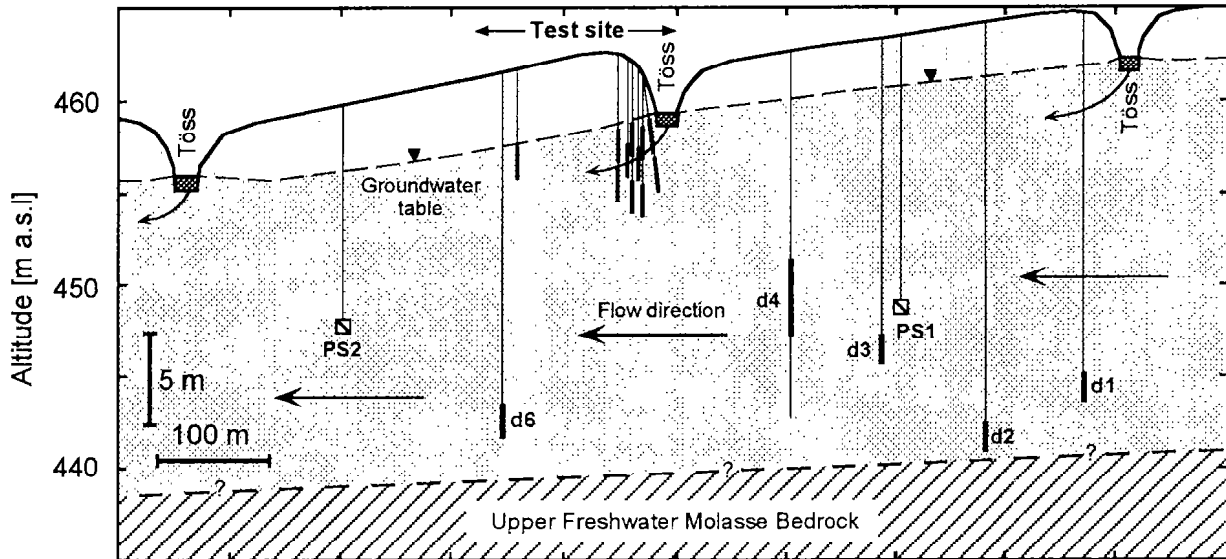


Figure 5.2: Vertical section through the Linsental aquifer. Well screens (in bold) are at the bottom of each borehole. Sample of borehole d4, which is along the whole length filtered, was taken at 11 m below water table.

Hydraulically, the Linsental aquifer is predominantly influenced by withdrawal of groundwater as a potable water resource from the pumping stations Sennschür (PS1) and Obere Au (PS2) (Figure 5.1) and by infiltration from the river Töss. The latter is controlled by the river discharge, the respective aquifer and river water levels, and the hydraulic conductivity of the river bed. During recent years, several boreholes were installed in the Linsental from which sampling is possible between 3 m and 25 m below surface. Closely spaced boreholes were drilled in the vicinity of the river to observe the local river infiltration ('test site' in Figures. 5.1 and 5.2).

Local precipitation controls the runoff dynamics of the river Töss. During floods, the discharge is two orders of magnitude higher than in dry periods (Figure 5.3). River temperatures vary between 18°C in summer and 0°C in winter. The mean annual temperature of the riverine water is 8.6°C (Figure 5.3) and is slightly lower than the mean annual air temperature of 9.2°C at the altitude of the Linsental (460 m a.s.l.) (Schüepp, 1981).

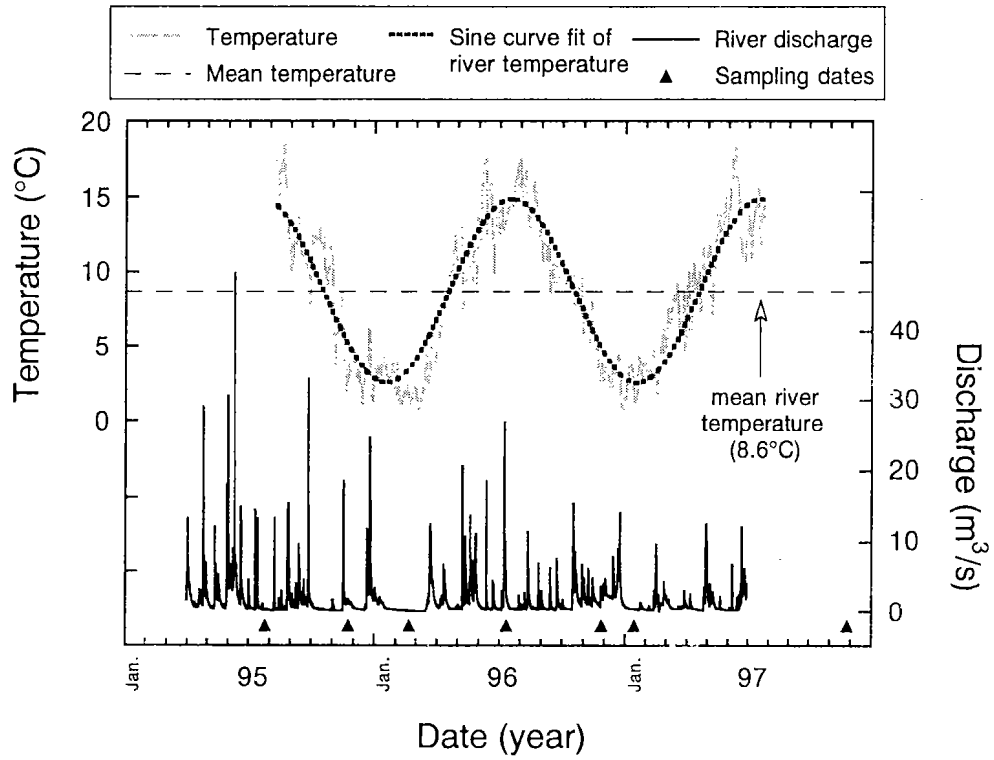


Figure 5.3: Daily discharge of the river Töss compared with the daily mean temperature of the river for the time period between 1995 and 1997.

5.3 Methods

5.3.1 Sampling and analysis

More than 60 samples of groundwater and river water from the Linsental were collected between 1995 and 1997. Groundwater samples were taken from 18 boreholes and two pumping stations by submersible pumps. The water for the noble gas, ^3H and CFC analysis was immediately transferred to 45-mL copper tubes and sealed with pinch-off clamps (Kipfer, 1991). The O_2 concentration was directly measured by Winkler titration.

Usually all noble gases (^3He , ^4He , Ne, Ar, Kr, Xe) were measured, with the exception of samples taken in July 1995 and January 1997 when only the ^3He , ^4He and Ne concentrations were analyzed. The ^3H concentration was measured in about every third sample, as variations in ^3H concentrations were expected to be small assuming residence times of a few months only. The CFC-11 (CFCl_3) and CFC-12 (CF_2Cl_2) concentrations were measured for most of the samples except for those taken in November 1996/97.

For the noble gas mass spectrometric analysis, the samples were quantitatively degassed on a vacuum line by water vapor transport through a capillary on liquid nitrogen cooled cold traps. The light noble gases He and Ne were analyzed according to the procedures described by Kipfer et al. (1994). After He and Ne analysis, the extracted water vapor (about 0.5 g) and all other condensable gases were released from the cold traps by heating to 180°C . After passing through a molecular sieve (3 Å pore diameter) to remove the water vapor, the gas was expanded to a 2 L reservoir. A split of 0.7 cm^3 was taken, passed through a series of getters to remove the reactive gases, and then admitted to the mass spectrometer for simultaneous analysis of Ar, Kr, and Xe. To improve the precision of the Xe measurement, in a larger gas split only the Xe concentration was measured. This time the Xe was separated from the other heavy noble gases by freezing on a cold trap at -100°C and later releasing it by heating to 180°C . The degassed water was transferred into the original copper tube and after several months the sample was reanalyzed for ^3He produced by the decay of ^3H .

For information on experimental details on noble gas, ^3H and CFC measurements refer to (Beyerle et al., in preparation), Kipfer et al. (1994) and Hofer and Imboden (1998), respectively.

The gas amounts of the samples are regularly calibrated against an air standard. Aliquots of an internal freshwater standard are routinely analyzed for the purpose of quality control. The typical precision of the $^3\text{He}/^4\text{He}$ ratios and the He, Ne, Ar, Kr concentrations for water samples, expressed as the reproducibility of the noble gas concentration of the water standard, are typically better than $\pm 1\%$ (1σ error). The typical precision of ^3H measurements is better than ± 1 TU, whereas the analytical error of the CFC measurement is less than $\pm 5\%$. Since the water samples were measured within 4 months after sampling, anoxic degradation of CFC-11 during storage is not significant compared to the error of the CFC-11 measurement (Hofer and Imboden, 1998).

5.3.2 Evaluation of noble gas temperature and excess air

The equilibrium concentration of dissolved atmospheric gases in groundwater (e.g. noble gases, CFCs and O_2) is determined by the individual partial pressure in the atmosphere, the water temperature at the groundwater table and the solubility of the gas, i.e. its Henry coefficient. In contrast to surface waters, at recharge groundwater commonly dissolves an excess of atmospheric gases in addition to the expected equilibrium concentration ('excess air') (Heaton and Vogel, 1981). The formation of excess air is poorly understood. Nevertheless, it has to be taken into account to calculate the initial concentration of dissolved gases in groundwater at recharge.

The amount of excess air and the recharge temperature both can be determined by measuring the concentration of Ne, Ar, Kr, Xe in groundwater, because the physical processes responsible for dissolution of atmospheric noble gases can be adequately modeled (see Aeschbach-Hertig et al., 1999). It is usually assumed that the elemental

composition of the excess air component corresponds to unfractionated atmospheric air, i.e. air bubbles trapped during recharge and later dissolved completely (Andrews, 1992). Therefore it is possible to calculate the two unknown variables, i.e. noble gas temperature (NGT) and excess air component from the known noble gas concentrations. Usually He can neither be used to derive the NGT nor the amount of excess air, because radiogenic He and tritiogenic ^3He often accounts for most of the observed ^3He and ^4He excess. In some aquifer systems, the composition of the excess air appears to deviate from that of atmospheric air. Partial loss of the excess air due to diffusive gas exchange at the water table has been proposed as a conceptual model to interpret the measured noble gas abundance pattern in such situations (Stute et al., 1995b). Thus, one additional parameter, the degree of re-equilibration may be needed to describe noble gas concentrations in groundwater. To calculate NGT we used the fitting procedure established by Aeschbach-Hertig et al. (1999). Solubility data of noble gases in water are taken from the following references: Weiss (1971) for He and Ne; Weiss (1970b) for Ar; Weiss and Kyser (1978) for Kr and Clever (1979) for Xe, respectively.

The NGT measures the soil temperature at recharge and corresponds typically to the annual mean air temperature (Stute et al., 1995a). Differences between annual mean air temperature and NGT may occur in cases where infiltration rates are very high, the water table is very close or far from the surface, or where water predominately infiltrates during warmer/colder periods (Stute and Schlosser, 1993). However, no data about NGT are available for river-bank infiltrated groundwater.

5.3.3 $^3\text{H}/^3\text{He}$ dating of groundwater

Tritium (^3H), the radioactive isotope of hydrogen with a half life of 12.38 years (Oliver et al., 1987), has been extensively used to study hydrologic systems such as oceans, lakes and groundwater. Most studies used the ^3H release from nuclear bomb tests in the atmosphere as a time marker. In addition, ^3H has been combined with its decay product $^3\text{He}_{\text{tri}}$ (tritiogenic ^3He) to determine the so called $^3\text{H}/^3\text{He}$ water age

(Schlosser et al., 1988; Solomon et al., 1992; Aeschbach-Hertig et al., 1998). Since residence times in the Linsental aquifer are expected to be on the order of months, ^3H alone can not be used. The $^3\text{He}/^3\text{H}$ ratio provides information on the groundwater age. The concentration of dissolved ^3He increases as soon as the groundwater is isolated from the atmosphere, because ^3He produced by ^3H decay can no longer escape. Therefore the $^3\text{He}_{\text{tri}}/^3\text{H}$ ratio is a measure for the time elapsed since a water parcel was last in contact with the atmosphere. The $^3\text{H}/^3\text{He}$ age τ is defined as (Tolstikhin and Kamenskiy, 1969):

$$\tau = \frac{1}{\lambda} \cdot \ln \left(1 + \frac{^3\text{He}_{\text{tri}}}{^3\text{H}} \right) \quad [\text{yr}] \quad (5.1)$$

where $\lambda = 0.0556 \text{ yr}^{-1}$ is the decay constant of ^3H and ^3H the measured ^3H concentration. It is usually expressed in tritium units (TU). 1 TU corresponds to a $^3\text{H}/^1\text{H}$ ratio of 10^{-18} and decays to $2.488 \times 10^{-15} \text{ cm}^3\text{STP}^3\text{He}/\text{g}_{\text{water}}$. $^3\text{He}_{\text{tri}}$ is defined as the fraction of the total ^3He produced by ^3H decay, i.e. the difference between the measured concentration $^3\text{He}_{\text{tot}}$ and the concentrations of all other ^3He components ($^3\text{He}_{\text{eq}}$: equilibrium, $^3\text{He}_{\text{ex}}$: excess air, $^3\text{He}_{\text{terr}}$: terrigenic):

$$^3\text{He}_{\text{tri}} = ^3\text{He}_{\text{tot}} - ^3\text{He}_{\text{eq}} - ^3\text{He}_{\text{ex}} - ^3\text{He}_{\text{terr}} \quad [\text{cm}^3\text{STP}/\text{g}_{\text{water}}] \quad (5.2)$$

The equilibrium concentration in water $^3\text{He}_{\text{eq}}$ is determined by the water temperature and the ambient pressure during recharge. Solubility data for He and Ne isotopes are taken from Weiss (1970) and from Benson and Krause (1980). The atmospheric excess $^3\text{He}_{\text{ex}}$ can be calculated from the Ne or also from the ^4He excess, provided the latter is exclusively of atmospheric origin. Isotopic and elemental compositions of the atmosphere are taken from Ozima and Podosek (1983). The $^3\text{He}_{\text{terr}}$ can be derived from the terrigenic ^4He , if the $^3\text{He}/^4\text{He}$ ratio of the injected He is reasonably well known. In this study the $^3\text{He}_{\text{terr}}$ was calculated using the average $^3\text{He}/^4\text{He}$ production ratio in crustal rocks of 2×10^{-8} (Mamyrin and Tolstikhin, 1984). However, since the radiogenic ^4He component in the groundwater of the Linsental is in the range of a few percent, the $^3\text{He}_{\text{terr}}$ is almost negligible. As an example, the 1.2 year old groundwater sample taken from the pumping station PS1 has the following relative ^3He fractions: 80% $^3\text{He}_{\text{eq}}$, 14% $^3\text{He}_{\text{ex}}$, 6% $^3\text{He}_{\text{tri}}$, and 0.04% $^3\text{He}_{\text{terr}}$ assuming a radiogenic $^3\text{He}/^4\text{He}$ ratio of 2×10^{-8} .

5.4 Results and discussion

5.4.1 $^3\text{H}/^3\text{He}$ groundwater ages

Between 1995 and 1997 ^3H concentrations hardly varied in the Linsental aquifer (Table 5.1), but were significantly larger than the average ^3H content in precipitation of northern Switzerland (17.7 ± 1.8 TU in 1993, Aeschbach-Hertig, 1994). Local tritium enrichments are reported from other highly industrialized parts of Switzerland (Völkle et al., 1996). Whereas ^3H variations in the groundwater are small (deep: 26.0 ± 1.3 TU, shallow: 27.3 ± 1.7 TU), ^3H fluctuates considerably in the river water (30.2 ± 3.3 TU). Assuming the mean ^3H of the river to be constant over time, the differences in ^3H concentrations between the river and the groundwater can be roughly interpreted in terms of a residence time that is in the order of 2 to 3 years.

More precise estimates of groundwater residence times can be gained if ^3H and $^3\text{He}_{\text{tri}}$ are combined to calculate $^3\text{H}/^3\text{He}$ ages according to Eqs. (5.1) and (5.2). For water samples in which ^3H was not measured, ^3H concentrations were assumed to be equal to the average ^3H concentration of the Linsental aquifer (Table 5.1). The tritiogenic ^3He was calculated using the following assumptions: (1) during recharge the water temperature is either equal to the calculated NGT or the measured groundwater temperature, (2) the pressure at the water table corresponds to a mean atmospheric pressure at the altitude of the Linsental (960 mbar at 460 m a.s.l.) and (3) the observed non-tritiogenic ^3He excess originates from the complete dissolution of air, and in case of a radiogenic ^4He component, from terrigenic He injection with a $^3\text{He}/^4\text{He}$ ratio of 2×10^{-8} .

Note that in case of low water ages (< 3 years) and approximately constant ^3H concentrations as in the Linsental aquifer, the $^3\text{He}_{\text{tri}}$ concentration is almost linearly related to the calculated $^3\text{H}/^3\text{He}$ age and the age error induced by the measured ^3H value is negligible. The error in the calculated age is mainly caused by errors of the $^3\text{He}/^4\text{He}$ ratio and the concentrations of He and Ne. If no radiogenic He component is present in a given sample, ^4He is used instead of Ne for excess air correction. This excess air correction leads to smaller errors in age because the $^3\text{He}/^4\text{He}$ ratio is measured with a better precision than the $^3\text{He}/\text{Ne}$ ratio (about ± 40 days instead of ± 100 days).

Table 5.1: Noble gas temperature (NGT), tritium concentration (^3H) and $^3\text{H}/^3\text{He}$ ages of river Töss, the shallow boreholes from the test site (depth: 3-8 m) and the deep borehole d6 (depth: 19 m)

Date	NGT (°C)			^3H (TU)			$^3\text{H}/^3\text{He}$ age (days)	
	River ⁽¹⁾	Shallow ⁽²⁾	Deep(d6) ⁽³⁾	River ⁽²⁾	Shallow ⁽³⁾	Deep(d6) ⁽²⁾	Shallow ⁽³⁾	Deep(d6) ⁽³⁾
26 July 95	-	-	-	28.2±0.9	27.2±0.4	24.4±1.2	20±30	640±130
24 Nov. 95	5.7±0.1	9.3±0.2	8.4±0.2	30.1±0.7	25.8±1.0	26.8±1.3	450±70	620±110
21 Feb. 96	4.7±0.2	7.2±0.3	8.3±0.2	26.2±0.6	25.2±0.6	24.1±0.6	400±130	660±100
12 July 96	13.9±0.1	10.2±0.8 ⁽⁵⁾	8.1±0.2	31.8±0.8	26.8±0.7	26.0±0.7	40±60	450±70
27 Nov. 96	-	8.8±0.2	8.9±0.2	-	29.1±0.7 ⁽²⁾	26.8±0.7	70±30 ⁽²⁾	550±100
14 Jan. 97	-	-	-	34.9±0.8	29.5±1.3	27.3±0.6	140±30	450±100
26 Nov. 97	-	-	9.1±0.2	-	-	26.9±0.7	-	560±100
Average ⁽⁴⁾	8.1±5.1	8.9±1.3	8.6±0.4	30.2±3.3	27.3±1.7	26.0±1.3	190±190	560±90

⁽¹⁾ NGT and its error derived from Ne, Ar, Kr, and Xe concentrations by fitting temperature and excess air to minimize the sum of the weighted least square differences between measured and predicted concentrations (Aeschbach-Hertig et al., 1999)

⁽²⁾ error is equal to the analytical error of the measured value (1 σ error)

⁽³⁾ error is equal to the standard deviation between the values for each shallow borehole

⁽⁴⁾ error is equal to the standard deviation between the values for each sampling date

⁽⁵⁾ satisfactory fit only if an additional parameter for partial re-equilibrium after formation of excess air (degassing) is assumed

The $^3\text{H}/^3\text{He}$ ages in the Linsental aquifer show a distinct variation over time. The samples from the deep part of the aquifer have an almost constant water age, whereas water ages of the shallow aquifer depend on the time of sampling (Table 5.1). Occasionally the mean age of the shallow part is similar to the age of the deep groundwater, at other times most ages from the shallow boreholes do not differ significantly from zero. This variation of the water ages is shown in Figure 5.4 in which $^3\text{H}/^3\text{He}$ ages are plotted against the horizontal distances from the river. Samples with younger water ages can be interpreted as a binary mixture between locally infiltrated river water in different proportions and older groundwater. As the local infiltration is

reduced or even cut off, only older groundwater remains and therefore the $^3\text{H}/^3\text{He}$ age of the groundwater close to the river is comparable to the age of the deep aquifer.

To illustrate this, in February 1996 the mean water age of the shallow aquifer was 400 days with a standard deviation of ± 130 days. This mean residence time of the shallow part of the aquifer is comparable to the groundwater age of the deep aquifer of 660 ± 100 days leading to the conclusion that local river infiltration was small. In contrast, the mean water age of the shallow groundwater in July 1996 had decreased to 40 ± 60 days (Table 5.1, Figure 5.4b) which indicates that locally infiltrated river water dominates. Indeed, in winter there was no major flood recorded in the Töss valley for almost 30 days prior to the February sampling, whereas in July 1996 heavy rain and flooding events were common (see Figure 5.3).

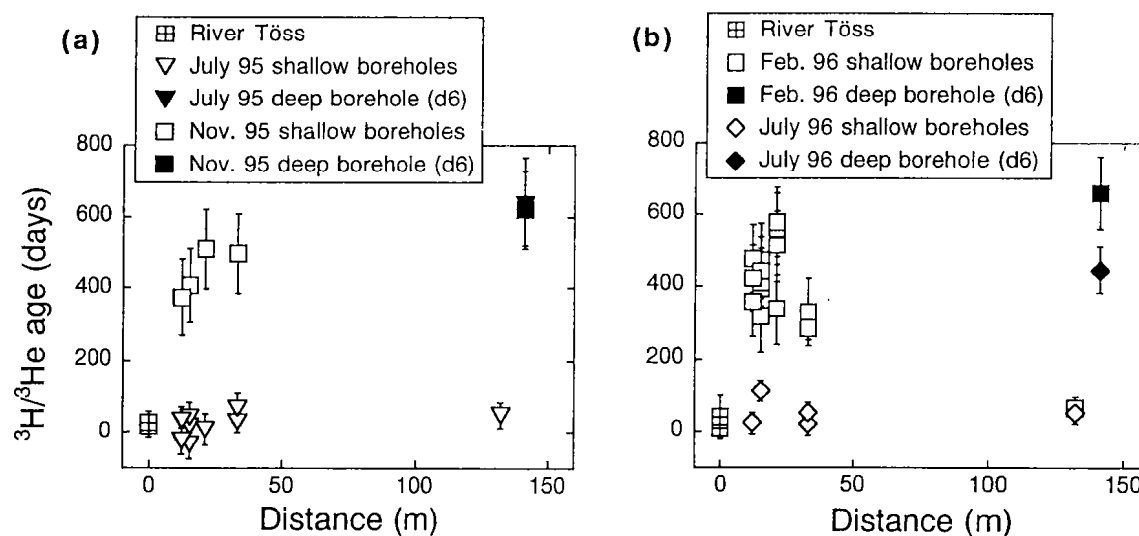


Figure 5.4: $^3\text{H}/^3\text{He}$ groundwater ages versus distance from the river Töss of samples taken at the test site (cf. Figures 5.1 and 5.2).

In Table 5.2 the $^3\text{H}/^3\text{He}$ water ages of the deep boreholes reaching the molasse bedrock are compared to the water ages found in the pumping stations (PS1, PS2) which extract groundwater a few meters above the molasse bedrock. The pumping stations operate at about 100 L/min for 5 to 6 hours in the evenings. Samples were taken in the morning subsequent to pumping during 30 minutes. The water ages in the pumping stations were found to be about 1 year. The mean age is much higher than the communal water supply authorities previously expected and is far larger than the threshold of 10 days quoted in the groundwater regulations (Pedroli, 1982). Model calculations using current average pumping rates as boundary conditions indicate that the youngest components of water attracted by the pumping stations have residence times from infiltration to the well along a single flow track of more than 10 days (Mattle, 1999). Assuming that the pumped water in PS1 is a binary mixture of recently infiltrated river water (age ≈ 0 days) and older groundwater that is similar to the one at the nearby borehole, d1 (960 ± 100 days), the older component accounts for roughly 50%. A similar mixing ratio for PS2 can be estimated, assuming that the older component is equal to the one at the nearby borehole, d6 (560 ± 90 days).

Table 5.2: $^3\text{H}/^3\text{He}$ groundwater ages of the samples from the deep boreholes (d1-d6) and the pumping stations Sennschür (PS1) and Obere Au (PS2) from different sampling dates.

$^3\text{H}/^3\text{He}$ age (days)							
d1	d2	d3	d4	d5	d6	PS1	PS2
960 ± 100 ⁽⁴⁾	750 ± 100 ⁽¹⁾	190 ± 40 ⁽¹⁾	550 ± 70 ⁽¹⁾	290 ± 90 ⁽⁴⁾	560 ± 90 ⁽⁵⁾	480 ± 90 ⁽⁴⁾	290 ± 90 ⁽²⁾
	800 ± 100 ⁽³⁾	320 ± 40 ⁽³⁾					
	910 ± 90 ⁽⁴⁾						

⁽¹⁾ 12 July 1996

⁽²⁾ 27 November 1996

⁽³⁾ 14 January 1997

⁽⁴⁾ 26 November 1997

⁽⁵⁾ average, cf. Table 5.1

5.4.2 Noble gas data from the Linsental aquifer

Groundwater is commonly supersaturated with atmospheric air (excess air). Since the light noble gases are far less soluble in water than the heavier noble gases, He and Ne react more sensitively to excess air than Ar, Kr and Xe. Indeed, measured He and Ne concentrations confirm that the supersaturation of noble gases is essentially controlled by the complete dissolution of air, as usually the elemental ratio of the light noble gas excess is in agreement with the atmospheric value ($Ne_{ex}/He_{ex} = (Ne/He)_{air} = 3.47$; Figure 5.5). But in some samples, He tends to be enriched relative to Ne which is indicative of a small non-atmospheric He component, most probably of radiogenic origin. This interpretation is in accordance with the observation that the largest 4He excesses are found in the oldest groundwater samples (see section 4.5).

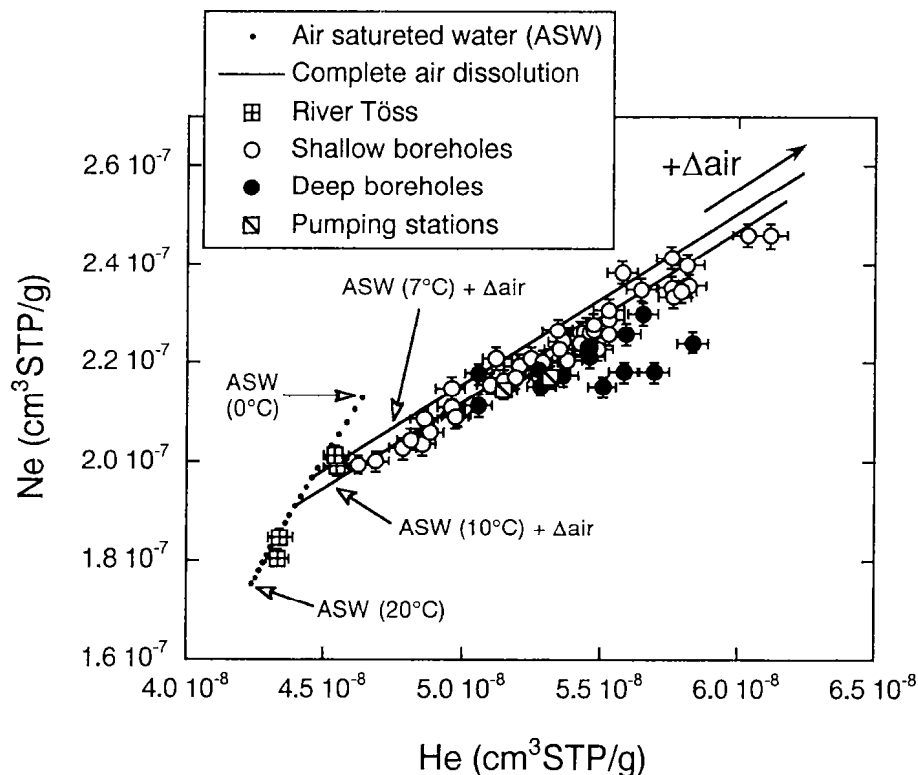


Figure 5.5: He versus Ne concentrations from the Linsental aquifer and the river Töss. Error bars correspond to the analytical error (1σ).

The noble gas temperature (NGT) and the amount of excess air of the samples were determined by using the optimization algorithm of Aeschbach-Hertig et al. (1999). In fact, although the river water is close to equilibrium, all groundwater samples contain appreciable amounts of excess air, even those from wells within meters of the river bank and with near zero $^3\text{H}/^3\text{He}$ ages. The amount of excess air in the groundwater varies between 5×10^{-4} and 3×10^{-3} $\text{cm}^3\text{STP/g}$ (5 to 30 % ΔNe). Except for 4 of the 47 samples, it is not necessary to assume a fractionation of the excess air in order to achieve a good fit. Since most of the samples have a, albeit small, radiogenic He component, the inclusion of He to fit NGT and excess air is usually not possible.

For the 42 samples with unfractionated excess air, temperature can be determined with a precision of $\pm 0.2^\circ\text{C}$, ranging from 6.6 to 9.6°C . Thus, if we take the error estimate at face value, the scatter of the noble gas temperatures must indicate real temperature variations. The effects of temperature and excess air on noble gas concentrations can be visualized in a graph of Xe versus Ne concentrations (Figure 5.6).

Xe reacts most sensitively to temperature, whereas Ne reflects mainly the effects of excess air. The noble gas data form clusters which are separated from each other mainly by different Xe concentrations. These concentration clusters indicate different regimes of groundwater recharge at different temperatures and therefore samples from shallow depths tend to exhibit seasonal variations. The samples taken in February 1996 have the highest Xe concentrations, corresponding to the lowest temperatures, yielding a mean temperature of 7.2°C with a standard deviation of only $\pm 0.3^\circ\text{C}$. The relatively warm mean NGT of 9.3°C from November 1995 suggests that this groundwater was infiltrated not in late autumn but during summer (Table 5.1). The NGTs of the deep borehole (d6) are almost constant over time (mean 8.6°C) and correspond well to the mean annual temperature of the river Töss (8.6°C , Figure 5.3). It appears that the mean NGT is closer to the mean river temperature than to the mean atmospheric temperature of 9.2°C . The variability of calculated NGTs is small compared to the fluctuation of the river temperature, as in general the amplitude of temperature oscillations exponentially decreases with depth in soils and groundwater (e.g., Stute and Schlosser, 1993; Matthess, 1982).

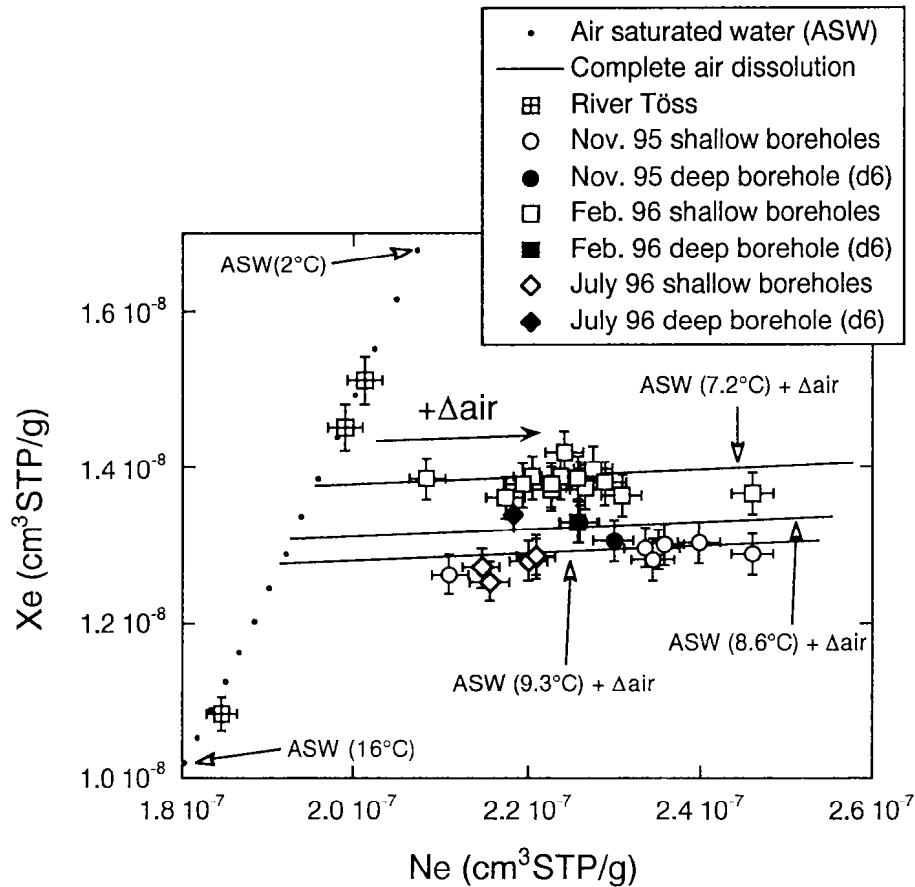


Figure 5.6: Ne versus Xe concentrations from the Linsental aquifer and the river Töss.

The four samples taken from the shallow part of the aquifer during July 1996 have similar Xe concentrations as the November samples (Figure 5.6). However, the NGT cannot be satisfactorily fitted assuming that excess air corresponds to unfractionated air. Yet, a model with an additional parameter for partial re-equilibration after formation of the excess air yields reasonable fits (Stute et al., 1995b; Aeschbach-Hertig et al., 1999). With this model, the mean NGT of the samples from July 1996 is 10.2°C (Table 5.1). Unfortunately, the error of the calculated NGT is considerably higher than that derived with the simple excess air model. The mean temperature error for the five samples taken in July is $\pm 0.6^\circ\text{C}$, although noble gas concentrations were determined with a precision of $\pm 1\%$.

The major conclusions of this section are that excess air is formed within days after infiltration and within meters from the river, and that this excess air is mainly unfractionated. If this is the case, infiltration temperatures can be determined with high precision ($\pm 0.2^\circ\text{C}$), allowing to easily detect seasonal variations of only about $\pm 1^\circ\text{C}$.

5.4.3 CFCs excess caused by contamination

Chlorofluorocarbons (CFCs) have been used in hydrology to date groundwaters (Thompson and Hayes, 1979; Busenberg and Plummer, 1992; Dunkle et al., 1993). In the Linsental aquifer, the following two reasons exclude the direct application of the CFC method to obtain information about the groundwater residence times: Atmospheric CFC concentrations did not increase significantly during the last few years (Elkins et al., 1993), and even more importantly, CFC concentrations in the Linsental aquifer are in excess compared to the expected initial concentration in groundwater.

As for all atmospheric gases, the initial concentration of CFCs in groundwater is determined by the atmospheric concentration, atmospheric pressure, solubility and the amount of excess air. The solubility is controlled by the recharge temperature of the groundwater, with CFC-11 being more soluble in water than CFC-12 (Warner and Weiss, 1985). The impact of excess air on CFC concentrations is very small, e.g. a typical supersaturation of 15% in Ne (dissolution of atmospheric air of $1.5 \times 10^{-3} \text{ cm}^3\text{STP/g}$) corresponds to a CFC excess of only about 1%.

The CFC content of the atmosphere in the Linsental is deduced from the riverine CFC concentration, assuming that the river Töss is in atmospheric equilibrium as indicated by the noble gas concentrations (Figures 5.5 and 5.6). The calculated atmospheric CFC abundances are almost constant over the entire observation period. The mean atmospheric CFC concentration is slightly higher than modern atmospheric values (Cook and Solomon, 1997), possibly caused by local industrial activity (400 pptv vs. 300 pptv for CFC-11 and 620 pptv vs. 550 pptv for CFC-12). For the given atmospheric CFC concentrations and the recharge temperatures, the expected CFC

concentrations of the groundwater in the Linsental aquifer should be in the range of 800 to 1500 pg/kg for CFC-11 and of 300 to 500 pg/kg for CFC-12. However, the CFC concentrations in the Linsental aquifer vary from 1000 up to 4100 pg/kg for CFC-11 and from 320 up to 730 pg/kg for CFC-12. As a result it is concluded that the groundwater in the Linsental is influenced by non directly atmospheric CFCs which limits the use of CFC for dating.

The CFC excess (ΔCFC) is derived by subtracting the calculated equilibrium concentration and the amount due to excess air from the measured CFC concentration:

$$\Delta CFC = CFC_{tot} - CFC_{eq} - CFC_{ex} \quad [\text{pg/kg}] \quad (5.3)$$

In the Linsental aquifer ΔCFC -11 increases linearly with ΔCFC -12 yielding a constant ΔCFC -11/ ΔCFC -12 ratio of 10 ± 1 (Figure 5.7). Since this ratio is higher than the CFC-11/CFC-12 ratio both in air $(CFC\text{-}11/CFC\text{-}12)_{air} \sim 0.6$ and in equilibrated water $(CFC\text{-}11/CFC\text{-}12)_{eq} \sim 3$ (for 8 - 10°C), CFC-11 is enriched over CFC-12 in the CFC excess compared to atmosphere derived CFCs. The comparison of ΔCFC s with groundwater age shows a linear increase as well (Figure 5.8).

Most probably, the observed CFC concentrations represent a mixture between locally infiltrated, uncontaminated river water and contaminated, older groundwater from the deep aquifer. Consequently, this older groundwater, which recharges and is contaminated at some distance, must have a constant CFC-11/CFC-12 ratio of around 10. About the source of the contamination we can only speculate. Either industrial pollution (Thompson and Hayes, 1979; Busenberg and Plummer, 1992) or sorption and desorption of the CFCs from soil surface are responsible for this CFC excess (Russell and Thompson, 1983). In Linsental, CFCs do not provide direct information on groundwater residence time, but they provide information on groundwater mixing and river bank controlled groundwater recharge.

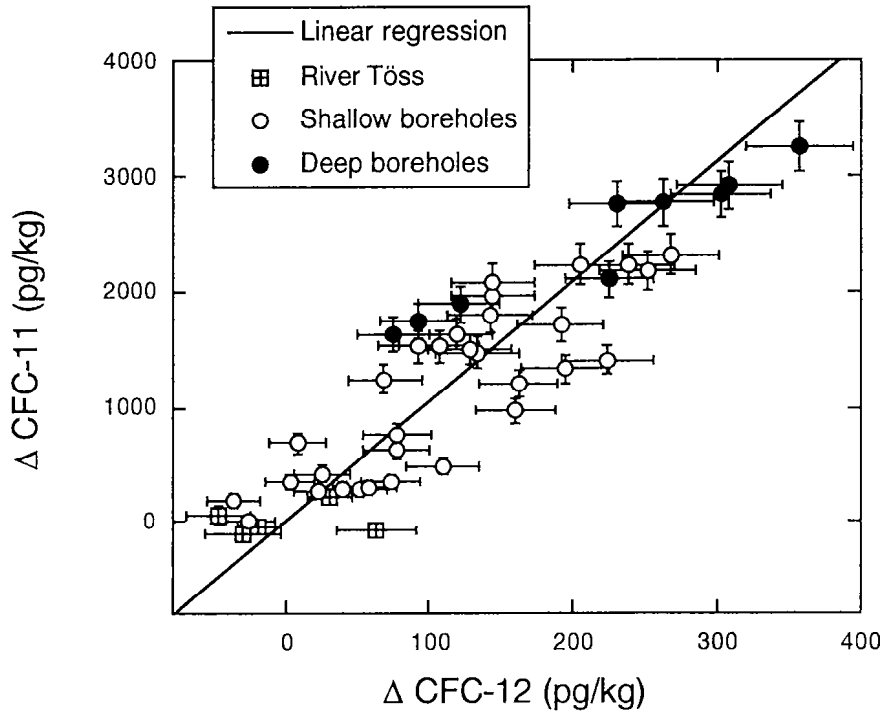


Figure 5.7: CFC-12 excess ($\Delta\text{CFC-12}$) plotted against CFC-11 excess ($\Delta\text{CFC-11}$) in the Linsental aquifer yielding a $\Delta\text{CFC-11}/\Delta\text{CFC-12}$ ratio of 10 ± 1 .

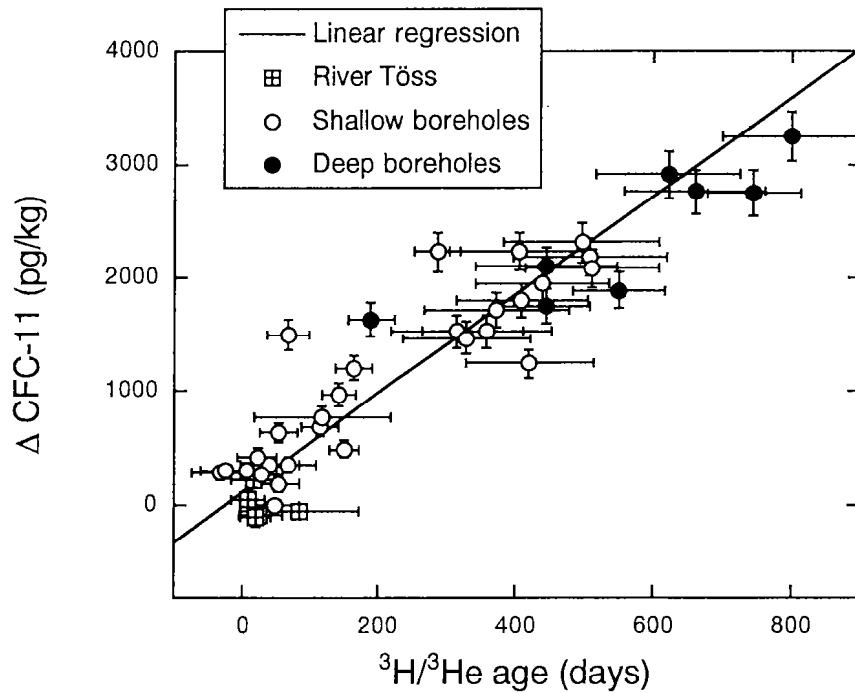


Figure 5.8: CFC-11 excess ($\Delta\text{CFC-11}$) plotted against calculated $^3\text{H}/^3\text{He}$ groundwater age in the Linsental aquifer.

5.4.4 Variation in the dissolved oxygen concentration

The concentration of dissolved oxygen generally decreases with residence time because of bacterial metabolic activity in the groundwater and can be used as an indicator of groundwater age. In alluvial aquifers oxygen consumption starts immediately after air-saturated river water infiltrates into the hyporheic zone which separates riverine water from groundwater (Triska et al., 1989). Due to high metabolic activity, the O_2 concentration sharply decreases during the passage of the water through the hyporheic zone. The hyporheic respiration rates of rivers are large (Malard and Hervant, 1999), e.g. about $4 \text{ mg } O_2 \text{ L}^{-1} \text{ h}^{-1}$ for the Nekar river (Naegeli et al., 1995). After passing the hyporheic zone and reaching the 'real' groundwater flow, the O_2 degradation decreases by more than three orders of magnitude (Malard and Hervant, 1999). The strong variability of oxygen consumption in and below the hyporheic zone reflects mainly the availability of organic matter and bacterial activity.

In Figure 5.9 the O_2 deficit in the Linsental aquifer is plotted against the calculated groundwater age. We define the reduction in O_2 as the difference between the measured O_2 concentration and the initial O_2 content at recharge which is given by the sum of the expected atmospheric equilibrium concentration and the excess air component:

$$\Delta O_2 = O_{2 \text{ tot}} - O_{2 \text{ eq}} - O_{2 \text{ ex}} \quad [\text{mg/L}] \quad (5.4)$$

Equilibrium and excess air O_2 can be derived from atmospheric noble gas concentrations. Note that in contrast to Eq. (5.4), O_2 consumption is commonly calculated relative to atmospheric equilibrium conditions although the existence of excess air is evident. In the Linsental aquifer samples with negligible $^3\text{H}/^3\text{He}$ age indeed do show a significant O_2 reduction of about 2.8 mg/L which can be easily explained by a fast O_2 consumption in the hyporheic zone within about an hour. However, the rate of change of dissolved O_2 in the groundwater, which has a measurable residence time, is only $(1.2 \pm 0.2) \text{ mg/L yr}^{-1}$ (Figure 5.9). As for the CFCs, the linear relation between ΔO_2 and $^3\text{H}/^3\text{He}$ age may also be interpreted in terms of mixing of riverine water after passing the hyporheic zone and older groundwater from the deeper aquifer.

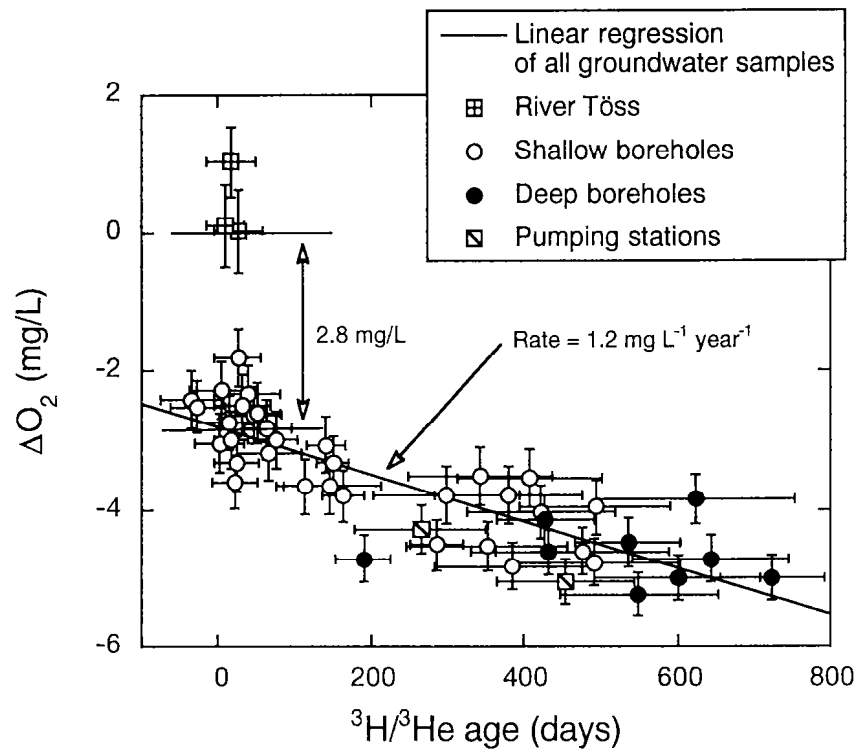


Figure 5.9: Oxygen deficit (ΔO_2) plotted against calculated $^3\text{H}/^3\text{He}$ groundwater age.

5.4.5 Radiogenic ^4He accumulation in the Linsental aquifer

Radiogenic ^4He ($^4\text{He}_{\text{rad}}$) has been widely used to estimate water residence times of up to 10^8 years in old groundwater systems (e.g., Andrews and Lee, 1979; Andrews et al., 1985; Torgersen and Clarke, 1985). Groundwater ^4He ages are based on the assumption that $^4\text{He}_{\text{rad}}$ is generated by the decay of U and Th in the aquifer matrix and accumulates continuously in the groundwater. However, the use of ^4He for calculating groundwater ages requires a detailed knowledge of the aquifer characteristics, such as porosity and the concentrations and spatial distributions of U and Th. Furthermore, the $^4\text{He}_{\text{rad}}$ accumulation rate is often much larger than the expected ^4He production due to U/Th decay in the aquifer matrix. Increased ^4He accumulation rates are explained either by (1) a ^4He -flux from the entire continental crust into the aquifer (Torgersen and Clarke, 1985), (2) ^4He transport from reservoirs in the upper most part of the continental crust (Lehmann and Loosli, 1991), or (3) by ^4He that accumulated over long time scales in the past in solid rock, which has relatively recently been eroded to form the aquifer matrix and now releases the stored ^4He by diffusion from the small grains (Solomon et al., 1996). Since the strength of an additional $^4\text{He}_{\text{rad}}$ source is highly uncertain, $^4\text{He}_{\text{rad}}$ accumulation rates can only be reasonable estimated if cross calibration with other dating methods is possible (e.g. $^3\text{H}/^3\text{He}$, CFC, ^{14}C , or hydrodynamic model ages).

The $^4\text{He}_{\text{rad}}$ in Figure 5.10 is calculated as the difference between the measured ^4He ($^4\text{He}_{\text{tot}}$) and the atmospheric ^4He component given by the equilibrium concentration ($^4\text{He}_{\text{eq}}$) and the excess air component ($^4\text{He}_{\text{ex}}$):

$$^4\text{He}_{\text{rad}} = ^4\text{He}_{\text{tot}} - ^4\text{He}_{\text{eq}} - ^4\text{He}_{\text{ex}} \quad [\text{cm}^3\text{STP/g}] \quad (5.5)$$

The in situ $^4\text{He}_{\text{rad}}$ production rate of gravel aquifers, as in the Linsental, is less than $10^{-11} \text{ cm}^3\text{STP/g}_{\text{water}} \text{ yr}^{-1}$ (Lehmann and Purtschert, 1997). However, the observed $^4\text{He}_{\text{rad}}$ increases with water age up to $5 \times 10^{-9} \text{ cm}^3\text{STP/g}_{\text{water}}$ (Figure 5.10).

A linear fit through the data yields a ^4He accumulation rate of $(1.9 \pm 0.2) \times 10^{-9} \text{ cm}^3\text{STP/g yr}^{-1}$. The observed $^4\text{He}_{\text{rad}}$ accumulation rate in the Linsental aquifer is at least two orders of magnitude larger than the expected in situ production rate. Furthermore, the estimated accumulation agrees within previous estimates of ^4He accumulation rates determined in different prealpine Swiss lakes (Aeschbach-Hertig, 1994). Although caution prevails in interpreting the available data on ^4He accumulation, the found constancy in the ^4He accumulation may indicate that the ^4He emanation seems to be constant within a factor of 5 in a region as large as Switzerland.

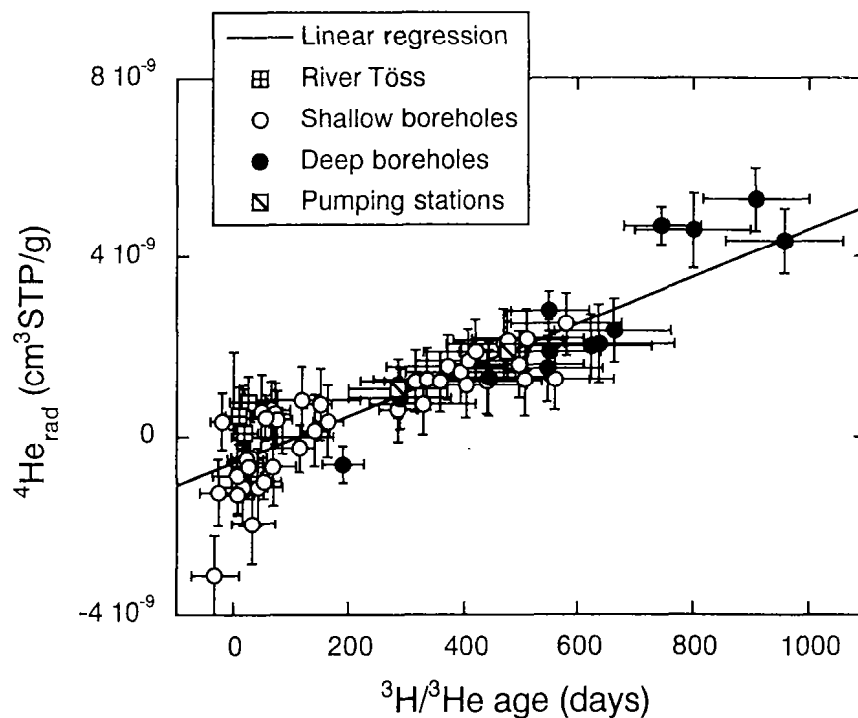


Figure 5.10: Radiogenic ^4He ($^4\text{He}_{\text{rad}}$) plotted against calculated $^3\text{H}/^3\text{He}$ groundwater age yielding a ^4He accumulation rate of $(1.9 \pm 0.2) \times 10^{-9} \text{ cm}^3\text{STP/g yr}^{-1}$.

5.5 Summary and conclusions

This study demonstrates that the $^3\text{H}/^3\text{He}$ dating method provides valuable information on the recharge dynamics and residence time of a river-bank infiltrated groundwater system. On the one hand deep groundwater in the Linsental is characterized by a relatively constant water age of about 2 years representing the mean residence time in the aquifer. On the other hand the measured $^3\text{H}/^3\text{He}$ ages of the shallow boreholes close to the river can be interpreted in terms of mixing of recently infiltrated river water with older groundwater. This idea is strongly supported by the fact that groundwater from the shallow boreholes have almost zero $^3\text{H}/^3\text{He}$ water ages subsequent to higher river discharge rates. The $^3\text{H}/^3\text{He}$ age data have important consequences for the water management in the Linsental. The water age at the pumping stations used for public water supply was found to be considerably higher than expected. The major conclusion from this result is that at least 50% of the pumped water originates from the deep aquifer.

Concerning the planned renaturalisation of the Töss river at the test site, the two major results are: (1) Although the quantity of locally infiltrated river water depends on the discharge of the river Töss, the residence time of the deep groundwater is not affected by different infiltration regimes; (2) In contrast to the previous idea that the water of the pumping stations originates directly from the river Töss, at least half of the water comes from the deep aquifer which contains older groundwater. These results indicate that safety regulations for drinking water can be met even if the distance between the river and the pumping stations is reduced.

In the Linsental the non-tritiogenic ^3He component is mainly of atmospheric origin and can be deduced from the concentration of dissolved atmospheric noble gases. Additionally, knowing the noble gas recharge temperature and the amount of excess air, the initial concentration of any other dissolved atmospheric gas can be calculated. Consequently, any process that modifies this initial gas concentration during groundwater flow can be observed (e.g., accumulation, consumption and mixing).

CFCs cannot be used for dating purposes in the Linsental. Yet, the CFC excess increases linearly with $^3\text{H}/^3\text{He}$ age. This observation reinforces the conclusion that the shallow groundwater can be interpreted as a mixture between river water and deep

groundwater, which has elevated concentrations of CFCs. Therefore CFCs are useful even though a non-atmospheric contribution is present. The knowledge of initial O₂ concentrations (equilibrium plus excess air component) and groundwater residence times, allows the rate of O₂ change to be quantified. In the Linsental the degradation of O₂ during groundwater flow was found to be much slower than the fast O₂ consumption in the hyporheic zone. Finally, the data from the Linsental aquifer allow us to calculate a ⁴He accumulation rate of $(1.9 \pm 0.2) \times 10^{-9} \text{ cm}^3 \text{STP/g}_{\text{water}} \text{ yr}^{-1}$, which is two orders of magnitude higher than the in situ production. This result shows that ⁴He can be used as a dating tool also in young groundwaters provided that ⁴He accumulation rates can be determined by calibration using e.g. the ³H/³He dating method. However at present a generally accepted model for the accumulation of radiogenic ⁴He in groundwater bodies is still missing.

Acknowledgements

We would like to thank the communal water supply of Winterthur (Wasserversorgung der Stadt Winterthur) for allowing us to take samples of the Linsental groundwater. This project was supported by the Swiss National Science Foundation (project no. 20-47060.96) and the EAWAG Priority Research Program 1993-97: Sustainable Management of Resources.

Climate and groundwater recharge during the last glaciation in an ice-covered region

U. Beyerle¹, R. Purtschert², W. Aeschbach-Hertig¹, D. M. Imboden¹, H. H. Loosli², R. Wieler³, and R. Kipfer¹

¹ Department of Environmental Physics, Swiss Federal Institute of Technology (ETH) Zurich and Swiss Federal Institute of Environmental Science and Technology (EAWAG), CH-8600 Dübendorf, Switzerland

² Physics Institute, University of Berne, CH-3012 Berne, Switzerland

³ Isotope Geology, Department of Earth Sciences, Swiss Federal Institute of Technology (ETH), NO C61, CH-8092 Zurich, Switzerland

(printed in *Science* (1998), **282**, 731-734)

Abstract

A multitracer study of a small aquifer in northern Switzerland indicates that the atmosphere in central Europe cooled by at least 5°C during the last glacial period. The relation between oxygen isotope ratios ($\delta^{18}\text{O}$) and recharge temperatures reconstructed for this period is similar to the present-day one if a shift in the $\delta^{18}\text{O}$ value of the oceans during the ice age is taken into account. This similarity suggests that the present-day $\delta^{18}\text{O}$ -temperature relation can be used to reconstruct paleoclimate conditions in northern Switzerland. A gap in calculated groundwater age between about 17,000 and 25,000 years before the present indicates that during the last glacial maximum, local groundwater recharge was prevented by overlying glaciers.

Continental climate records from mid-latitude regions that experienced ice cover during the last glacial period are scarce. Groundwaters have been used as paleoclimate archives in permanently ice-free regions (Rudolph et al., 1984; Stute et al., 1992a; Stute et al. 1992b; Andrews et al., 1994; Stute et al., 1995a; Stute et al., 1995b). Here we present groundwater data from the Glatt Valley, Switzerland, which was ice-covered after a glacial advance during the last glacial maximum (Schlüchter et al., 1987). The impact of glaciation on groundwater recharge and dynamics is not well known, but numerical models have shown that glaciers can dramatically change groundwater flow (Boulton et al., 1995; Piotrowski, 1997). In groundwater, past values of climate variables can be derived from the stable isotope composition of water molecules (Münnich and Vogel, 1962; Degens, 1962) and the concentrations of dissolved atmospheric noble gases (Mazor, 1972). Besides the local air temperature, many factors control the isotopic composition of groundwater ⁽¹⁾. In contrast, the concentrations of atmospheric noble gases dissolved in groundwater are determined mainly by the solubility equilibrium during infiltration, given by the mean local atmospheric pressure (specified by the altitude of the recharge area), and by the water temperature prevailing during recharge. The so-called noble gas temperature (NGT) is therefore a measure of the temperature at which groundwater equilibrated with the atmosphere during infiltration, and it commonly corresponds to the mean annual air temperature (Stute and Schlosser, 1993). Consequently, information on stable isotopes and noble gases taken together allows one to evaluate the oxygen isotope $\delta^{18}\text{O}$ -temperature relation over long time scales.

The deep Glatt Valley aquifer (GVA), situated about 100 m below ground level, is 15 km long, 3 km wide, and has an average thickness of 10 m (Figure 6.1). It is formed of gravel and sand and has a permeability of 10^{-5} to 10^{-6} m s⁻¹ (Wyssling, 1988). Poorly permeable Pleistocene sediments separate the GVA from a shallow unconfined groundwater system, the Aathal aquifer. The presumed recharge area of the GVA is located near borehole 0 at an elevation of about 540 m. In 1995 and 1996, samples from boreholes tapping the GVA were collected by means of a submersed pump. Hydrochemistry, noble gases, radionuclides (³H, ⁸⁵Kr, ³⁷Ar, ³⁹Ar, and ¹⁴C) and stable isotope ratios ($\delta^{13}\text{C}$, $\delta^2\text{H}$, and $\delta^{18}\text{O}$) were measured (Table 6.1).

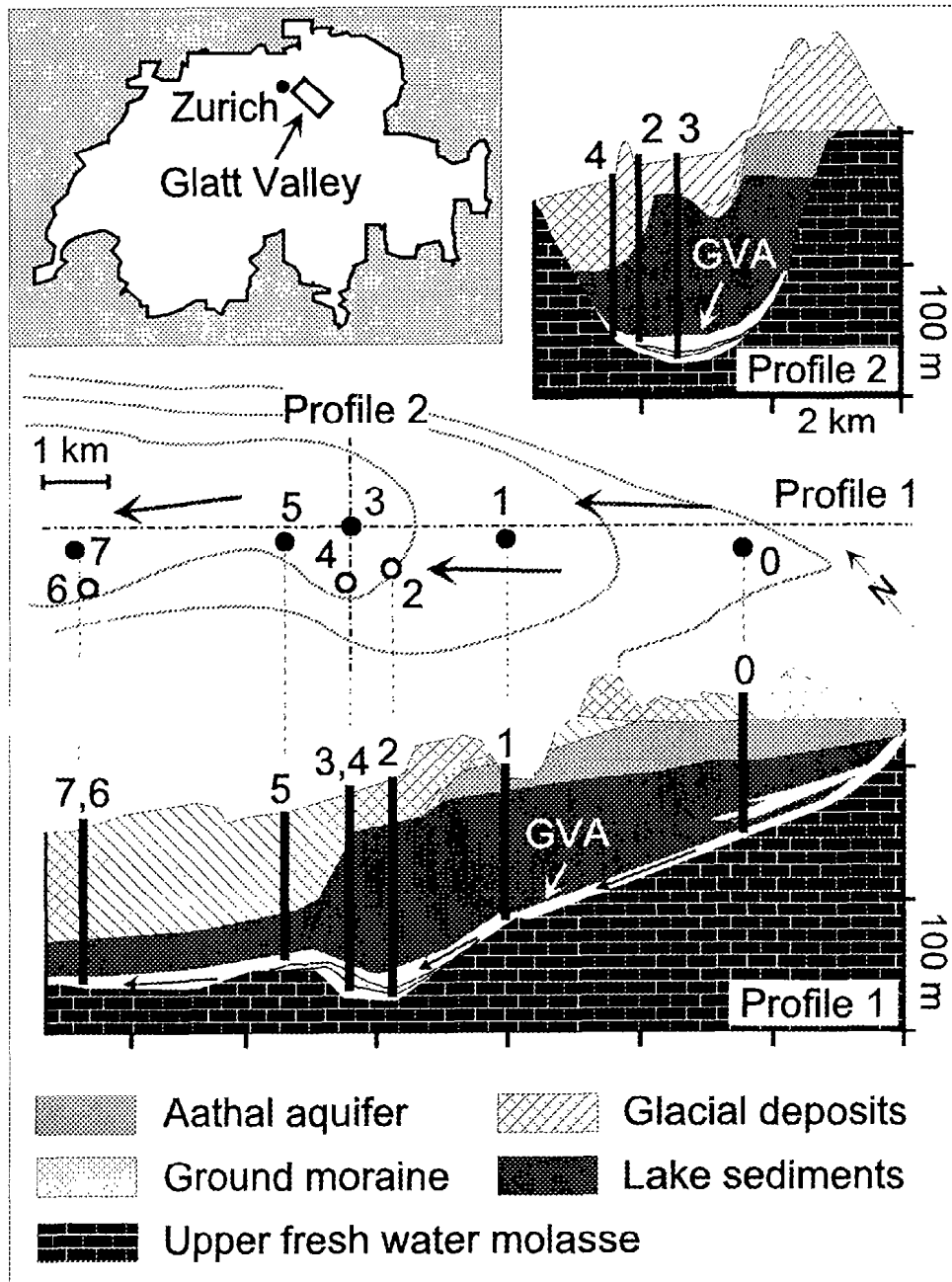


Figure. 6.1: (Top left) Map showing the location of the Glatt Valley, Switzerland. (Center) Detailed map of the study area showing boreholes 0 through 7. Open circles represent boreholes yielding a mixture of an older and a younger groundwater; solid circles represent boreholes without mixture; dash-dotted lines indicate location of profiles 1 and 2 (shown top right and bottom); and thin solid lines indicate the contours of the underlying molasse bedrock (shown at 50-m intervals). The presumed recharge area lies south-east of borehole 0, where the confining sediments outcrop (Wyssling, 1988). Arrows indicate the general direction of groundwater flow.

NGTs are calculated from noble gas concentrations by accounting for their temperature-dependent solubilities and for the common excess air component found in groundwater (Andrews, 1992; Heaton and Vogel, 1981)⁽²⁾. Groundwater ages were determined from the ^{14}C activities of the total dissolved inorganic carbon. Conventional correction models (Ingerson and Pearson, 1964; Fontes and Garnier, 1979) using chemical and isotopic balances were applied to convert activity values into ^{14}C ages. Conversion into calibrated years before present (B.P.) is based on (Bard et al., 1990; Stuiver and Reimer, 1993).

Only the water from the recharge area (borehole 0) contains significant amounts of ^3H (half-life, 12.4 years) and ^{85}Kr (half-life, 10.8 years). The ^3H and ^{85}Kr values indicate a mean residence time of 15 years. Water from three boreholes (2, 4, and 6) turned out to be binary mixtures of an older and a younger component (Table 6.2). The proportion and residence time of the younger component were determined by measuring the concentrations of Cl^- and of the radioactive isotopes ^3H and ^{39}Ar (half-life, 269 years)⁽³⁾. The presence of atmospheric ^{39}Ar and the absence of ^3H in the samples from boreholes 2, 4, and 6 (Table 6.1) imply that the younger component has a residence time of a few hundred years. The ^{14}C ages and NGTs of the older component in these samples were calculated by correcting for the younger component. This correction is the cause of the large uncertainty in the ^{14}C ages at boreholes 2, 4, and 6. In the following, calibrated ^{14}C ages, NGTs and $\delta^{18}\text{O}$ values refer only to the older component.

Table 6.1: Noble gas, stable and radioactive isotope, and chloride data from the GVA groundwater samples. Sampling locations are given in Figure 6.1. ΔNe is the contribution of excess air to the Ne concentration normalized to the solubility equilibrium component at the temperature equal to the NGT. NGT is the noble gas temperature derived from Ne, Ar, Kr, and Xe by optimizing temperature and excess air to minimize the sum of the weighted least square difference between measured and predicted concentrations (Aeschbach-Hertig et al. 1999; Weiss, 1970b, 1971; Weiss and Kyser, 1978; Clever 1979b). ^{14}C , ^{39}Ar and ^{85}Kr activities were measured by low-level counting (Andrews et al., 1984). STP, standard temperature and pressure; pmc, percent modern carbon; TU, tritium unit; dpm, decay per minute; NA, not analyzed.

Borehole	$\delta^2\text{H}$ (‰)	$\delta^{18}\text{O}$ (‰)	He (10^{-8})	Ne (10^{-7})	Ar (10^{-4})	Kr (10^{-8})	Xe (10^{-8})	ΔNe (%)	NGT (°C)
			(cm ³ STP/g)						
0	-70.0	-9.8	5.67	2.39	4.13	9.40	1.34	24	7.8 ±0.6
1	-70.6	-9.7	11.3	2.16	3.94	9.22	1.39	11	7.3 ±0.5
2	-71.2	-10.0	49.6	2.41	4.23	9.79	1.50	22	5.6 ±0.7
3	-80.5	-11.0	26.5	2.42	4.38	10.24	1.65	20	3.8 ±1.1
4	-73.1	-9.8	27.3	2.42	4.21	9.64	1.37	24	6.8 ±0.6
5	-85.5	-11.5	51.3	2.16	4.32	10.45	1.74	6	2.4 ±1.4
6	-74.4	-10.5	89.5	2.37	4.29	10.02	1.54	19	4.9 ±0.6
7	-94.9	-12.8	91.9	3.13	4.64	10.60	1.70	54	3.2 ±1.7
1σ error	±1.5	±0.1	±1%	±1%	±1%	±1%	±1.5%	±3	

Borehole	^{14}C (pmc)	^{13}C (‰)	^{39}Ar (%modern)	^3H (TU)	^{85}Kr (dpm / cm ³ STP Kr)	Cl ⁻ (μmol/L)
0	78.9 ±0.9	-15.1	114 ±8	30.0 ±1.3	29.8 ±0.6	129.8
1	22.1 ±0.4	-10.3	9 ±5	0.4 ±0.1	0.8 ±0.6	11.3
2	24.5 ±0.5	-11.1	27 ±5	0.3 ±0.1	NA	19.7
3	9.2 ±0.5	-11.0	12 ±3	0.1 ±0.1	0.4 ±0.4	11.3
4	39.3 ±0.1	-14.7	54 ±8	0.3 ±0.1	0.6 ±0.4	22.6
5	1.7 ±0.2	-8.1	NA	0.7 ±0.1	NA	14.1
6	5.1 ±0.2	-10.3	35 ±6	0.1 ±0.1	NA	19.7
7	1.9 ±0.2	-10.3	≤18	0.1 ±0.1	NA	16.9
1σ error		±0.4				±3%

Table 6.2: Proportion of the younger component ⁽³⁾ and corrected data for the older component of mixed samples. Noble gas concentrations and stable isotope ratios for the older component were calculated by assuming that the younger component had the same composition as the sample from borehole 0.

Borehole	Proportion of the younger component (%)	Corrected data for the older component		
		$\delta^2\text{H}$ (‰)	$\delta^{18}\text{O}$ (‰)	NGT (°C)
2	35 ±5	-71.9 ±2.5	-10.1 ±0.2	4.6 ±1.1
4	50 ±5	-72.4 ±3.4	-9.8 ±0.2	6.1 ±0.7
6	8 ±5	-74.8 ±1.7	-10.6 ±0.1	4.7 ±0.6

The NGTs vary significantly with time (Figure 6.2). NGTs of groundwater samples younger than 7000 years (7 kyr) agree with the recent mean annual air temperature of 8.3°C in the recharge area (Schüep, 1981) and demonstrate the validity of the noble gas "thermometer" for modern climate. The intermediate NGTs at boreholes 2 and 4 are most likely the results of dispersive mixing within the aquifer under a climatic transition to present-day conditions. The lower NGTs of the samples with ¹⁴C ages of 15 kyr B.P. (borehole 3) and around 28 kyr B.P. (boreholes 5 and 7) indicate a climate that was 5°C colder than it is now. During the last glacial maximum (around 18 kyr B.P.) (CLIMAP, 1976), the temperature drop may have been even greater than 5°C, but no samples with ages between 25 and 17 kyr B.P. were found. An indication of a similar age gap has also been found in a study of a Triassic sandstone aquifer in England (Bath et al., 1979). In our study, it is unlikely that insufficient spatial resolution of the sampling boreholes is responsible for the observed age gap. Borehole 5 (27 kyr B.P.) and borehole 3 (15 kyr B.P.) are separated by less than 1 km along the direction of the flow. Adopting the mean observed flow velocity of 0.4 m year⁻¹ between boreholes 0 and 3, 1 km corresponds to an age increase of only 2.5 kyr. The gap is therefore interpreted to be the result of an almost complete cessation of groundwater recharge between 25 and 17 kyr B.P.. The inference that groundwater formation was interrupted during the last glacial maximum is consistent with the glaciological and climatological history of the Glatt Valley and adjacent areas: The Glatt Valley was ice-free before 28 kyr B.P. and after 14.5 kyr B.P.

(Schlüchter et al., 1987). The climate was dry and cold between about 33.5 and 28.5 kyr B.P. (Schlüchter et al., 1987), during which time infiltration may have been reduced or even interrupted. However, enhanced biological activity around 28 kyr B.P. (Schlüchter et al., 1987), corresponding to the age of the samples from boreholes 5 through 7, indicates the occurrence of a brief warm period during which infiltration was possible.

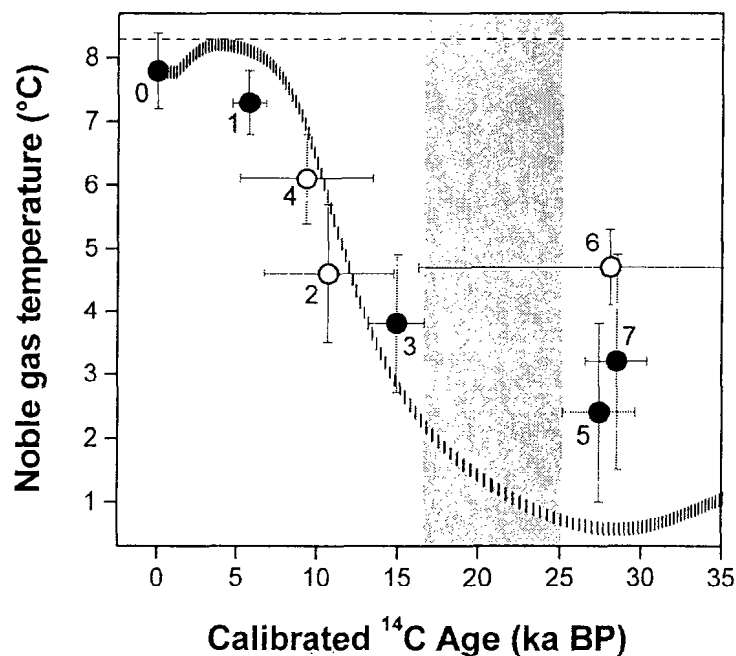


Figure 6.2: NGT versus calibrated ^{14}C age. Error bars correspond to 1σ . The sample numbers refer to the boreholes shown in Figure 6.1. Solid circles indicate samples without mixture. For samples containing a mixture of an older and a younger component (open circles) the values shown refer to the older component only. The horizontal dashed line indicates the modern mean annual air temperature of 8.3°C (Schüep, 1981). No water was found for the period between 25 and 17 kyr B.P. (shaded area). The curve is derived from a model that shows how a temperature evolution similar to that recorded in the oxygen isotope profiles of Greenland ice cores would be transferred through a dispersive flow system. The larger distance between the bars of the curve in the age range of the assumed recharge gap (from 25 to 17 kyr B.P.) reflects the reduced probability of finding a water sample with a mean residence time between 25 and 17 kyr B.P.

The curve in Figure 6.2 is derived from a model based on the following assumptions:

- (i) the temperature evolution during the last 30 kyr in central Europe is similar to that derived from $\delta^{18}\text{O}$ measurements in Greenland ice cores (Johnson et al., 1995);
- (ii) the maximum $\delta^{18}\text{O}$ change corresponds to a temperature decrease of 8.6°C relative to present-day conditions (Stute et al., 1992b; Frenzel, 1980);
- (iii) the recharge rate is constant except between 25 and 17 kyr B.P., when recharge is assumed to be zero; and
- (iv) the dispersivity of the water flow in the GVA is 100 m, which is representative of an aquifer of the size of the GVA (Gelhar et al., 1992).

The model and noble gas data correspond well with ^{14}C ages up to 15 kyr B.P., strengthening our confidence in the ^{14}C dating. However, for the older groundwaters around 28 kyr B.P. the NGTs exceed the model predictions. Lithological profiles (Schlüchter et al., 1987) and Greenland $\delta^{18}\text{O}$ ice records (Johnson et al., 1995) consistently point to dramatic temperature fluctuations during the Denekamp Interstadial (18 to 33 kyr B.P.). If groundwater recharge was interrupted during colder intervals, the NGTs would selectively reflect the signals of the warmer periods, which could explain the deviation from the model.

All $\delta^2\text{H}$ and $\delta^{18}\text{O}$ values (Tables 6.1 and 6.2) lie close to the global regression line of $\delta^2\text{H} = 8.2 \delta^{18}\text{O} + 10.8$ (Yurtsever and Gat, 1981), which indicates that $\delta^{18}\text{O}$ was not modified significantly by isotope exchange within the aquifer. We corrected the $\delta^{18}\text{O}$ values for the variation in the isotopic composition of seawater due to increased ice volume (Sowers et al., 1993). The calculated slope of the linear fit to the $\delta^{18}\text{O}$ and NGT data ⁽⁴⁾, which represents the long-term $\delta^{18}\text{O}$ -temperature relation in the recharge area, is 0.49 ± 0.17 per mil (‰) per $^\circ\text{C}$ (Figure 6.3). This slope is in good agreement with both the present-day spatial ($0.56\text{‰ per }^\circ\text{C}$) and seasonal ($0.45\text{‰ per }^\circ\text{C}$) slopes for the Swiss Plateau (Siegenthaler and Oeschger, 1980; Kullin and Schmassmann, 1991). This finding should help in the interpretation of stable isotope data from other archives as temperature proxies.

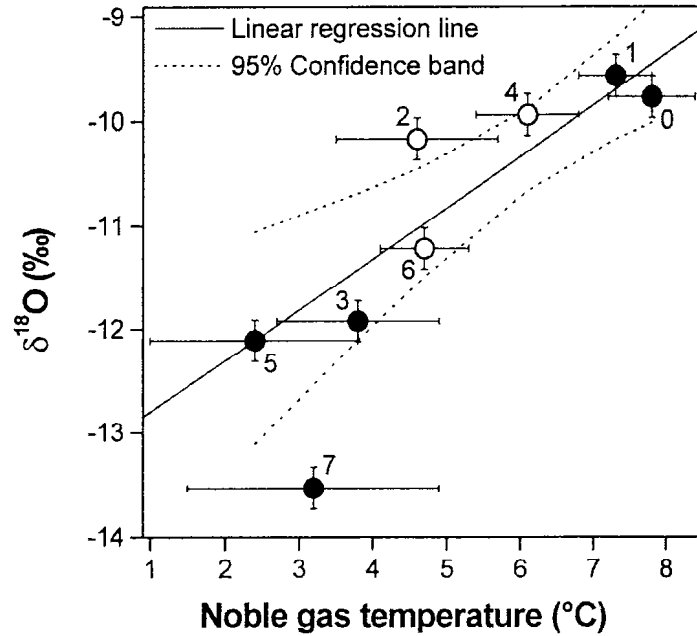


Figure 6.3: Relation between $\delta^{18}\text{O}$ and NGT. Error bars correspond to 1σ . The sample numbers refer to the boreholes shown in Figure 6.1. Solid circles indicate samples without mixture. For samples containing a mixture of an older and a younger component (open circles), the values shown refer to the older component only. The $\delta^{18}\text{O}$ shift in the ocean during the ice age (Sowers et al., 1993) is taken into account. The slope of the $\delta^{18}\text{O}$ -NGT regression line inferred from the corrected $\delta^{18}\text{O}$ data is 0.49 ± 0.17 ‰ per $^{\circ}\text{C}$ ⁽⁴⁾ which agrees with the present-day $\delta^{18}\text{O}$ -temperature spatial and seasonal relations (Siegenthaler and Oeschger, 1980; Kullin and Schmassmann, 1991).

Notes

- (1) Stable isotope composition in groundwaters is controlled by the temperature and humidity prevailing during evaporation and during the condensation of precipitation, and by the large-scale atmospheric circulation patterns. It can later be altered by local evaporation, by mixing with melting ice or snow, and by water-rock interaction within the aquifer (Mazor, 1997).
- (2) The processes responsible for this excess of atmospheric gases are not yet fully understood. Some experimental data indicate that the elemental ratios of the noble gas excesses correspond to the composition of unfractionated atmospheric air (Stute et al., 1995a). A more sophisticated correction scheme, accounting for a fractionation of the excess air, has been proposed for cases when otherwise no consistent temperatures can be obtained from the different noble gases (Stute et al., 1995b). In our study, the common correction with an excess of atmospheric composition yields coherent results, and no additional correction for fractionation is required.
- (3) For each borehole j , the following three balance equations can be defined: $C_{k,s}^j = x^j \cdot C_{k,y}^j + (1 - x^j) \cdot C_{k,o}^j$, where x^j is the mixing ratio of the younger component and C_k^j is the concentration or activity ($k = \text{Cl}^-$, ^{39}Ar or ^{14}C) of the sample (s), of the younger component (y) and of the older component (o). To allow the calculation of x^j , it was assumed that (i) the ^{14}C activity of the younger component is similar to the calculated initial activity of the sample; (ii) the dissolved inorganic carbon concentrations in the two components are comparable; (iii) the subsurface background ^{39}Ar equilibrium activity is constant in the whole aquifer (an assumption supported by constant ^{222}Rn and ^{37}Ar activities) and given by the lowest measured values at boreholes 1, 3 and 7 (~10 %modern, Table 6.1); (iv) the older component contains no atmospheric ^{39}Ar ; and (v) the ^{39}Ar activity and the Cl^- concentration of the younger component are the same in all samples.
- (4) The data from borehole 7 have been disregarded because the low $\delta^{18}\text{O}$ value and large excess air component of this sample (Table 6.1) may indicate that meltwater infiltrated during the short warmer climate period around 28 kyr B.P. This might

also account for the somewhat disturbed noble gas pattern, which results in a relatively large error in the calculated NGT at borehole 7.

Acknowledgment

This project was supported by the Swiss National Science Foundation (project no. 20-47060.96). We are grateful to H. Baur, T. Graf, M. Möll and S. Reese for assisting in the measurements; E. Hoehn for discussions; an anonymous reviewer for his or her comments; and D. Livingstone for linguistic improvements in the text.

References

- Aeschbach-Hertig, W. (1994) Helium und Tritium als Tracer für physikalische Prozesse in Seen. Diss. ETH Nr. 10714, ETH Zürich.
- Aeschbach-Hertig, W., R. Kipfer, M. Hofer, D. M. Imboden and H. Baur (1996) Density-driven exchange between the basins of Lake Lucerne (Switzerland) traced with the ^3H - ^3He method. *Limnol. Oceanogr.*, **41**(4), 707-721.
- Aeschbach-Hertig, W., P. Schlosser, M. Stute, H. J. Simpson, A. Ludin and J. F. Clark (1998) A $^3\text{H}/^3\text{He}$ study of ground water flow in a fractured bedrock aquifer. *Ground Water*, **36**(4), 661-670.
- Aeschbach-Hertig, W., F. Peeters, U. Beyerle and R. Kipfer (1999) Interpretation of dissolved atmospheric noble gases in natural waters. *Water Resour. Res.*, **35** (9), 2779-2792.
- Andrews, J. N. and D. J. Lee (1979) Inert gases in groundwater from the Bunter Sandstone of England as indicators of age and palaeoclimatic trends. *J. Hydrol.*, **41**, 233-252.
- Andrews, J. N., W. Balderer, A. H. Bath, H. B. Clausen, G. V. Evans, T. Florkowski, J. E. Goldbrunner, M. Ivanovich, H. Loosli and H. Zojer (1984) Environmental isotope studies in two aquifer systems. In: *Isotope Hydrology 1983, Vol. IAEA-SM-270* (Ed. by IAEA), pp. 535-577. IAEA, Vienna.
- Andrews, J. N. (1985) The isotopic composition of radiogenic helium and its use to study groundwater movement in confined aquifers. *Chem. Geol.*, **49**, 339-351.
- Andrews, J. N., J. E. Goldbrunner, W. G. Darling, P. J. Hooker, G. B. Wilson, M. J. Youngman, L. Eichinger, W. Rauert and W. Stichler (1985) A radiochemical, hydrochemical and dissolved gas study of groundwaters in the Molasse basin of Upper Austria. *Earth Planet. Sci. Lett.*, **73**, 317-332.
- Andrews, J. N., S. N. Davis, J. Fabryka-Martin, J.-C. Fontes, B. E. Lehmann, H. H. Loosli, J.-L. Michelot, H. Moser, B. Smith and M. Wolf (1989) The in situ production of radioisotopes in rock matrices with particular reference to the Stripa granite. *Geochim. Cosmochim. Acta*, **53**, 1803-1815.

References

- Andrews, J. N. (1992) Mechanisms for noble gas dissolution by groundwaters. In: *Isotopes of Noble Gases as Tracers in Environmental Studies* (Ed. by IAEA), pp. 87-110. IAEA, Vienna.
- Andrews, J. N. and J.-C. Fontes (1992) Importance of the in situ production of ^{36}Cl , ^{36}Ar and ^{14}C in hydrology and hydrogeochemistry. In: *Isotope techniques in water resource development 1991, Vol. IAEA-SM-319/12* (Ed. by IAEA), pp. 245-269. IAEA, Vienna.
- Andrews, J. N., J.-C. Fontes, J.-F. Aranyossy, A. Dodo, W. M. Edmunds, A. Joseph and Y. Travi (1994) The evolution of alkaline groundwaters in the continental intercalaire aquifer of the Irhazer Plain, Niger. *Water Resour. Res.*, **30**(1), 45-61.
- Balderer, W. and B. E. Lehmann (1991) Isotopes formed by underground production: ^3He and ^4He . In: *Applied Isotope Hydrogeology, a Case Study in Northern Switzerland* (Ed. by F. J. Pearson, W. Balderer, H. H. Loosli, B. E. Lehmann, A. Matter, T. Peters, H. Schmassmann and A. Gautschi), pp. 276-287. Elsevier, Amsterdam
- Bard, E., B. Hamelin, R. G. Fairbanks and A. Zindler (1990) Calibration of the ^{14}C timescale over the past 30,000 years using mass spectrometric U-Th ages from Barbados corals. *Nature*, **345**, 405-409.
- Bath, A. H., W. M. Edmunds and J. N. Andrews (1979) Palaeoclimatic trends deduced from the hydrochemistry of a Triassic sandstone aquifer, United Kingdom. In: *Isotope Hydrology 1978, Vol. 2* (Ed. by IAEA), pp. 545-568. IAEA, Neuherberg.
- Baur, H. (1980) Numerische Simulation und praktische Erprobung einer rotationssymmetrischen Ionenquelle für Gasmassenspektrometer. Diss. ETH Nr. 6596, ETH Zürich.
- Bayer, R., P. Schlosser, G. Bönisch, H. Rupp, F. Zaucker and G. Zimmek (1989) Performance and Blank Components of a Mass Spectrometric System for Routine Measurement of Helium Isotopes and Tritium by the ^3He Ingrowth Method. Springer-Verlag.
- Benson, B. B. and D. Krause (1976) Empirical laws for dilute aqueous solutions of nonpolar gases. *J. Chem. Phys.*, **64**(2), 689-709.
- Benson, B. B. and D. Krause (1980a) Isotopic fractionation of helium during solution: A probe for the liquid state. *J. Solution Chem.*, **9**(12), 895-909.
- Benson, B. B. and D. Krause (1980b) The concentration and isotopic fractionation of gases dissolved in freshwater in equilibrium with the atmosphere. 1. Oxygen. *Limnol. Oceanogr.*, **25**(4), 662-671.

References

- Beyerle, U., W. Aeschbach-Hertig, R. Kipfer, F. Peeters, D. M. Imboden, R. Purtschert, B. Lehmann, H. H. Loosli and A. Love (1998a) Some noble gas recharge temperatures from the Great Artesian Basin (GAB) indicating 5°C cooling in Australia on time scales of 10⁵ years. In: *ICOG-9, Vol. 43 Supp.*, pp. 10. Chinese Science Bulletin, Chinese Academy of Science, Beijing.
- Beyerle, U., R. Purtschert, W. Aeschbach-Hertig, D. M. Imboden, H. H. Loosli, R. Wieler and R. Kipfer (1998b) Climate and groundwater recharge during the last glaciation in an ice-covered region. *Science*, **282**, 731-734.
- Beyerle, U., W. Aeschbach-Hertig, M. Hofer, D. M. Imboden, H. Baur and R. Kipfer (1999a) Infiltration of river water to shallow aquifer investigated with ³H/³He, noble gases and CFCs. *J. Hydrol.*, **220**, 169-185.
- Beyerle, U., W. Aeschbach-Hertig, D. M. Imboden, H. Baur, T. Graf and R. Kipfer (1999b) A mass spectrometric system for the analysis of noble gases and tritium from water samples. *Environ. Sci. Technol.*, submitted.
- Bieri, R. H. (1971) Dissolved Noble Gases in Marine Waters. *Earth Planet. Sci. Lett.*, **10**, 329-333.
- Bottomley, D. J., J. D. Ross and W. B. Clarke (1984) Helium and neon isotope geochemistry of some ground waters from the Canadian Precambrian Shield. *Geochim. Cosmochim. Acta*, **48**, 1973-1985.
- Boulton, G. S., P. E. Caban and K. Van Gijssel (1995) Groundwater flow beneath ice sheets: Part I - large scale patterns. *Quaternary Sci. Rev.*, **14**, 545-562.
- Bouwer, H. (1978) *Groundwater Hydrology*. McGraw-Hill Book Company, New York, 480 pp.
- Busenberg, E. and L. N. Plummer. (1992) Use of chlorofluorocarbons (CCl₃F and CCl₂F₂) as hydrologic tracers and age-dating tools: The alluvium and terrace system of central Oklahoma. *Water Resour. Res.*, **28**(9), 2257-2284.
- Butzin, M. (1994) Bestimmung der Löslichkeiten von Helium und Neon in destilliertem Wasser und in Seewasser. Diplomarbeit, Universität Bremen.
- Clarke, W. B., W. J. Jenkins and Z. Top (1976) Determination of tritium by mass spectrometric measurement of ³He. *Int. J. appl. Radiat. Isotopes*, **27**, 515-522.
- Clever, H. L. (1979a) Helium and neon - gas solubilities. In: *Solubility data series, Vol. 1* (Ed. by I. U. o. P. a. A. Chemistry). Pergamon Press, Oxford.
- Clever, H. L. (1979b) Krypton, xenon and radon - gas solubilities. In: *Solubility data series, Vol. 2* (Ed. by I. U. o. P. a. A. Chemistry). Pergamon Press, Oxford.
- Clever, H. L. (1980) Argon. In: *Solubility data series, Vol. 4* (Ed. by I. U. o. P. a. A. Chemistry). Pergamon Press, Oxford.

References

- CLIMAP. (1976) The surface of the ice-age Earth. *Science*, **191**, 1131-1137.
- Cook, P. G. and D. K. Solomon (1995) Transport of atmospheric trace gases to the water table: Implications for groundwater dating with chlorofluorocarbons and krypton 85. *Water Resour. Res.*, **31**(2), 263-270.
- Cook, P. G. and D. K. Solomon (1997) Recent advances in dating young groundwater: chlorofluorocarbons, $^3\text{H}/^3\text{He}$ and ^{85}Kr . *J. Hydrol.*, **191**(1-4), 245-265.
- Craig, H. and D. Lal (1961) The production rate of natural tritium. *Tellus*, **13**(1), 85-105.
- Craig, H. and R. F. Weiss (1971) Dissolved gas saturation anomalies and excess helium in the ocean. *Earth Planet. Sci. Lett.*, **10**, 289-296.
- Craig, H. and J. E. Lupton (1976) Primordial Neon, Helium, and Hydrogen in Oceanic Basalts. *Earth Planet. Sci. Lett.*, **31**, 369-385.
- Degens, E.T. (1962) Geochemische Untersuchungen von Wasser aus der aegyptischen Sahara, *Geol Rundsch.*, **52**, 625.
- Dunai, T. J. and J. L. R. Touret (1993) A noble gas study of a granulite sample from the Nilgiri Hill, southern India: implications for granulite formation. *Earth Planet. Sci. Lett.*, **119**, 271-281.
- Dunkle, S. A., L. N. Plummer, E. Busenberg, P. J. Phillips, J. M. Denver, P. A. Hamilton, R. L. Michel and T. B. Coplen. (1993) Chlorofluorocarbons (CCl_3F and CCl_2F_2) as dating tools and hydrologic tracers in shallow groundwater of the Delmarva Peninsula, Atlantic Coastal Plain, United States. *Water Resour. Res.*, **29**(12), 3837-3860.
- Elkins, J. W., T. M. Thompson, T. H. Swanson, J. H. Butler, B. D. Hall, S. O. Cummings, D. A. Fisher and A. G. Raffo (1993) Decrease in the growth rates of atmospheric chlorofluorocarbons 11 and 12. *Nature*, **364**, 780-783.
- Fontes, J.-C. and J.-M. Garnier (1979) Determination of the initial ^{14}C activity of the total dissolved carbon: A review of the existing models and a new approach. *Water Resour. Res.*, **15**(2), 399-413.
- Forster, M., K. Ramm and P. Maier (1992) Argon-39 dating of groundwater and its limiting conditions. In: *Isotope techniques in water resource development 1991*, Vol. IAEA-SM-319/13 (Ed. by IAEA), pp. 203-214. IAEA, Vienna.
- Freeze, R. A. and J. A. Cherry (1979) *Groundwater*. Prentice-Hall, Englewood Cliffs.
- Frenzel, B. (1980) Das Klima der letzten Eiszeit in Europa. In: *Das Klima* (Ed. by H. Oeschger, B. Messerli and M. Svilar), pp. 45-63. Springer, Berlin.
- Gelhar, L. W., C. Welty and K. R. Rehfeldt (1992) A critical review of data on field-scale dispersion in aquifers. *Water Resour. Res.*, **28**, 1955-74.

References

- Gill, A. E. (1982) *Atmosphere-Ocean Dynamics*. Academic Press, San Diego, 662 pp.
- Greenkorn, R. A and D. P. Kessler (1972) *Transfer operations*. New York, McGraw-Hill, 548 pp.
- Greenkorn, R. A. (1983) Flow phenomena in porous Media: Fundamentals and applications in petroleum, Water and food production. New York, Marcel Dekker, 550 pp.
- Habermehl, M. A. (1980) The Great Artesian Basin, Australia. *Journal of Australian Geology & Geophysics*, **5**, 9-38.
- Hartmann, D. and P. Michel (1992) Grundwasserschutz in der Schweiz. *Gas Wasser Abwasser*, **72**(3), 167-173.
- Heaton, T. H. E. and J. C. Vogel. (1981) "Excess air" in groundwater. *J. Hydrol.*, **50**, 201-216.
- Helfferrich, F. (1966) In: *Ion exchange, a series of advances* (Ed. by J. A. Marinsky). pp. 65-100. New York, Marcel Dekker.
- Hofer, M. and D. M. Imboden (1998) Simultaneous determination of CFC-11, CFC-12, N₂ and Ar in water. *Anal. Chem.*, **70**(4), 724-729.
- Hohmann, R., M. Hofer, R. Kipfer, F. Peeters and D. M. Imboden. (1998) Distribution of helium and tritium in Lake Baikal. *J. Geophys. Res.*, **103**(C6), 12823-12838.
- IAEA. (1992) Statistical treatment of data on environmental isotopes in precipitation. International Atomic Energy Agency, IAEA.
- IAEA/WMO. (1998) Global Network of Isotopes in Precipitation. The GNIP Database. <http://www.iaea.or.at/programs/ri/gnip/gnipmain.htm>, IAEA.
- Ingerson, E. and F. J. Pearson (1964) Estimation of age and rate of motion of groundwater by the ¹⁴C-method. In: *Recent Researches in the Fields of Atmosphere, Hydrosphere and Nuclear Geochemistry*, pp. 263-283. Nagoya University, Nagoya, Japan.
- Jähne, B., G. Heinz and W. Dietrich (1987) Measurement of the diffusion coefficients of sparingly soluble gases in water. *J. Geophys. Res.*, **92**(C10), 10767-10776.
- Jean-Baptiste, P., F. Mantsi, A. Dapoigny and M. Stievenard (1992) Design and performance of a mass spectrometric facility for measuring helium isotopes in natural waters and for low-level tritium determination by the ³He ingrowth method. *Appl. Radiat. Isot.*, **43**(7), 881-891.
- Jenkins, W. J. and W. B. Clarke (1976) The distribution of ³He in the western Atlantic Ocean. *Deep-Sea Res.*, **23**, 481-494.

References

- Jenkins, W. J. (1987) ^3H and ^3He in the Beta Triangle: Observations of gyre ventilation and oxygen utilization rates. *J. Phys. Oceanogr.*, **17**, 763-783.
- Johnsen, S. J., D. Dahl-Jensen, W. Dansgaard and N. Gundestrup (1995) Greenland palaeotemperatures derived from GRIP bore hole temperature and ice core isotope profiles. *Tellus*, **47B**, 624-629.
- Kaufman, S. and W. F. Libby (1954) The natural distribution of tritium. *Phys. Rev.*, **93**(6), 1337-1344.
- Kempf, T., M. Freimoser, P. Haldimann, V. Longo, E. Müller, C. Schindler, G. Styger and L. Wyssling (1986) *Die Grundwasservorkommen im Kanton Zürich*. Kümmerly & Frei AG, Bern.
- Kennedy, B. M., H. Hiyagon and J. H. Reynolds (1990) Crustal neon: a striking uniformity. *Earth Planet. Sci. Lett.*, **98**, 277-286.
- Kipfer, R. (1991) Primordiale Edelgase als Tracer für Fluide aus dem Erdmantel. Diss. ETH Nr. 9463, ETH Zürich.
- Kipfer, R., W. Aeschbach-Hertig, H. Baur, M. Hofer, D. M. Imboden and P. Signer (1994) Injection of mantle type helium into Lake Van (Turkey): The clue for quantifying deep water renewal. *Earth Planet. Sci. Lett.*, **125**, 357-370.
- Kugler, G. and W. B. Clarke (1972) Mass-spectrometric measurements of ^3H , ^3He and ^4He produced in thermal-neutron ternary fission of ^{235}U : evidence for short-range ^4He . *Phys. Rev. C*, **5**(2), 551-559.
- Kullin, M. and H. Schmassmann (1991) Isotopic Composition of Modern Recharge. In: *Applied Isotope Hydrogeology, a Case Study in Northern Switzerland* (Ed. by F. J. Pearson, W. Balderer, H. H. Loosli, B. E. Lehmann, A. Matter, T. Peters, H. Schmassmann and A. Gautschi), pp. 65-89. Elsevier, Amsterdam.
- Lal, D. and B. Peters (1962) Cosmic ray produced isotopes and their application to problems in geophysics. *Elementary Particle and Cosmic Ray Physics*, **6**, 1-74.
- Lehmann, B. E., H. Oeschger, H. H. Loosli, G. S. Hurst, S. L. Allman, C. H. Chen, S. D. Kramer, M. G. Payne, R. C. Phillips, R. D. Willis and N. Thonnard (1985) Counting ^{81}Kr atoms for analysis of groundwater. *J. Geophys. Res.*, **90**(B13), 11547-11551.
- Lehmann, B. E. and H. H. Loosli (1991) Isotopes formed by underground production. In: *Applied Isotope Hydrogeology, a Case Study in Northern Switzerland* (Ed. by F. J. Pearson, W. Balderer, H. H. Loosli, B. E. Lehmann, A. Matter, T. Peters, H. Schmassmann and A. Gautschi), pp. 239-296. Elsevier, Amsterdam.
- Lehmann, B. E. and R. Purtschert (1997) Radioisotope dynamics - the origin and fate of nuclides in groundwater. *Appl. Geochem.*, **12**(6), 727-738.

References

- Lide, D. R. (1994) CRC handbook of chemistry and physics. CRC Press, Boca Raton.
- Loosli, H. H. and H. Oeschger (1978) Argon-39, carbon-14 and krypton-85 measurements in groundwater samples. In: *Isotope Hydrology, Vol. 2* (Ed. by IAEA), pp. 931-947. IAEA, Neuberberg. *Isotope Hydrology*.
- Loosli, H. H., B. E. Lehmann, C. Thalmann, J. N. Andrews and T. Florkowski (1991) Argon-37 and argon-39: measured concentrations in groundwater compared with calculated concentrations in rock. In: *Isotope Techniques in water resources development* (Ed. by IAEA), pp. 189-201. IAEA, Vienna.
- Lott, D. E. and W. J. Jenkins (1984) An automated cryogenic charcoal trap system for helium isotope mass spectrometry. *Rev. Sci. Instrum.*, **55**(12), 1982-1988.
- Malard, F. and F. Hervant (1999) Oxygen patterns and adaptive strategies of animals in groundwater. *Freshwater Biology*, **41**, 1-30
- Mamyrin, B. A., G. S. Anufriyev, I. L. Kamenskiy and I. N. Tolstikhin (1970) Determination of the isotopic composition of atmospheric helium. *Geochemistry International*, **7**, 498-505.
- Mamyrin, B. A. and I. N. Tolstikhin (1984) *Helium isotopes in nature*. Elsevier, Amsterdam, Oxford, New York, Tokyo, 273 pp.
- Marine, I. W. (1981) The use of radiogenic noble gases for dating groundwater. In: *The technology of high level nuclear waste disposal*, 42-64.
- Mather, J. R. (1984) *Water resources, distribution, use, and management*. John Wiley & Sons, Inc. and V.H. Winstzons & Sons, New York, Silver Spring Maryland, 439 pp.
- Matthess, G. (1982) *The Properties of Groundwater*. John Wiley & Sons, New York.
- Mattle, M. (1999) Interpretation von Tracermessungen in Grundwässern mittels Boxmodellen und numerischen Strömungs-/Transportmodellen. Ph.D. thesis, Universität Bern.
- Mazor, E. (1972) Paleotemperatures and other hydrological parameters deduced from gases dissolved in groundwaters, Jordan Rift Valley, Israel. *Geochem. Cosmochim. Acta*, **36**, 1321-1336.
- Mazor, E. (1977) Geothermal tracing with atmospheric and radiogenic noble gases. *Geothermics*, **5**, 21-36.
- Morrison, P. and J. Pine (1955) Radiogenic origin of the helium isotopes in rock. *Annals of the New York Academy of Sciences*, **62**, 69-92.
- Münnich, K. O. and J. C. Vogel (1962) Untersuchung an pluvialen Wassern der Ost-Sahara. *Geol. Rundsch.*, **52**, 611.

References

- Naegeli, M. W., U. Hartmann, E. I. Meyer and U. Uehlinger (1995) POM-dynamics and community respiration in the sediments of floodprone prealpine river (Necker, Switzerland) *Archiv für Hydrobiologie*, **133**, 339-347.
- Nier, O. A. (1950) A redetermination of the relative abundances of the isotopes of carbon, nitrogen, oxygen, argon and potassium. *Phys. Rev.*, **77**(6), 789-793.
- Oliver, B. M., H. Bradley and J. G. Farrar (1984) Helium concentration in the earth's lower atmosphere. *Geochim. Cosmochim. Acta*, **47**, 1759-1767.
- Oliver, B. M., H. Farrar IV and M. M. Bretscher (1987) Tritium half-life measured by helium-3 growth. *Appl. Radiat. Isot.*, **38**(11), 959-965.
- O'Nions, R. K. and E. R. Oxburgh. (1983) Heat and helium in the earth. *Nature*, **306**, 429-431.
- Osenbrück, K. (1991) Laborversuche zur Bildung des Luftüberschusses im Grundwasser. Diplomarbeit, Universität Heidelberg.
- Ozima, M. and F. A. Podosek (1983) *Noble gas geochemistry*. Cambridge Univ. Press, Cambridge, London, New York, 367 pp.
- Parkomenko E. I. (1967) *Electrical properties of rocks*. Plenum Press, New York, 268 pp.
- Pedroli, R. (1982) Wegleitung zur Ausscheidung von Gewässerschutzbereichen, Grundwasserschutzzonen und Grundwasserschutzarealen. Bundesamt für Umweltschutz, Bern.
- Phillips, F. M., M. K. Tansey and L. A. Peeters (1989) An isotopic investigation of groundwater in the Central San Juan Basin, New Mexico: carbon 14 dating as a basis for numerical flow modeling. *Water Resour. Res.*, **25**(10), 2259-2273.
- Piotrowski, J. A. (1997) Subglacial groundwater flow during the last glaciation in northwestern Germany. *Sediment. Geol.*, **111**, 217-224.
- Press, W. H., P. F. Flannery, S. A. Teukolsky and W. T. Vetterling (1986) *Numerical Recipes*. Cambridge University Press, Cambridge, 818 pp.
- Purdy, C. B., G. R. Helz, A. C. Mignerey, P. W. Kubik, D. Elmore, P. Sharma and T. Hemmick (1996) Aquia aquifer dissolved Cl⁻ and ³⁶Cl/Cl: Implications for flow velocities. *Water Resour. Res.*, **32**(5), 1163-1171.
- Roberts, P. V. and A. J. Valochi (1981) Principles of organic contaminant behavior during artificial recharge. In: *Quality of groundwater* (Ed. by W. Duijvenbooden, P. Glassberg and H. van Lelyveld), pp. 439-450. Elsevier, Amsterdam.
- Roether, W. (1967) Estimating the tritium input to groundwater from wine samples: Groundwater and direct run-off contribution to Central European surface waters. In: *Isotopes in Hydrology* (Ed. by IAEA), pp. 73-79. IAEA, Vienna.

References

- Rohling, E. J., M. Fenton, F. J. Jorissen, P. Bertrand, G. Ganssen and J. P. Caillet (1998) Magnitudes of sea-level lowstands of the past 500,000 years. *Nature*, **394**, 162-165.
- Rozanski, K., R. Gonfiantini and L. Araguas-Araguas (1991) Tritium in the global atmosphere: Distribution patterns and recent trends. *J. Phys. G: Nucl. Part. Phys.*, **17**, S523-S536.
- Rudolph, J., H. K. Rath and C. Sonntag (1984) Noble gases and stable isotopes in ¹⁴C-dated palaeowaters from Central Europa and the Sahara. In: *Isotope Hydrology 1983, Vol. IAEA-SM-270* (Ed. by IAEA), pp. 467-477. IAEA, Vienna.
- Russell, A. D. and G. M. Thompson. (1983) Mechanisms leading to enrichment of atmospheric fluorocarbons CCl₃F and CCl₂F in groundwater. *Water Resour. Res.*, **19**(1), 57-60.
- Schlosser, P., M. Stute, C. Dörr, C. Sonntag and K. O. Münnich (1988) Tritium/³He-dating of shallow groundwater. *Earth Planet. Sci. Lett.*, **89**, 353-362.
- Schlosser, P., G. Bönisch, B. Kromer, K. O. Münnich and K. P. Koltermann (1990) Ventilation rates of the waters in the Nansen Basin of the Arctic Ocean derived from a multitracer approach. *J. Geophys. Res.*, **95**(C3), 3265-3272.
- Schlosser, P. (1992) Tritium/³He dating of waters in natural systems. In: *Isotopes of noble gases as tracers in environmental studies*, pp. 123-145. IAEA, Vienna.
- Schlüchter, C., M. Maisch, J. Suter, P. Fitze, W. A. Keller, C. A. Burga and E. Wynistorf (1987) Das Schieferkohlen-Profil von Gossau (Kanton Zürich) und seine stratigraphische Stellung innerhalb der letzten Eiszeit. *Vierteljahresschrift der Naturforschenden Gesellschaft Zürich*, **132**(3), 135-174.
- Schüepp, M. and O. Gisler (1980) Luftdruck. In: Beihefte zu den Annalen der Schweiz. Meteorologischen Anstalt, Vol. 23. SMA, Zürich.
- Schüepp, M. (1981) Klima und Wetter. In: *Atlas der Schweiz* (Ed. by E. Spiess), pp. 11. Verlag der Eidgenössischen Landestopographie, Wabern-Bern.
- Shackleton, N. J., J. Imbrie and M. A. Hall (1983) Oxygen and carbon isotope record of the East Pacific core V19-30: implications for the formation of deep water in the late Pleistocene North Atlantic. *Earth Planet. Sci. Lett.*, **65**, 233-244.
- Siegenthaler, U. and H. Oeschger (1980) Correlation of ¹⁸O in precipitation with temperature and altitude. *Nature*, **285**, 314-317.
- Smith, G. D., F. Newhall, L. H. Robinson and D. Swanson (1964) Soil temperature regimes: Their characteristics and predictability. Report number SCS-TP-144, USDA, Soil Conservation Service.

- Smith, S. P. and B. M. Kennedy (1983) Solubility of noble gases in water and in NaCl brine. *Geochim. Cosmochim. Acta*, **47**, 503-515.
- Solomon, D. K., R. J. Poreda, S. L. Schiff and J. A. Cherry (1992) Tritium and helium 3 as groundwater age tracers in the Borden aquifer. *Water Resour. Res.*, **28**(3), 741-755.
- Solomon, D. K., A. Hunt and R. J. Poreda (1996) Source of radiogenic helium 4 in shallow aquifers: Implications for dating young groundwater. *Water Resour. Res.*, **32**, 1805-1813.
- Sowers, T., M. Bender, L. Labeyrie, D. Martinson, D. Raynaud, J. J. Pichon and A. Korotkevich (1993) A 135'000-year Vostok-Specmap common temporal framework. *Paleoceanogr.*, **8**, 737-766.
- Steiger, R. H. and E. Jäger (1977) Subcommittee on geochronology: convention on the use of decay constants in geo- and cosmochronology. *Earth Planet. Sci. Lett.*, **36**(359-62), 359-362.
- Stuiver, M., P.J. Reimer (1993) Radiocarbon calibration program Rev. 3.0.3c, *Radiocarbon*, **35**, 215-230.
- Stute, M. (1989) Edelgase im Grundwasser - Bestimmung von Paläotemperaturen und Untersuchung der Dynamik von Grundwasserfließsystemen. PhD thesis, Universität Heidelberg.
- Stute, M. and J. Deák (1989) Environmental isotope study (^{14}C , ^{13}C , ^{18}O , D, noble gases) on deep groundwater circulation systems in Hungary with reference to paleoclimate. *Radiocarbon*, **31**(3), 902-918.
- Stute, M. and C. Sonntag (1992) Paleotemperatures derived from noble gases dissolved in groundwater and in relation to soil temperature. In: *Isotopes of noble gases as tracers in environmental studies*, pp. 111-122. IAEA, Vienna.
- Stute, M., P. Schlosser, J. F. Clark and W. S. Broecker (1992a) Paleotemperatures in the Southwestern United States derived from noble gases in ground water. *Science*, **256**, 1000-1003.
- Stute, M., C. Sonntag, J. Deák and P. Schlosser (1992b) Helium in deep circulating groundwater in the Great Hungarian Plain: Flow dynamics and crustal and mantle helium fluxes. *Geochim. Cosmochim. Acta*, **56**, 2051-2067.
- Stute, M. and P. Schlosser (1993) Principles and applications of the noble gas paleothermometer. In: *Climate Change in Continental Isotopic Records, Vol. 78* (Ed. by P. K. Swart, K. C. Lohmann, J. McKenzie and S. Savin), pp. 89-100. American Geophysical Union, Washington, DC.

References

- Stute, M., J. F. Clark, F. M. Phillips and D. Elmore (1993) Reconstruction of late glacial climates from the groundwater archive: Cl⁻ and ³⁶Cl in the Carrizo Aquifer, Texas. In: *Isotope Techniques in the Study of Past and Current Environmental Changes in the Hydrosphere and the Atmosphere, Vol. IAEA-SM-329/70* (Ed. by IAEA), pp. 259-270. IAEA, Vienna.
- Stute, M., J. F. Clark, P. Schlosser and W. S. Broecker (1995a) A 30'000 yr continental paleotemperature record derived from noble gases dissolved in groundwater from the San Juan Basin, New Mexico. *Quatern. Res.*, **43**, 209-220.
- Stute, M., M. Forster, H. Frischkorn, A. Serejo, J. F. Clark, P. Schlosser, W. S. Broecker and G. Bonani (1995b) Cooling of tropical Brazil (5°C) during the Last Glacial Maximum. *Science*, **269**, 379-383.
- Stute, M., J. Deák, K. Révész, J. K. Böhlke, É. Deseö, R. Weppernig and P. Schlosser (1997) Tritium/³He dating of river infiltration: An example from the Danube in the Szigetkös area, Hungary. *Ground Water*, **35**(5), 905-911.
- Thiele, G. and J. L. Sarmiento (1990) Tracer dating and ocean ventilation. *J. Geophys. Res.*, **95**(C6), 9377-9391.
- Thompson, G. M. and J. M. Hayes (1979) Trichlorofluoromethan in groundwater - a possible tracer and indicator of groundwater age. *Water Resour. Res.*, **15**(3), 546-554.
- Tolstikhin, I. N. and I. L. Kamenskiy (1969) Determination of ground-water ages by the T-³He Method. *Geochemistry International*, **6**, 810-811.
- Top, Z., W. C. Eismont and W. B. Clarke (1987) Helium isotope effect and solubility of helium and neon in distilled water and seawater. *Deep-Sea Res.*, **34**(7), 1139-1148.
- Torgersen, T., Z. Top, W. B. Clarke, W. J. Jenkins and W. S. Broecker (1977) A new method for physical limnology - tritium-helium-3 ages - results for Lakes Erie, Huron and Ontario. *Limnol. Oceanogr.*, **22**(2), 181-193.
- Torgersen, T. and W. B. Clarke (1985) Helium accumulation in groundwater, I: An evaluation of sources and the continental flux of crustal ⁴He in the Great Artesian Basin, Australia. *Geochim. Cosmochim. Acta*, **49**, 1211-1218.
- Torgersen, T., B. M. Kennedy, H. Hiyagon, K. Y. Chiou, J. H. Reynolds and W. B. Clark (1989) Argon accumulation and the crustal degassing flux of ⁴⁰Ar in the Great Artesian Basin, Australia. *Earth Planet. Sci. Lett.*, **92**, 43-56.
- Triska, F. J., V. C. Kennedy and R. J. Avanzino (1989) Retention and transport of nutrients in a third-order stream in northwestern California: Hyporheic processes. *Ecology*, **70**(6), 1893-1905.

References

- Völkle, H., H. Surbeck, C. Murith and M. Gobet (1996) *Umweltradioaktivität und Strahlendosen in der Schweiz*. BAG, Abteilung Strahlenschutz, Bern.
- Warner, M. J. and R. F. Weiss (1985) Solubilities of chlorofluorocarbons 11 and 12 in water and seawater. *Deep-Sea Res.*, **32**(12), 1485-1497.
- Weise, S. M., P. Faber and M. Stute (1992) Neon-21 - a possible tool for dating very old groundwaters? In: *Isotope Techniques in water resources development 1991* (Ed. by IAEA), pp. 179-188. IAEA, Vienna.
- Weiss, R. F. (1970a) Helium isotope effect in solution in water and seawater. *Science*, **168**, 247-248.
- Weiss, R. F. (1970b) The solubility of nitrogen, oxygen and argon in water and seawater. *Deep-Sea Res.*, **17**, 721-735.
- Weiss, R. F. (1971) Solubility of helium and neon in water and seawater. *J. Chem. Eng. Data*, **16**(2), 235-241.
- Weiss, R., W. Roether and G. Bader (1976) Determination of blanks in low-level tritium measurement. *International Journal of Applied Radiation Isotopes*, **27**, 217-225.
- Weiss, R. F. and T. K. Kyser (1978) Solubility of krypton in water and seawater. *J. Chem. Eng. Data*, **23**(1), 69-72.
- Weiss, R. F. and B. A. Price (1989) Dead Sea gas solubilities. *Earth Planet. Sci. Lett.*, **92**(1), 7-10.
- Wilson, G. B. and G. W. McNeill (1997) Noble gas recharge temperatures and the excess air component. *Appl. Geochem.*, **12**(6), 747-762.
- Wüest, A., G. Piepke and J. D. Halfman (1996) Combined effects of dissolved solids and temperature on the density stratification of Lake Malawi. In: *The Limnology, Climatology and Paleoclimatology of the East African Lakes* (Ed. by T. C. Johnson and E. O. Odada), pp. 183-202. Gordon and Breach, Toronto.
- Wyssling, L. (1988) *Hydrogeologische Erforschung des tiefliegenden Grundwasserstromes im oberen Glattal/ZH*. Report Nr. 88.46, Baudirektion des Kantons Zürich, Amt für Gewässerschutz und Wasserbau, Zürich.
- Yurtsever, Y. and J. R. Gat (1981) Atmospheric Waters. In: *Stable Isotope Hydrology: Deuterium and Oxygen-18 in the Water Cycle* (Ed. by IAEA), pp. 103-142. IAEA, Vienna.
- Zuber, A. (1986) On the interpretation of tracer data in variable flow systems. *J. Hydrol.*, **86**, 45-57.

Seite Leer /
Blank leaf

Seite Leer /
Blank leaf

Appendix

A1 Solubility data of noble gases

In the following the coefficients and constants that were used to calculate the solubility of He, Ne, Ar, Kr, and Xe in water are listed. The nomenclature corresponds to the one used in section 2.2.

Equilibrium concentration C_{eq}^i , Weiss (1970b, 1971); Weiss and Kyser (1978)

$$\ln\left(C_{eq}^i(T, S, P_0)\right) = \left\{ A_1 + A_2 \frac{100}{T} + A_3 \cdot \ln\left(\frac{T}{100}\right) + A_4 \frac{T}{100} + S \cdot \left[B_1 + B_2 \frac{T}{100} + B_3 \left(\frac{T}{100}\right)^2 \right] \right\} / 1000 \quad (\text{A.1})$$

$C_{eq}^i(T, S, P_0)$ equilibrium concentration of noble gas i in water with moist air at a total atmospheric pressure of $P_0 = 1$ atm [cm³STP/gH₂O]

T temperature [K], where T(K) = T(°C) + 273.15

S salinity [‰]

$A_1, A_2, A_3, B_1, B_2, B_3$ constants see Table A.1

Table A.1: Constants of Weiss for calculating moist-air saturation concentrations of noble gases in water.

Noble gas	A_1	A_2	A_3	A_4	B_1	B_2	B_3
He	-167.2178	216.3442	139.2032	-22.6202	-0.044781	0.023541	-0.0034266
Ne	-170.6018	225.1946	140.8863	-22.629	-0.127113	0.079277	-0.0129095
Ar	-178.1725	251.8139	145.2337	-22.2046	-0.038729	0.017171	-0.0021281
Kr	-112.6840	153.5817	74.4690	-10.0189	-0.011213	-0.001844	0.0011201

Henry coefficient k_i , Clever (1979a, 1979b, 1980)

$$\ln\left(\frac{1}{k_i(T,0)}\right) = A + B\frac{100}{T} + C \cdot \ln\left(\frac{T}{100}\right) \quad (\text{A.2})$$

- $k_i(T,0)$ Henry coefficient for noble gas i in pure water $S = 0\text{‰}$ [atm]
 T temperature [K]
 S salinity [‰]
 A, B, C constants see Table A.2

Table A.2: Constants of Clever for calculating Henry coefficients in pure water.

Noble gas	A	B	C
He	-41.4611	42.5962	14.0094
Ne	-52.8573	61.0494	18.9157
Ar	-57.6661	74.7627	20.1398
Kr	-66.9928	91.0166	24.2207
Xe	-74.7398	105.2100	27.4664

Henry coefficient k_i , Benson and Krause (1976)

$$\ln\left(\frac{1}{k_i(T,0)}\right) = a_0 + a_1\frac{1}{T} + a_2\frac{1}{T^2} \quad (\text{A.3})$$

- $k_i(T,0)$ Henry coefficient for noble gas i in pure water $S = 0\text{‰}$ [atm]
 T temperature [K]
 S salinity [‰]
 a_0, a_1, a_2 constants see Table A.3

Table A.3: Constants of Benson and Krause for calculating Henry coefficients in pure water.

Noble gas	a_0	a_1	a_2
He	-5.0746	-4127.8	627250
Ne	-4.2988	-4871.1	793580
Ar	-4.2123	-5239.6	995240
Kr	-3.6326	-5664.0	1122400
Xe	-2.0917	-6693.5	1341700

Salting coefficient K_i , Smith and Kennedy (1983)

$$K_i(T) = B_1 + B_2 \frac{100}{T} + B_3 \cdot \ln\left(\frac{T}{100}\right) \quad (\text{A.4})$$

$K_i(T)$ salting coefficient [L/mol]

T temperature [K]

B_1, B_2, B_3 constants see Table A.4

Table A.4: Constants of Smith and Kennedy for calculating salting coefficients.

Noble gas	B_1	B_2	B_3
He	-9.6723	14.4725	4.6188
Ne	-11.5250	17.7408	5.3421
Ar	-10.2710	16.0950	4.7539
Kr	-9.5534	15.1039	4.4164
Xe	-14.1338	21.8772	6.5527

Molar volume V_i , calculated from Lide (1994)

Table A.5: Molar volumes of noble gases.

Noble gas	V_i [cm ³ STP/mol]
He	22436.4
Ne	22421.7
Ar	22386.5
Kr	22351.2
Xe	22280.4
ideal gas	22414.1

Water density ρ , Gill (1982)

$$\begin{aligned} \rho(T, 0) = \{ & 999.842594 + 6.793952 \cdot 10^{-2} \cdot T - 9.09529 \cdot 10^{-3} \cdot T^2 \\ & + 1.001685 \cdot 10^{-4} \cdot T^3 - 1.120083 \cdot 10^{-6} \cdot T^4 \\ & + 6.536332 \cdot 10^{-9} \cdot T^5 \} / 1000 \end{aligned} \quad (\text{A.5})$$

$\rho(T, 0)$ density of pure water, $S = 0\text{‰}$ [kg/L]
 T temperature [$^{\circ}\text{C}$]

$$\begin{aligned} \rho(T, S) = \rho(T, 0) + \{ & S \cdot [0.824493 - 4.0899 \cdot 10^{-3} \cdot T + 7.6438 \cdot 10^{-5} \cdot T^2 \\ & - 8.2467 \cdot 10^{-7} \cdot T^3 + 5.3875 \cdot 10^{-9} \cdot T^4] \\ & + S^{3/2} \cdot [-5.72466 \cdot 10^{-3} + 1.0227 \cdot 10^{-4} \cdot T - 1.6546 \cdot 10^{-6} \cdot T^2] \\ & + 4.8314 \cdot 10^{-4} \cdot S^2 \} / 1000 \end{aligned} \quad (\text{A.6})$$

$\rho(T, 0)$: density of water [kg/L]
 T : temperature [$^{\circ}\text{C}$]
 S : salinity [‰]

Dank

Die vier Jahre meiner Dissertation waren eine überaus wertvolle und gewinnbringende Zeit. Ich möchte an dieser Stelle allen danken, welche zum Gelingen dieser Arbeit beigetragen haben.

Dieter Imboden hat mich offen in seine Gruppe Umweltisotope (UI) an der EAWAG aufgenommen. Seine Fähigkeit physikalische Prozesse sofort zu verstehen und anschaulich darzulegen hat mich immer sehr beeindruckt. Ich mochte seine umgängliche und motivierende Art als Doktorvater wie auch seine kritischen Anregungen.

Christoph Schär danke ich für sein Korreferat und für seinen Vorschlag mich bei *Dieter Imboden* um eine Dissertationsstelle zu bewerben.

Meinen UI-Kollegen, *Rolf Kipfer*, *Werner Aeschbach-Hertig*, *Markus Hofer* und *Johannes Holoher*, die mich im Feld und bei den Messungen unterstützt haben, gilt mein besonderer Dank. Die enge und ausgezeichnete Zusammenarbeit innerhalb unserer Gruppe war für die vorliegende Arbeit einer der wichtigsten Stützpfiler.

Rolf Kipfer alias RoKi hat mich als Betreuer in die Mysterien der Edelgasmassenspektrometrie eingeweiht. Seine überaus kollegiale und dynamische Art hat mich immer wieder aufs Neue motiviert. Ich verdanke ihm viele konstruktive und kreative Ideen und das Wissen, wo es in Zürich die besten Cordon-bleus gibt.

Werner Aeschbach-Hertig hat mit seinen Anregungen und Korrekturen und seinem Wissen einen wesentlichen Beitrag zu dieser Arbeit geleistet. Herzlich danken möchte ich *Markus Hofer* für seine uneingeschränkte Hilfsbereitschaft, für die Messung der unzähligen CFC Proben und für die entspannenden Momente in seinem Labor. Ohne den "Fitter" von *Frank Peeters* hätte ich alle Edelgastemperaturen von Hand ausrechnen müssen - ihm und *Philippe Périsset*, der mich für den Mac begeisterte, gilt mein spezieller Dank.

Der Gruppe um *Rainer Wieler* danke ich für die vorbehaltlose Unterstützung im Edelgaslabor der Isotopen Geologie der ETH. Ohne *Heiri Baur*, seiner reichen Erfahrung und denen von ihm betreuten Massenspektrometern wären die Edelgas-

messungen unvorstellbar gewesen. *Urs Menet*, *Stephan Thürig* und *Thomas Graf* möchte ich für die unkomplizierte und kompetente Hilfe im Labor herzlich danken.

Mehrere Teile der vorliegenden Arbeit entstanden in enger Zusammenarbeit mit der Gruppe von *Hugo Loosli* der Klima- und Umweltphysik der Uni Bern. Ihm und im speziellen seinen Doktoranden *Roland Purtscher* und *Nobert Mattle* danke ich für die fruchtbare Zusammenarbeit im oberen Glattal und im Linsental Projekt.

David Livingstone und *Vijay Matta* danke ich für die sprachlichen Korrekturen.

Bei meinen D16-Bürokollegen *Martin Büssenschütt*, *Christoph Schlumpf* und *Andreas Schönborn* und den letzten echten UP-Mitdoktoranden *Gerhard Wagner* und *Christoph Mattenberger* möchte ich mich für die wundervolle Zeit bedanken.

Das überaus angenehme Klima an der Umweltphysik im besonderen und an der EAWAG im allgemeinen werde ich in Zukunft sicher vermissen. Aus diesem Grund sei allen, jetzt auch nicht namentlich erwähnten Personen, von ganzem Herzen gedankt.

Finanziell unterstützt wurde diese Arbeit durch den Schweizer Nationalfond (Kredit Nr. 20-47060.96).

Mein persönlicher Dank gilt meinen Eltern, die mich während meiner ganzen Ausbildung sowohl moralisch, wie auch finanziell unterstützt haben. Meiner Freundin Daniela möchte ich danken, dass sie mir half auch wieder genügend Abstand zur Arbeit zu gewinnen. Nicht zuletzt bedanke ich mich bei meiner Grossmutter dafür, dass sie immer an mich geglaubt hat.

Curriculum Vitae

Urs Beyerle

- | | |
|--------------|--|
| May 25, 1969 | Born in St. Gallen (Switzerland) |
| 1976 - 1982 | Primary school in St. Gallen |
| 1982 - 1984 | Secondary school in St. Gallen |
| 1984 - 1988 | High school in St. Gallen
School-leaving exam (Matura type C) |
| 1989 | Mandatory military service |
| 1989 - 1995 | Study of environmental science at the Swiss Federal Institute of Technology (ETH), Zürich |
| 1995 | Diploma thesis at the Institute for Atmospheric Science (LAPETH), ETH Zürich |
| 1995 | Diploma in natural sciences (Dipl. Natw. ETH) |
| 1995 - 1999 | Ph.D. student in the Department of Environmental Science, Swiss Federal Institute of Technology (ETH), Zürich; and in the Department of Environmental Physics, Swiss Federal Institute for Environmental Science and Technology (EAWAG), Dübendorf |